2015

ORIGIN AND QUANTIFICATION OF DIFFUSE CO2 AND H2S EMISSION AT CRATER HILLS, YELLOWSTONE NATIONAL PARK

Peipei Lin
Michigan Technological University

ORIGIN AND QUANTIFICATION OF DIFFUSE CO_2 AND H_2S EMISSION AT CRATER HILLS, YELLOWSTONE NATIONAL PARK

By
Peipei Lin

A THESIS
Submitted in partial fulfillment of the requirements for the degree of
MASTER OF SCIENCE
In Geology
MICHIGAN TECHNOLOGICAL UNIVERSITY
2015

This thesis has been approved in partial fulfillment of the requirements for the Degree of MASTER OF SCIENCE in Geology.

Department of Geological and Mining Engineering and Sciences

Thesis Advisor: *Dr. Chad D. Deering*

Committee Member: *Dr. Cynthia Werner*

Committee Member: *Dr. Simon A. Carn*

Department Chair: *Dr. John S. Gierke*

Table of Contents

List of Figures

List of Tables

Abstract

At Crater Hills, a thermally-altered area adjoining the Sour Creek resurgent dome that is located within the Yellowstone Caldera, we characterized volatile emissions based upon our soil degassing measurements and soil gas chemistry in 2014 and fumarole gas chemistry in 2007 (Bergfeld et al., 2011). The investigation at Crater Hills on its diffuse gases isotopes and CO_2, H_2S emission improve our understanding on its gas emission mode – including total emission and spatial distribution, and contribute to a more accurate estimation of total CO_2 emission at Yellowstone volcanic system. The total emission of CO_2 interpolated by sequential Gaussian simulation method (sGs) was 66 to 109 t d^{-1} with 95% confidence, which is an underestimation due to the inability to measure a high flux area on a slope as well as the absence of fumarole and pool emissions. Indicated by gas chemistry data of the fumarole at Crater Hills in 2007, the proportion of CO_2 derived from magma would be at least 38% if considering the worst and unreasonable scenario; other scenarios give a much higher proportion of magma component, which would be over 50%. Faults or fractures covered by overlying alluvium are very likely to exist at Crater Hills, based on the similarity between the connection of high flux areas and the trend of the regional faults. The estimated emission of H_2S was 0.39 t d^{-1}, based on the linear correlation between H_2S and CO_2. The heat output was also estimated to be ~35MW with average heat flux of ~100 W m^{-2} based upon CO_2-H_2O-heat relations. The temperature of liquid-dominated reservoir was estimated to be 270-300 ^{0}C estimated by Fournier (1989), and was 213 ^{0}C to 217 ^{0}C for the vapor-dominated reservoir which is the source for the sampled fumarole gas in 2007.

1. Introduction

The magmatic system underlying the Yellowstone Caldera is the source of the ground's thermal activities. It is a two-layered system, with the deeper magmatic system releasing heat and gases and the upper hydrothermal system transmitting the heat and gases to the ground mainly through thermal areas (Fournier, 1989). According to Werner & Brantley (2003), both the total CO_2 emission and the areal CO_2 emission from Yellowstone are comparable to that of other large volcanic systems.

The magmatic gases entering the hydrothermal system are transmitted to the ground in two forms: via the dissolved solute from the thermal waters (liquid-dominated hydrothermal system) *or* the volatiles from thermal features like water pools, fumaroles and diffused soils (i.e., a vapor-dominated hydrothermal system) (Fournier, 1989). The neutral-chloride thermal areas, mainly located at the western part of the 0.6 Ma-caldera, host the discharging thermal waters; and the acid-sulfate thermal areas at the eastern part of the 0.6 Ma-caldera, where there is higher elevation, constitute the main pathway for emitted gases at Yellowstone. The vapor-dominated hydrothermal system is derived from the boiling of the underlying hot-water system, thus is high in less dissolvable gases like CO_2.

The earliest investigations of geochemistry in Yellowstone were mainly focused on the Cl-rich waters from a liquid-dominated hydrothermal system. However, Werner & Brantley (2003) indicated that the CO_2 emission from neutral-chloride thermal areas was comparably low compared to that from acid-sulfate areas, from which >96% of total CO_2 emissions were found.

In July-August 2014, a field campaign was performed at Crater Hills, an acid-sulfate thermal area previously simply investigated by Werner and Brantley (2003) as high CO_2 flux area, to 1) characterize and quantify the emission rate of CO_2 and H_2S at diffused soil; 2) compare the emission rate and gas component with other thermal areas at Yellowstone; and 3) estimate the heat flux.

2. Geologic Setting

The Yellowstone Plateau Volcanic Field is located on the North America Plate, under which the Farallon Plate has almost completely subducted on the western side, leaving the North America Plate in contact with the Pacific Plate. Under the North America Plate, a continental hot spot has

developed from the ascent of a mantle plume, which is responsible for the enhanced magma production and the resulting voluminous volcanism.

2.1 Eruption History

The eruptive history of the Yellowstone hot spot has been dated back to 17 Ma in the region of eastern Oregon, western Idaho and northern Nevada, where flood basalts formed today's Columbia and Oregon Plateaus and dispersed rhyolites (Pierce and Morgan, 1992).The volcanism then followed a northeastward track, passing through the Snake River Plain between 14 Ma and 4 Ma to the current Yellowstone Plateau at ~2.1 Ma. This northeastward track of volcanism on the fixed mantle plume indicates the southwestward motion of the North America Plate at the rate of 62 km/m.y. (17-10 Ma) and ~25 km/m.y. (10 Ma - current) (Pierce and Morgan, 2009).

The Yellowstone Plateau Volcanic Field formed during three volcanic cycles over the past 2.1 million years and includes two of the world's largest eruptions. The location and size of each caldera is shown in Figure 1. The first eruption, occurring at 2.059±0.004 Ma (Lanphere et al., 2002), created >2450 km3 Huckleberry Ridge Tuff and the Island Park Caldera (80 km wide and 65 km long). The second eruption at 1.285±0.004 Ma (Lanphere et al., 2002) produced over 280 km^3 Mesa Falls Tuff and Henry's Fork Caldera that is located inside the west part of the Island Park Caldera. The Henry's Fork Caldera is 37 km wide and 29 km long. The most recent eruption started at 0.639±0.002 Ma (Lanphere et al., 2002) with the production of >1000 km^3 of the Lava Creek Tuff and the resulting 45 by 85 km Yellowstone Caldera *(http://volcanoes.usgs.gov/about/volcanoes/yellowstone.php)*.

After the formation and collapse of the Yellowstone Caldera, uplift within the caldera created Mallard Lake resurgent dome located at south-west of the Yellowstone Caldera and the Sour Creek resurgent dome at north-east of the Yellowstone Caldera (Christiansen, 2001) (Figure 1). The Sour Creek resurgent dome in the east was formed soon after the caldera collapse, based on $^{40}Ar/^{39}Ar$ dating of the overlying Canyon flow indicating an age of 484±15 ka, (Gansecki et al., 1996). The Sour Creek resurgent dome has a gentle slope with maximum dips on the flanks of ~15 degrees. The northwest-trending faults developed on the resurgent dome are related to its uplift and emplacement (Christiansen, 2001) (Figure 2). The Mallard Lake dome is much younger (160 ka) as indicated by K-Ar dating; however, an older resurgent dome may have formed at a similar time as the Sour Creek dome (Christiansen, 2001).

Post-resurgent eruptions occurred during two major episodes, and filled the caldera with over 600 km^3 lavas, forming the Rhyolite Plateau. The first episode began at 600±20 ka (Morgan and

Shanks, 2005) or 516±7 ka (Gansecki et al., 1996) and continued to 257±13 ka (Christiansen et al., 2007), which formed the Upper Basin Member. The second episode started at ~170 ka and continued to 72±4 ka (Christiansen et al., 2007) to form the Central Plateau Member. This effusive eruption produced >600 km^3 rhyolite lavas and filled the Yellowstone Caldera through the NW-SE trending vents. During the second episode, at least two major explosive eruptions occurred in the Central Plateau Member, one depositing the Bluff Point tuff during the creation of the West Thumb Caldera, and another depositing the Cold Mountain Creek tuff (Christiansen, 2001; Christiansen et al., 2007).

Can you add a section here or perhaps later that discusses what Crater Hills is? Why is it a hill? Is it a volcanic feature, or do we know? How does it relate to the Sour Creek dome or these other deposits. What is exposed at the surfaces at Crater Hills?

2.2 Magmatic System

The magmatic system under the Yellowstone Caldera consists of an upper crustal reservoir and an underlying basaltic system at the lower crust and upper mantle (Figure 3). The upper crustal reservoir measuring 6-12km deep (Miller and Smith, 1999) is comprised of porous granite filled by a mixture of partially crystallized rhyolite melt, water and dissolved gases (Chu et al., 2010; Husen et al., 2004). As indicated by Lowenstern and Hurwitz (2008), the high flux of magma derived volatiles from Yellowstone Plateau Volcanic Field exceeding the capacity of the upper siliceous crustal reservoir is a clear implication for a deeper basaltic system that stores more CO_2. Moreover, the inconsistence in the relative proportion of emitted volatile from the magmatic-hydrothermal system that has high magnitude in CO_2 than in Cl, F and S, and the degassing of upper silicic magma abundant in Cl and F however less in CO_2 and S indicates an underlying basaltic system. This basaltic magma is considered to be successively provided by the underlying hot spot (Porritt et al., 2014; Schmandt and Humphreys, 2010; Smith et al., 2009). Werner and Brantley (2003) showed that the total CO_2 emission for Yellowstone is consistent with the CO_2 release expected from the emplacement of basaltic magma from the lower crust into shallower crustal reservoirs.

2.3 Hydrothermal system

The hydrothermal system overlying the magmatic system receives the heat and volatiles released from magmas, releases heat and volatiles through thermal features, and controls the soil

types. The thermal features developed throughout Yellowstone National Park indicate a wide distribution of the hydrothermal system (Figure 4). Thermal water at YPVF can be classified according to its water chemistry into neutral-chloride, acid sulfate and travertine deposits. Indicated by water stable isotopes, the thermal water discharged in YPVF is derived from a parent fluid (335-370 ^{0}C, 310-400 ppm Cl^{-}, δD of -149‰) modified by boiling and mixing with cold dilute water at depth as well as gas-water-rock reaction at an shallower depth (Fournier et al., 1976; Truesdell and Fournier, 1976; Truesdell et al., 1977). The difference in water chemistry is related to the pathways they travelled where encountered different rock types and different topography. In addition, the interaction between hydrothermal water and some sedimentary rocks (e.g. limestone) would generate CO_2, contributing to the CO_2 released from hydrothermal system.

The neutral chloride water is normally from high-temperature, felsic-rock-hosted hydrothermal system, as the result of the full neutralization of parent magmatic fluid (Giggenbach, 1988). The neutralization process includes rock dissolution which incorporates metals like Na, K, Mg and Ca with similar ratio as the original rocks, and the precipitation process that deposits Mg- and Ca-rich as well as sulfur-incorporated products. The resulted water derived from complete interactions between parent magmatic fluid and rocks is enriched in Cl^{-} and depleted in SO_4^{2-}, Ca^{2-} and Mg^{2-} (Fournier, 1989; Hurwitz et al., 2012). The neutral chloride hydrothermal systems are mainly located at western part of Yellowstone where elevation is low compared to eastern Yellowstone at low elevation basins (Morgan et al., 2009) with high water table at or near ground surface..

The acid sulfate hydrothermal system is primarily formed due to the steam heating process, by which the underlying neutral waters boils to generate steam and less soluble volatile (CO_2, H_2S, H_2, CH_4, etc.). The generated H_2S-rich steam rises to fill faults and fractures beneath an impermeable lava cap to form a vapor-dominated system (Fournier, 1989) and perched over the cap. Common surficial expression of the vapor-dominated system are fumaroles, mud pots, and acid boiling pools (Allen and Day, 1935; White et al., 1971). At Yellowstone, the acid sulfate hydrothermal system is mainly located at eastern part with a higher elevation than western has (Farrell et al., 2014; Husen et al., 2004; Miller and Smith, 1999). The acid water derived from boiled neutral water released at higher topography, while the neutral water flows horizontally to outflow directly at lower elevation.

The travertine type, mainly located at Mammoth Hot Springs, is rich in carbonate and saturated in calcium carbonate. Its pH is around 6 but quickly increases with the degassing of CO_2 (Kharaka et al., 2000; Sorey and Colvard, 1997). Compared to other thermal waters, travertine is rich in Ca^{2+}, Mg^{2+}, HCO^{3-}, SO_4^{2-}.

2.4 Soil

Based on fluid chemistry, the soil over the hydrothermal systems is categorized into acid-sulfate, travertine, and neutral-chloride (Rodman et al., 1996) (Figure 4). In travertine-depositing areas at Mammoth Terraces, the weathering of travertine deposits contributes to the soil; thus, the soils are characterized by travertine fragments. Neutral-chloride soils fed by alkaline-chloride thermal waters have a neutral pH of 5.0 - 6.9. This pH range is a favorable condition for deposition of SiO_2 from silica-saturated solutions. The hot-spring-derived siliceous deposits are then weathered into soils and siliceous rock fragments, and mixed with non-hydrothermally derived rhyolite soils, forming the neutral-chloride soil.

Acid-sulfate soils are formed in the existing deposit are associated with pedogenic activities occurring in the upper 20-30cm and hydrothermal alteration processes at depth. In the area above the water table, soils are moistened by acid steam from the boiling thermal water or water produced through capillary action, associated with the pH of 2.1-5.3 and the temperature of ambient to 78 degrees Celsius. The soil normally has a bleached appearance from the loss of Fe and other times seems darkened due to organic matter. In addition, it generally is lacking in vegetation due to the high soil temperature and high acidity, for example, the Crater Hills shown in Figure 5.

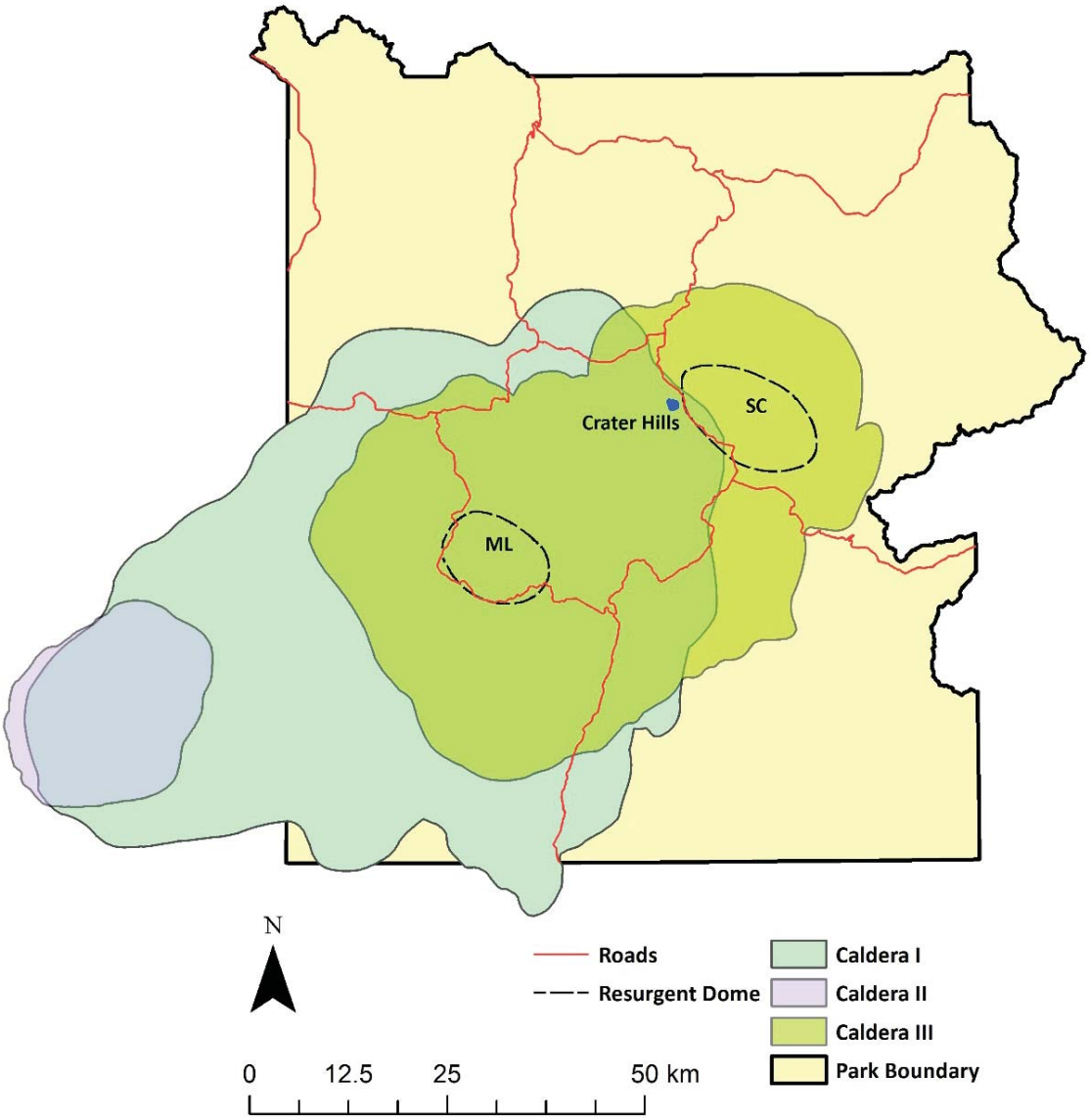

Figure 1 The caldera complex formed from three eruptions over the past 2.1 Ma. The Crater Hills' thermal area (outlined by the small blue dots) is located inside the third caldera and at the edge of the first caldera.

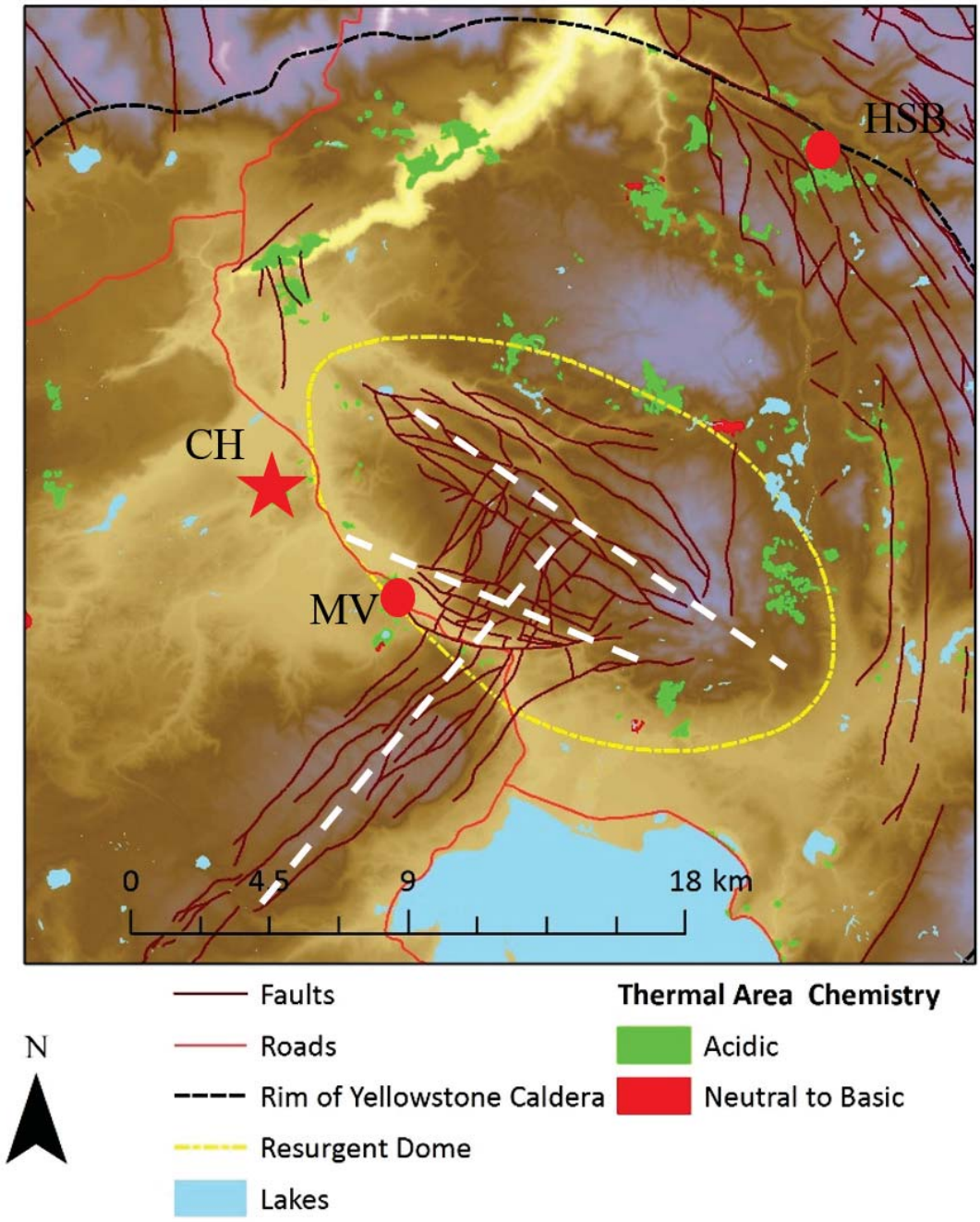

Figure 2 Map of regional faults for Sour Creek resurgent dome region. The white dashed line is the trend of major faults groups, which are NW, WNW and NE directions.. Crater Hills (CH) is labeled by star; Mud Volcano (MV) and Hot Spring Basin (HSB) are labled by circles.

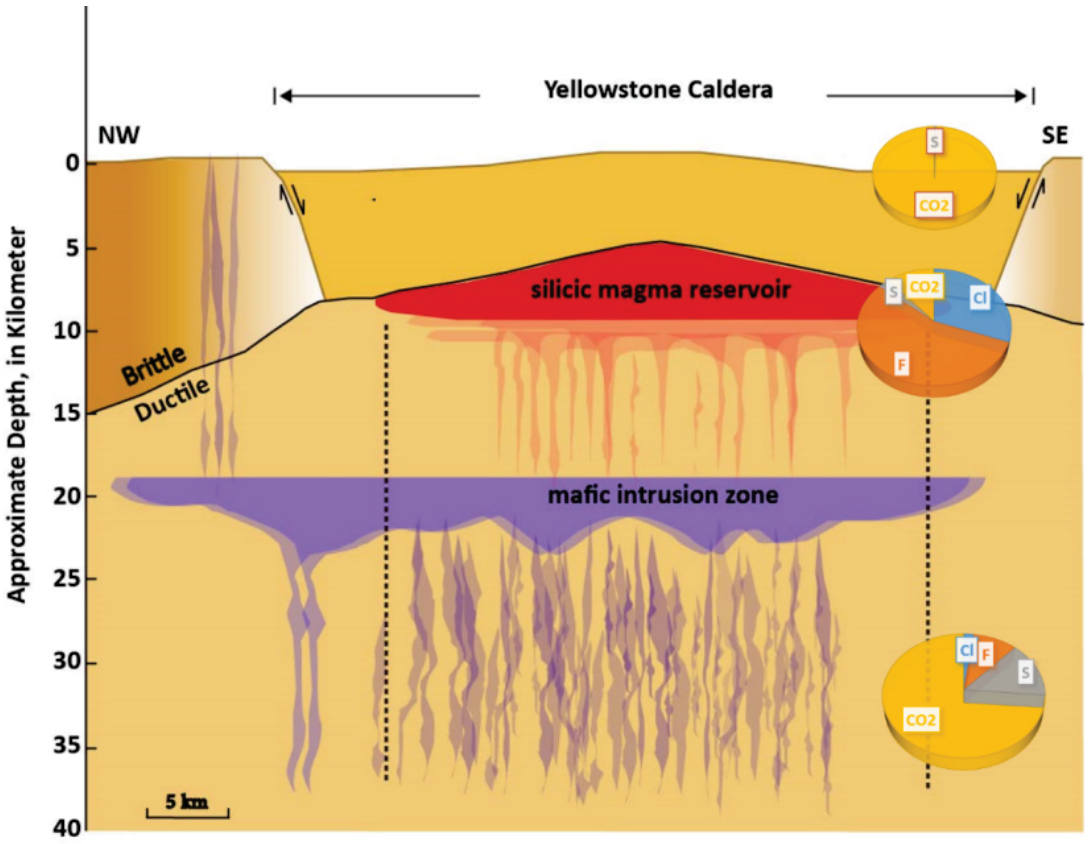

Figure 3 Cross-section of the Yellowstone magmatic system. The magmatic system mainly consists of a deeper mafic intrusion zone and a shallow silicic magma reservoir. The pie chart indicates the proportion of the released gas component at different depths. Modified from Lowenstern and Hurwitz, (2008).

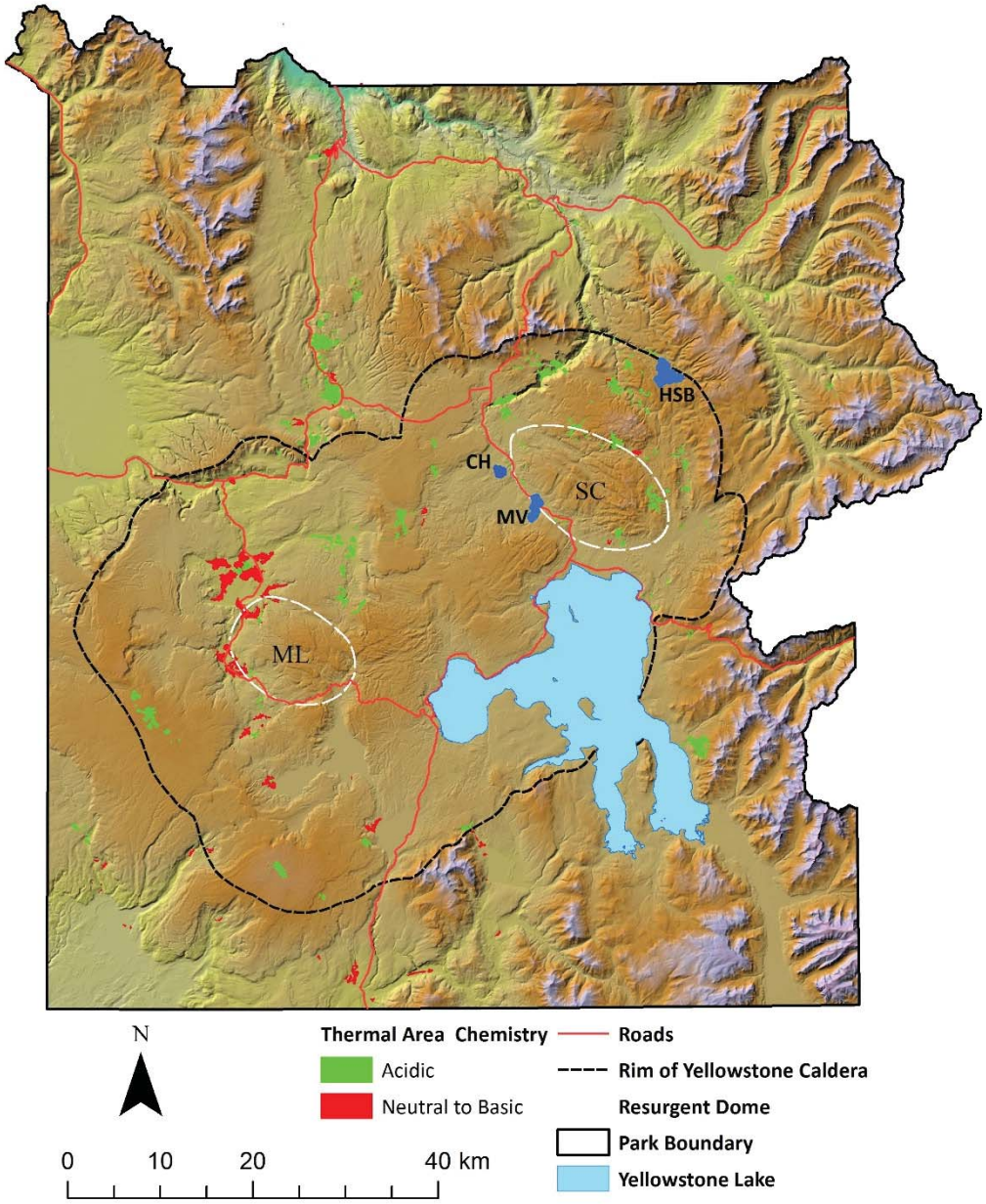

Figure 4 Map of Yellowstone National Park, including information showing the boundaries of the Yellowstone Caldera, the location of the resurgent domes, and the distribution and chemistry properties of thermal areas. Crater Hills (CH), Mud Volcano (MV) and Hot Spring Basin (HSB) thermal regions are also outlined. The GIS data used for the map design have been downloaded from the Yellowstone Geologic GIS Data Center, Wyoming State Geological Survey (http://www.wsgs.wyo.gov/Research/Yellowstone/GIS.aspx).

Figure 5 Overview of Crater Hills, acid sulfate area with bleached soil color. Source: Google earth V 7.1.2.2041. (June 18, 2013). Crater Hills, Yellowstone National Park. 44.653751°, -110.481026°, Eye alt 3.24 km. DigitalGlobe 2015. http://www.earth.google.com [July 23, 2015].

3. Field Description

Crater Hills is located inside the Yellowstone Caldera and on the northwest rim of a resurgent dome. It covers about 0.34 km^2 and has a barren surface with minimal vegetation (satellite image, Figure 5). According to the satellite image, the surface color is grey, and field observations reveal a lighter color (i.e., grey) for less-active areas and a darker color (i.e., brown and even black) for highly-active areas. The highly-active and less active areas could be outlined based on the existence of thermal features and soil color from satellite image (Figure 6). The ground surface at Crater Hills is not flat because the northern part ("Crater Hills") is a high elevation area with an average height of ~2410 meters, about 30 meters higher than the southern part that has an average elevation of ~2380 meters (Figure 7).

Crater Hills is characterized as an acid sulfate thermal region. However the water discharged from Sulfur Spring inside Crater Hills is acid but also chloride-rich. The existence of this acid, chloride-rich hot spring is related to the direct uptake of parent magmatic fluid and the neutralization process (Fournier, 1989; Giggenbach, 1988; Guo et al., 2014). Faults at Sour Creek region have NW, WNW and NE trend; but none of them traverses Crater Hills based on the geological map (Figure 2) generated by U.S. Geological Survey in 1977. However, hidden faults covered by sediments were pointed out at Mallard Lake resurgent dome region (Jaworowski et al., 2010). As Crater Hills areas is covered by alluvium (Christiansen, 2001) and the existence of faults or fractures is required for the upward flow, Crater Hills is likely to have the same situation as Mallard Lake resurgent dome region.

A reconnaissance field campaign on diffuse CO_2 was previously performed in the south-eastern part of Crater Hills in 2007 (according to written communication with Werner), using the same accumulation chamber method but with a slightly larger spacing of 25-30 meters. The gases of a fumarole, located in the eastern part of Crater Hills, was collected and analyzed by USGS in 2007 (Bergfeld et al., 2011). Location of the 2007 data and the measured fumarole is shown in Figure 8. The gas chemistry of the fumarole is shown in Table 2.

Table 1 *Fumarole gas isotope data for Crater Hills (Bergfeld et al., 2011).*

Date	Feature	Temp °C	Easting meters	Northing meters	Xg (%)	CO_2 mol%	H_2S mol%	NH_3 mol%	He mol%	H_2 mol%	Ar mol%	O_2 mol%	N_2 mol%
2007/9/18	fum	90.9	541392	4944637	3	98.4	1.27	<0.0002	0.0026	0.016	0.0047	0.001	0.245
						CH_4 mol%	C_2H_6 mol%	HCl mol%	R/Ra	Rc/Ra	$^4He/^{40}Ar*$	$\delta^{13}C\text{-}CO_2$ (C) per mil	N_2/Ar
						0.056	0.00004	<0.001	10.37	10.37	2.4	-2.9	52.1

Figure 6. The location map of highly active areas. These highly active areas are determined based on the existence of thermal features, the soil temperature and color. The image is derived from Google Earth. Source: Google earth V 7.1.2.2041. (June 18, 2013). Crater Hills, Yellowstone National Park. 44.653751°, -110.481026°, Eye alt 3.24 km. DigitalGlobe 2015. http://www.earth.google.com [July 23, 2015].

Figure 7. Contour map for Crater Hills area. The blue area is the Crater Hills area. The coordinate system used as x, y coordinates is the UTM system in meters.

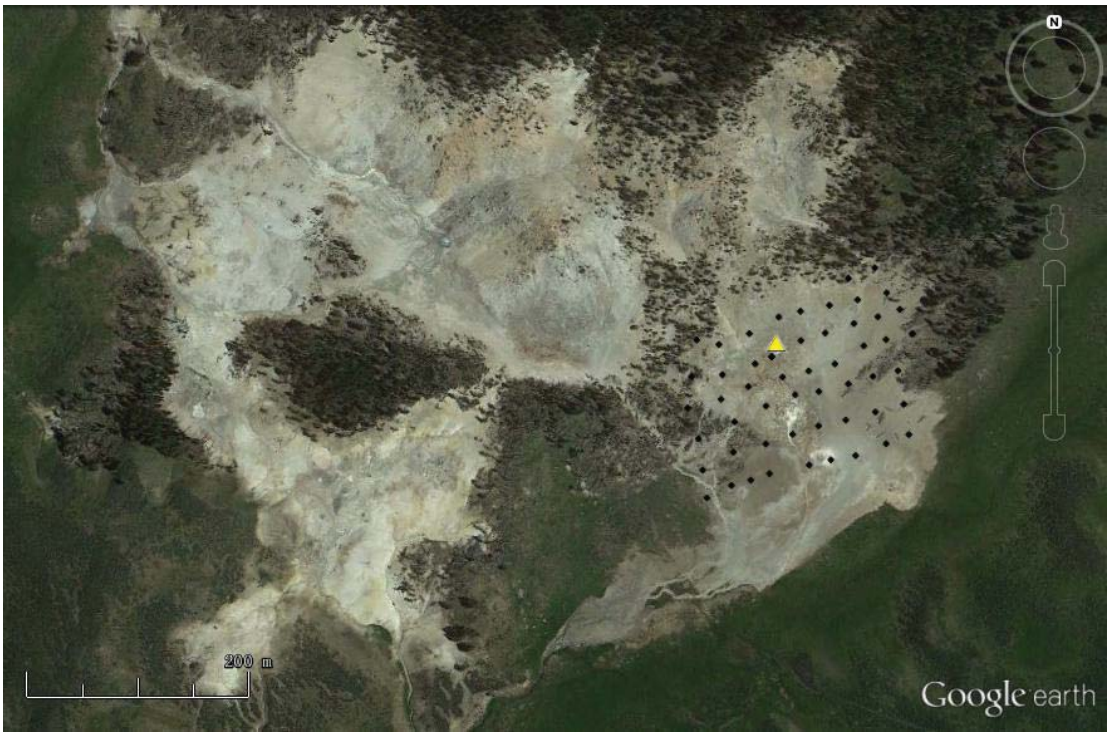

Figure 8. Location of the 2007 reconnaissance field campaign data and the fumarole data measured in 2007. The black points are the sample sites for diffuse CO2. The yellow triangle is the location of the measured fumarole. Source: Google earth V 7.1.2.2041. (June 18, 2013). Crater Hills, Yellowstone National Park. 44.653751°, -110.481026°, Eye alt 3.24 km. DigitalGlobe 2015. http://www.earth.google.com [July 23, 2015].

4. Method

4.1 Soil Gas Measurements

4.1.2 Soil Gas Fluxes

In order to quantify the flux of diffuse CO_2 and H_2S soil gas emissions at Crater Hills, we utilized the accumulation chamber method (ref). This method estimates gas fluxes based on the rate of increase in the gas concentration within the accumulation chamber placed over the ground surface. At Crater Hills, we used a systematic sampling approach with grid spacing of ~15 m for non-vegetated areas and spacing of ~25-35 m for vegetated areas (Figure 9). The routes followed each day for measurements were pre-planned with the GPS as parallel sampling lines to maintain spacing of 15m and to ensure complete coverage of the area of interest. Soil temperatures were also measured at a depth of ~15 cm within 1m of the accumulation chamber. The soil is hard due to the

existence of sinter and crushed stones, which required a heavy-duty thermal probe and still prevented the consistent measurement at 15 cm depth. Air temperature, humidity, and wind speed are measured at the start of each measurement and after every 10 consecutive measurements of flux and soil temperature.

The instrument consists of the following: 1) a West Systems® Type B accumulation chamber, with an internal diameter of 0.2m, internal height of 0.198m, and internal volume of 6.231×10^{-3} m^3 (Figure 10); 2) a LI-COR 820 CO_2 gas analyzer to measure the concentration of CO_2 over a range of 0- 20,000 ppm; 3) TOX05 H_2S gas analyzers to measure the concentration of H_2S over the range of 0-20 ppm; 4) a Trimble® portable computer, mainly used to store concentration data and display the curve of concentration vs. time, and also recorded the information of location, elevation, temperature and pressure; 5) a Garmin® GPS to record the location of measurements with accuracy (the black instrument in the middle of Figure 11); and 6) a Fluke 51-2T thermometer to measure soil temperature (the one on the right in Figure 11).

The diffuse gas gathered in the chamber is pumped out to CO_2 and H_2S gas analyzers to allow concentration to be measured and thus to derive the flux based on the concentration-time relation. The utilized accumulation chamber (Type B chamber ordered from the West System®) is designed to measure high fluxes that exceed 10,000 g m^{-2} d^{-1} with higher accuracy. In order to eliminate air contamination, the accumulation chamber was placed on the soil in a specific manner so as to maintain a good seal when making the measurements. The software FluxManager in Trimble displayed the concentration vs. time plot and calculated slope over the measurement time interval, which could be used as a quick check for the performance of the analyzers in the field. In the later data processing step, a more accurate linear regression was performed for the concentration-time relation and expressed as the angular coefficient (α) for the regression, which is calculated using equation 1,

$$\alpha = \frac{\sum x \cdot y - \frac{\sum x \cdot \sum y}{n}}{\sum x^2 - \frac{(\sum x)^2}{n}} \quad (1)$$

where x is the time in seconds, y is the concentration in ppm, and n is the number of points used for flux calculation. The angular coefficient α is in ppm/s. The performance of the linear regression is evaluated by the following linear regression quality factor (ErrQ, equation 2).

$$\mathrm{ErrQ} = \frac{(\sum x \cdot y - \frac{\sum x \cdot \sum y}{n})^2}{[\sum x^2 - \frac{(\sum x)^2}{n}][\sum y^2 - \frac{(\sum y)^2}{n}]} \quad (2)$$

The value of ErrQ varies from 0 to 1. The value close to 0 (ErrQ < 0.5) indicates a poor regression,

and close to 1 (ErrQ > 0.9) indicates an acceptable regression.

The determination of flux depends on the volume of the accumulation chamber and is affected by air temperature, barometric pressure and humidity. In order to eliminate the effects of humidity, all measurements are taken on dry soil. To eliminate the effects of air temperature and barometric pressure, the STP-normalized flux is calculated from the rate of increase in gas concentration,

$$\text{Flux} = \text{k}\left(\frac{P}{P_0}\right)\left(\frac{T_0}{T}\right)\left(\frac{V}{A}\right)\left(\frac{dc}{dt}\right) \quad (3)$$

where P is the barometric pressure (bar/kPa), T is the measured air temperature (K), V is the volume of the accumulation chamber, and A is the internal surface of the chamber. For normalization, T_0 and P_0 represent standard temperature and pressure (298K and 101.3kPa).

The detection limits of CO_2 and H_2S flux are 2-32,000 g m^{-2} d^{-1} and 1.7-47 g m^{-2} d^{-1}, respectively. The error is estimated at ±15% (Chiodini, 1996) and -12% (Evans et al., 2001). Since the low flux of H_2S is easily affected by previous high flux measurements, the instrument was run for over 10 seconds before placing the accumulation chamber on the soil. This procedure ensured the concentration of H_2S decreased to a low concentration. In cases where the concentration vs. time plot showed an increasing trend followed by a rapid decrease trend, the data was considered invalid for the determination of the flux.

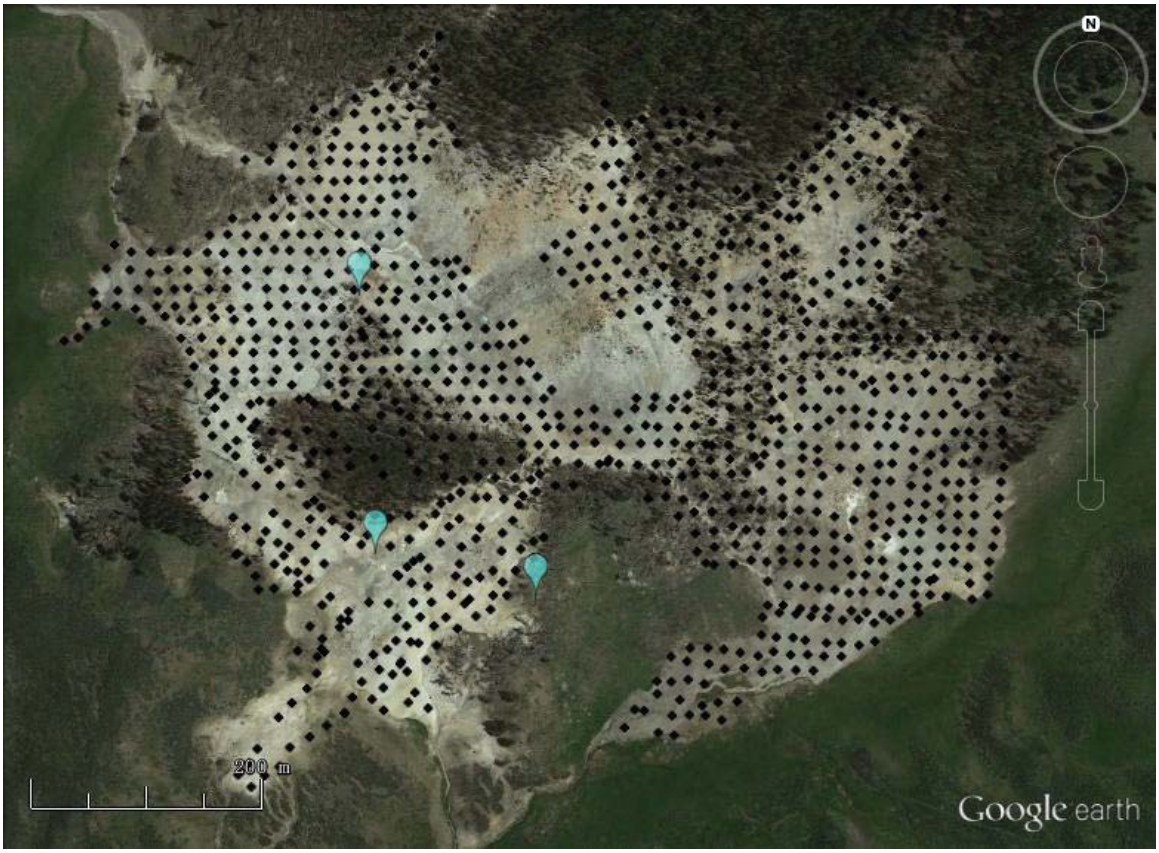

Figure 9 Satellite image of Crater Hills' area, with sampled points marked in black circles. The location marked by the blue bubble is the sample sites where diffused soil gases are collected for isotope analysis. The number for the scale is 200m. Source: Google earth V 7.1.2.2041. (June 18, 2013). Crater Hills, Yellowstone National Park. 44.653751°, -110.481026°, Eye alt 3.24 km. DigitalGlobe 2015. http://www.earth.google.com [July 23, 2015].

Figure 10 The cylinder placed on the ground is the accumulation chamber. It is connected to the yellow box, where the H_2S and CO_2 gas analyzer is placed.

Figure 11 Instruments used in the field. From left to right are a field book, the Garmin® GPS, and the Fluke® thermometer.

4.1.2 Carbon Isotope Measurements

At some sites, the diffused gases were collected using 1) an Isotech® gas bag (Figure 12) and 2) a syringe and vessel (Figure 13). The sampled sites for carbon isotope analysis were selected based on the following criteria: 1) Low or no H_2S flux (< 2 g m^{-2} d^{-1}), as the gas bag is not able to contain the H_2S; but 2) not too low CO_2 flux (> 20 g m^{-2} d^{-1}). For the syringe gas collection, the syringe was inserted into the septum of the accumulation chamber to obtain/collect the gases. Unfortunately, for the isotope analysis, the data collected via the syringe could not be analyzed due to the insufficient amount of gases collected into the vessel. For the gas bag collection, a hand pump was used to extract the gases from the accumulation chamber, which was operated at least 1 minute before collection. The gas bag was filled after 10-15 squeezes. The gas bag contained enough gas for carbon isotope measurements, which were later made by Isotech®. The information of the sample location and the instrument for gas collection are listed in Table 2. The three analyzed data is marked on Figure 9.

Table 2 *Detailed information on carbon isotope samples.*

Sample No.	Sample Date	Longitude	Latitude	Instrument
1	08/09/2014 10:53	-110.48093^0	44.65255^0	Gas bag 1 & Vessel 1
2	08/09/2014 11:02	-110.48074^0	44.65295^0	Vessel 2
3	08/09/2014 11:16	-110.48033^0	44.65377^0	Vessel 3
4	08/09/2014 11:37	-110.48319^0	44.65494^0	Gas bag 2 & Vessel 4
5	08/09/2014 11:48	-110.48398^0	44.65486^0	Vessel 5
6	08/09/2014 12:08	-110.48302^0	44.65289^0	Gas bag 3 & Vessel 6
7	08/15/2014 10:46	-110.47968^0	44.65368^0	Vessel 7
8	08/15/2014 11:50	-110.48452^0	44.65288^0	Vessel 8

Figure 12 Isotech® gas bags and the bucket for protecting the bags while they are transported during transportation. (Image downloaded from Isotech® website: http://www.isotechlabs.com/products/other/gasbags.html).

Figure 13 Syringe and vessel used for diffused soil gases' collection. However, insufficient gases were inserted into the vessel for isotope analysis.

4.2 Data Analysis

In order to estimate the flux of CO_2 and H_2S, the unit conversion from ppm s^{-1} to g m^{-2} d^{-1} was first performed. The geographic statistical approach (GSA) and sequential Gaussian simulation (sGs) were utilized to estimate the flux and total emission of diffused CO_2. Considering the lack of valid H_2S data, the H_2S-CO_2 was used to estimate the total emission of H_2S.

4.2.1 Unit Conversion

The coordinate system was converted from a geographic coordinate system (longitude and latitude) to the Universal Transverse Mercator (UTM) to change the map units from degrees to meters for subsequent processing. The measured rate of increase in concentration in ppm s^{-1} was converted to flux in g m^{-2} d^{-1} by factoring in the barometric pressure, air temperature, and area and volume of the accumulation chamber using the following A.c.K. equation (from the West System® handbook:

$$K = \frac{86400 * P}{10^6 * R * T_k} * \frac{V}{A} \quad (4)$$

where P is the barometric pressure expressed in mBar (HPa); R is the gas constant of 0.08314510 bar L K^{-1} mol^{-1}; T_k is the air temperature expressed in Kelvin degree; V is the chamber net volume in cubic meters, which is 6.186×10^{-3} m^3 for this type of B chamber; and A is the chamber inlet net area in square meters, which is 3.140×10^{-2} m^2 for the type B chamber. The dimensions of the A.c.K. are

$$K = \frac{moles * meter^{-2} * day^{-1}}{ppm * sec^{-1}} \quad (5)$$

The dimensions of flux in moles m^{-2} day^{-1} are then converted to grams m^{-2} day^{-1}. The flux value under the detection limit were marked UD in the sample data (Appendix I), but were represented by the value of 0.1 for simulation.

4.2.2 Graphical Statistical Approach (GSA)

The graphical statistical approach (GSA) (Chiodini et al., 1998) performs the following functions: 1) It partitions the flux data into groups based on the log-normal probability plot (Sinclair, 1974), 2) calculates the mean flux and the 95% confidence interval of each group using Sichel's t-estimator (David, 1977), and 3) calculates the total gas emission by summing up the gas emission of each group, calculated by multiplying the mean value with the corresponding area of the group. The area covered by each group is obtained as follows:

$$S_i = f_i \cdot S \quad (6)$$

where S represents the total ground area and f_i is the proportion of the group in the flux dataset. The total soil gas emission was estimated using the following equation:

$$\mathrm{E} = \sum E_i = \sum m_i \cdot S_i \quad (7)$$

where m_i is the mean value of each group. The advantage of the GSA is that it allows scientists to determine the confidence interval of the estimation. However, one limitation of the GSA is that it does not consider the spatial correlation between the data.

4.2.3 Sequential Gaussian Simulation

The sequential Gaussian simulation (sGs) technique is a stochastic simulation algorithm that not only allows scientists to define the uncertainty of the estimation but also considers the spatial correlation between the data. The basic function of this algorithm is to generate a set of equiprobable representations (realizations) of the spatial distribution of the attribute *and* to use the differences in the realizations to measure the uncertainty (Goovaerts, 2001).

The basic elements of an effective map using sGs is a proper sample design that accurately defines the spatial dependency of the data points (e.g. variogram) and a derived statistical distribution for each 1 by 1 grid based on the variogram. The program used for sGs is *sgsim* in GSLIB –an acronym for Geostatistical Software LIBrary which is a collection of geospatial programs (Deutch and Journel, 1992) and the processes of the sGs are described below (Deutch and Journel, 1992; Pyrcz and Deutsch, 2014):

1) Perform a declustering of the raw data and a normal-score transformation of the declustered data.
2) Randomly pick a non-simulated grid.
3) Estimate the function of the local probability distribution for the grid based on its mean and the standard deviation, calculated using the previous simulated data for the grid and the surrounding points.
4) Repeat 2-3 times until all grid locations are assigned a value, which indicates the completion of one realization.

For this study's dataset, the number of simulations was set to 1000 realizations and a spacing of 1-meter was specified for CO_2 flux and soil. Information of the detailed process can be found in Appendix II.

5. Results

5.1 Field Observation at Crater Hills

Crater Hills could be categorized into two groups - the highly-active area and the less-active areas - based on the significant discrepancy of their CO_2 flux, the existence of thermal features, the soil temperature, and the soil color discovered in field observations. The two groups could also be classified through satellite images showing the color of the soil and the roughness of the ground. From satellite images, the active areas have a much rougher surface as illustrated by the abundance of thermal features such as hot springs, mud pots and fumaroles, a comparably darker soil color, higher soil temperature, and higher CO_2 flux.

There are five main active areas outlined in Figure 14 (same with Figure 6) in Crater Hills: the middle eastern area (Area 1 in Figure 14), the northeastern area (Area 3 in Figure 14), the middle area (Area 2 in Figure 14) and two low elevation zones in the southwestern part (Areas 4 and 5 in Figure 14). Detailed descriptions for each area are as follows:

1) Thermal features like fumaroles and mud pots were highly developed in Area 1, and there also existed the discharge of hot springs. The geochemistry of a fumarole gas was measured in 2007 by USGS in Area 1 (Bergfeld et al., 2011). No measurements on the flow rate and chemistry were available for this spring. The highest soil temperature of 92.3 degrees Celsius and the CO_2 flux of 44281 g m^{-2} d^{-1} in the Crater Hill campaign were measured in Area 1. The soil color was quite dark, ranging from brown to even black.

2) In Area 2, only fumaroles existed; they were highly developed on the slope (~30 degrees). At several points, the soil temperature was quite high, with the highest point registering at 92 degrees Celsius. The soil color was not too dark, ranging from yellow to brown. The presence of yellow indicates the existence of the sulfur deposits.

3) Area 3 suffered high elevation change, with a slope of 20-30 degrees. Fumaroles were highly developed on the slopes, the steam from which could be clearly seen in the morning (Figure 15 & 16). There existed a 6m-diameter discharging hot spring, called Sulfur Spring or Crater Hills geyser, at the toe of the slope with 3-5m high explosions several times a day (Figure 17). The spring water chemistry was presented by Fournier (1989) and the temperature and pH were re-measured in 2000 provided by Montana State University in the Yellowstone Geothermal Features Database (http://www.rcn.montana.edu/Features/Detail.aspx?id=717). The soil color varied from

grey to brown to black and sometimes yellow.

4) In Area 4, mud pots were highly developed, including the mud pot holes on the left and mud pots on the muddy ground on the right in Figure 18; and there existed a small hot spring and very few fumaroles. The soil color there varied from grey to black (Figure 18).

5) In Area 5, mud pots were highly developed, and one 7.5m-diameter discharging hot spring existed. Unfortunately, we did not get chemistry data for this spring so that we did not have the information about the flux of HCO3- and SO42- from this spring. The soil color ranged from dark grey to black.

Figure 14 The location map of highly active areas. These highly active areas are determined based on the existence of thermal features, the soil temperature and color. The image is derived from Google Earth.

Figure 15. The clearly-seen steam from fumaroles on the slope, taken at the middle part of Crater Hills (Area 2 in Figure 14).

Figure 16. Fumaroles at the flank of the slope, at the middle part, releasing steam.

Figure 17. The 6m-diameter discharging hot spring, called Sulfur Spring, at the toe of the slope at middle part, with 3-5m high explosions several times a day.

Figure 18 The mud pot holes and muddy ground at south part of Crater Hills (Area 4 in Figure 14).

5.2 Diffuse soil gas flux

5.2.1 CO_2 flux and soil temperature

Among the measured locations, 1029 sites resulted in CO_2 flux measurements over the detection limit, ranging from 2 to 44281 g m^{-2} d^{-1}. The 1083 measured soil temperatures ranged from 11.2 to 92.3 ^{0}C (the boiling point at 2380 m is ~92^{0}C). The maximum CO_2 flux and highest soil temperature were measured at the same location. The soil temperature of the points where CO_2 fluxes under the detection limit ranged from 12.5 to 45.6 ^{0}C, and most of the soil temperatures were under 30 ^{0}C. At locations where CO_2 flux exceeded 200 g m^{-2} d^{-1}, soil temperatures ranged from 14.6 to 92.3 ^{0}C, with most of the temperatures over 30 ^{0}C. The scatter plot of logarithm CO_2 and soil temperature at 15m-depth also indicates a positive correlation between CO_2 and soil temperature (Figure 19).

The sGs-derived CO_2 flux map shows several areas of high flux (Figure 20), which is

consistent with the highly-active areas circled out based on field observation. The largest two areas were located at the lower eastern part (Area 1, Figure 14) and middle part (Area 2, Figure 14), and other small high flux areas were scattered around the study area. The middle high-flux area (Area 2) located on a slope that had many fumaroles, the steam from which were clearly observed in the morning. In the eastern area, the maximum flux and highest soil temperatures were measured and active thermal features like mud pots, pools and fumaroles were highly developed. The probability map (Figure 21) is consistent with the flux map, in particular in identifying where the potentiality of high flux was similar with the measured high flux areas. The high flux CO_2 areas is matching the high-soil-temperature areas shown in Figure 22.

The declustered mean of CO_2 flux for Crater Hills was 212 g m^{-2} d^{-1}. The mean emission rate was 84 t d^{-1} for the modeled area. Applying the 95% confidence limit results in total emission ranges that from 66 to 109 t d^{-1}. Several active but unstable areas were unable to be measured for CO_2 flux. In addition, the contribution of thermal features (i.e., fumaroles, hot springs and mud pots) over the whole area is not included. Moreover, part of Area 2 (back-slashed area in Figure 20) is considered highly active based on the abundance of fumaroles, where the CO_2 flux should be higher than surrounding measured locations indicated by the trend of increasing flux towards center. However, that area was not measured due to the instability of that area and the extrapolation done by sGs would only assign values equal or lower than the surrounding values. Thus, the results of the CO_2 flux in that area are underestimated.

Although the geographical statistical approach (GSA) is thought to be questionable in accuracy (Cardellini, 2003), the GSA analysis could be used as a complementary technique for determining the total emission rate. Based on the log-normal probability plot (Figure 23), the CO_2 flux was divided into two groups, each of which encompassed about 50 percent of the data. Group A ranged from under detection to 41.0 g m-2 d-1 with the mean of 13.7 g m-2 d-1 and the median of 10.6 g m-2 d-1. Group B ranged from 41.1 to 44281 g m-2 d-1 with the mean of 576.5 g m-2 d-1 and the median of 180 g m-2 d-1. According to this grouping, the mean of the CO2 flux was 295 g m-2 d-1 and the total CO_2 emission was 100 t d-1, which is 20% higher than the estimation derived from sGs.

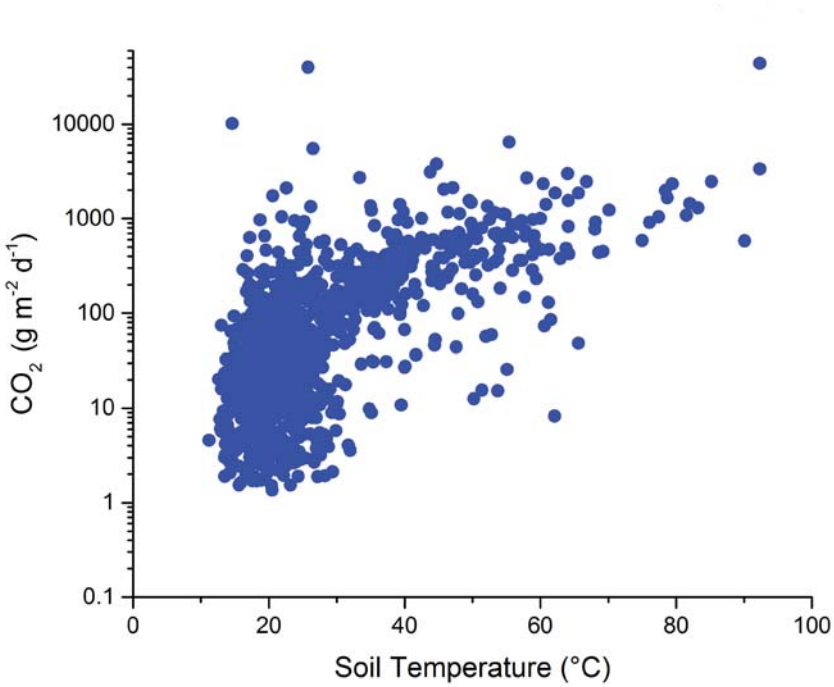

Figure 19. Scatter plot of the CO_2 and soil temperature, indicating a positive relation between CO_2 and soil temperature.

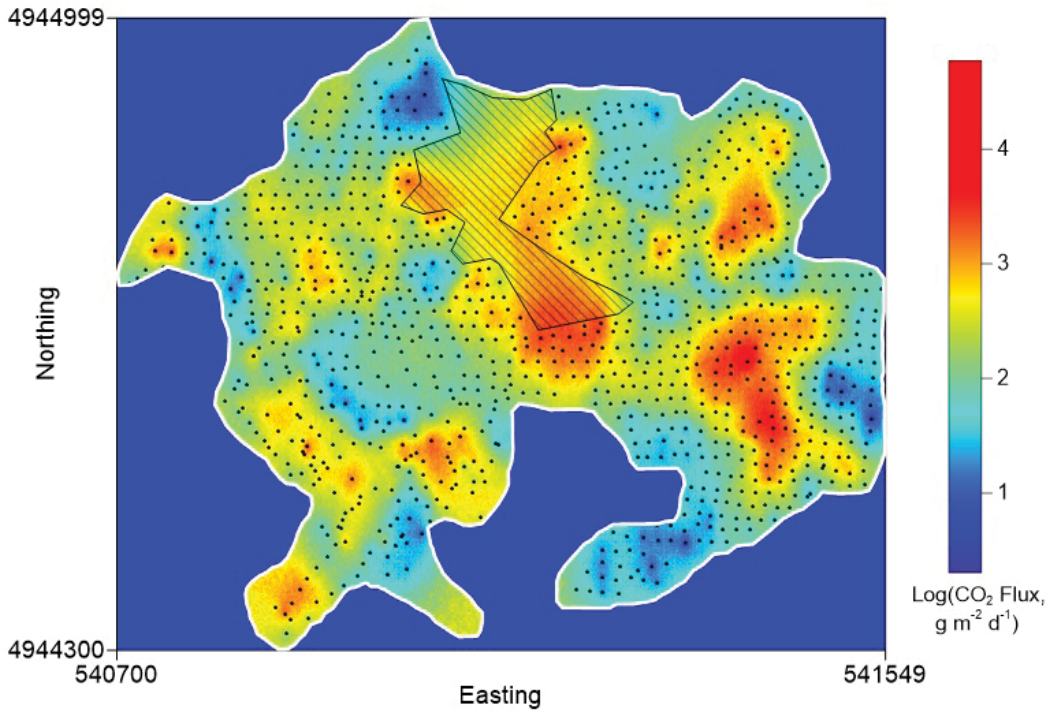

Figure 20. CO_2 flux map, showing the spatial distribution of the fluxes. The black points are the sample sites. The high temperature areas are mainly located in the eastern and middle areas. The back-slashed region is the place which is determined as high-active but without no sufficient measurements; thus the CO_2 flux estimated there is thought to be underestimated.

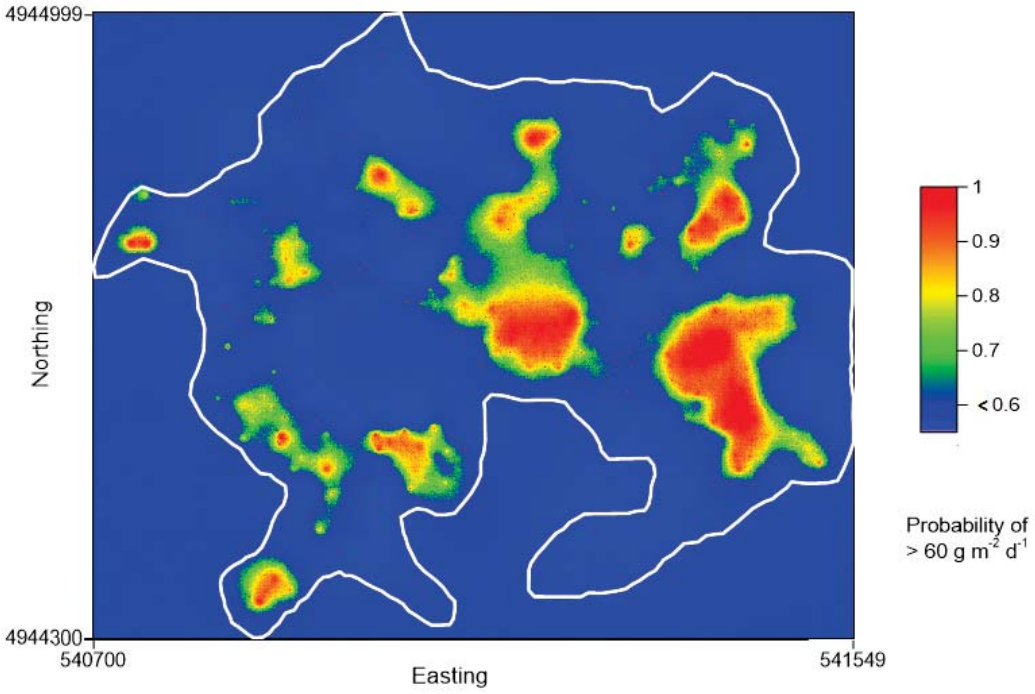

Figure 21 Probability map for the CO_2 flux increases the credibility of the flux map. The threshold of 130 g m^{-2} d^{-1} is the value of the inflection point in the GSA plot, where the CO_2 flux data are separated into two groups. The black points are the sample sites.

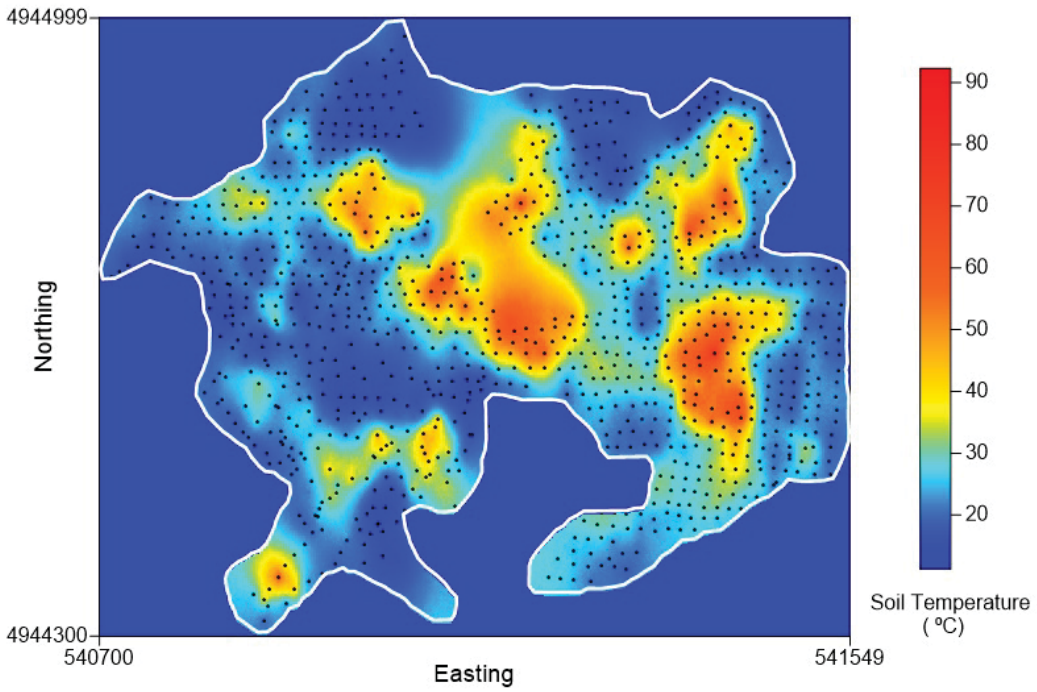

Figure 22. The soil temperature map, showing the spatial distribution of soil temperature. The high temperature areas were mainly located in the eastern and middle parts. The black points are the sample sites.

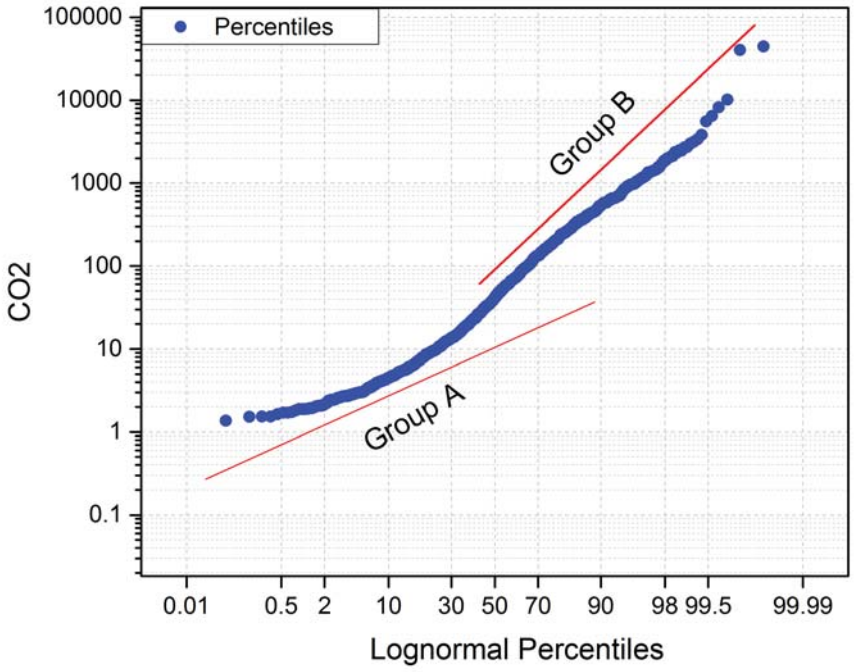

Figure 23. Log-normal probability plot for CO_2 flux at Crater Hills. The data were separated into two groups, A and B, representing diffused CO_2 from two different sources. Group A represents the mixture of biological and hydrothermal source. Group B represents the pure hydrothermal source.

5.2.2 H_2S Flux

In total, 798 H_2S flux measurements were made, ranging from below detection to 106 g m^{-2} d^{-1}; however, only 19 of them were over the detection limit, the number of which is not significant enough for the sGs simulation. Thus the correlation between H_2S and CO_2 was used for the extrapolation of H_2S. For those nineteen valid H_2S flux data, a strong positive correlation to CO_2 was indicated (r^2=0.72 for linear regression); statistical evaluation (i.e., R-squared, T-test, Koenker statistic, Jarque-Bera statistics and scatter plot of residuals, and the detailed analysis in Appendix III) for the model performance indicates the linear regression model used for prediction of H_2S flux using CO_2 as an independent variable is acceptable. This strong linear correlation between CO_2 and H_2S was also demonstrated by Werner et al. (2008) from the diffuse soil gas data at the Hot Spring Basin, as indicated by the scatter plot (Figure 24). The derived H_2S flux map (Figure 25) was based on the linear regression equation below (Equation 8) and used the CO_2 flux threshold of 286 g m^{-2}

d^{-1} as the minimum CO_2 flux for the estimation of the H_2S flux (all CO_2 flux corresponding to a valid H_2S flux was over 286 g m^{-2} d^{-1} except at one point). The maximum predicted H_2S flux was 102 g m^{-2} d^{-1} with a minimum value of 4.3 g m^{-2} d^{-1}; and the predicted total emission was 0.39 t d^{-1}.

$$H_2S = 0.00238 \times CO_2 + 3.707167 \quad (8)$$

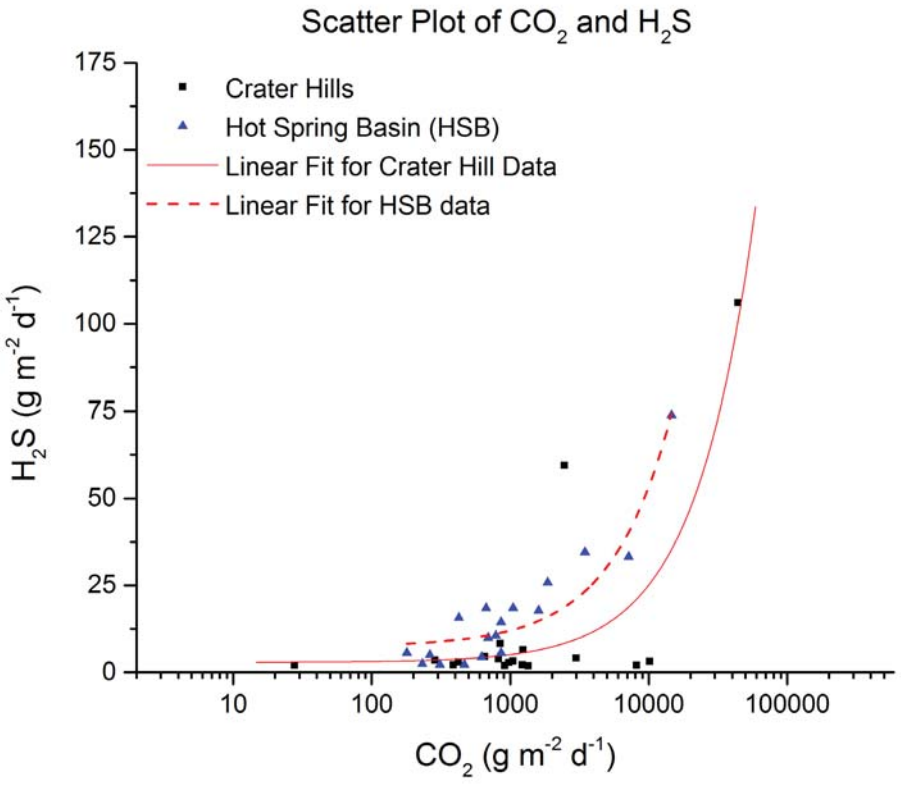

Figure 24. Scatter plot of CO_2 vs. H_2S. Two sets of CO_2-H_2S data, one from Crater Hills in 2014 and another from Hot Spring Basin in 2008, are included to prove the strong correlation between CO_2 and H_2S. The data from Hot Spring Basin are provided by Cynthia Werner.

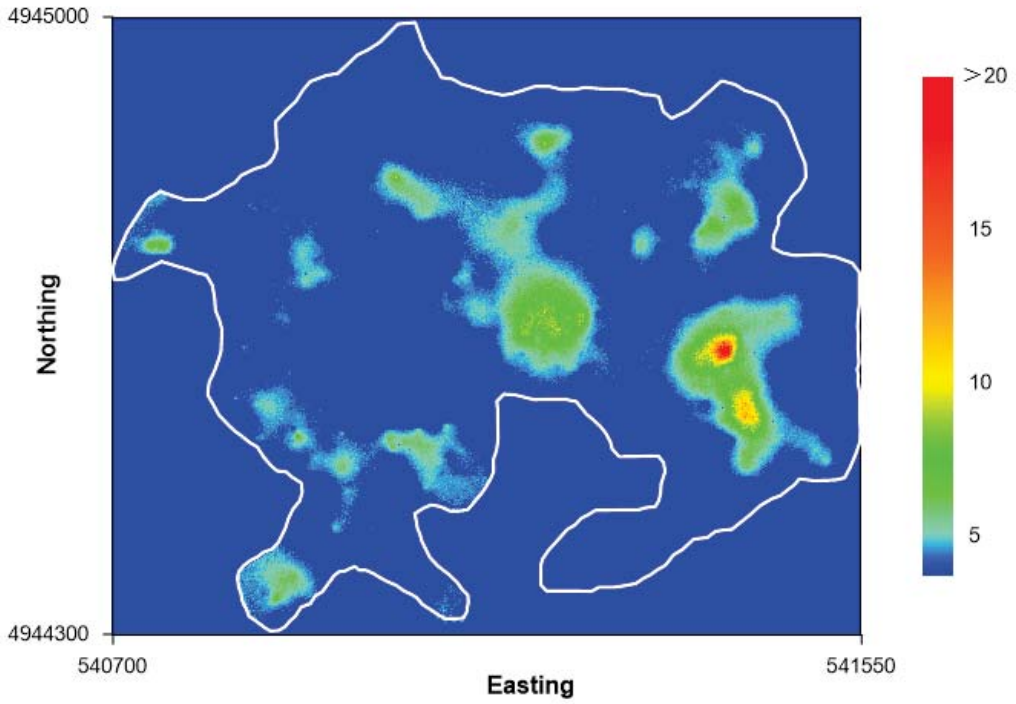

Figure 25. The map of H_2S flux was derived from the map of CO_2 flux, based on the linear regression for CO_2 and H_2S. Additionally, the threshold of the CO_2 flux of 286 g m^{-2} d^{-1} was utilized to define the minimum CO_2 flux used to estimate the H_2S flux.

5.3 Gas geochemistry

Gas samples from diffuse soil measured on Aug. 15th, 2014, were primarily composed of N_2, O_2 like atmospheric air; but the range of CO_2 from 0.42% to 1.31% was much higher than the ratio found in the atmospheric air. The carbon isotope value of CO_2 ($\delta^{13}CO_2$) ranged from -2.48‰ to -4.27‰. The value was close to that of the fumarole, except for the CH-3 sample with the value of -4.27‰. The results are shown in Table 3.

Table 3 *Diffused soil gas data for Crater Hills measured in 2014*

Sample No.	Sample Date	Longitude Degrees	Latitude Degrees	Analysis Date	He %	H_2 %	Ar %	O_2 %	CO_2 %	N_2 %	$\delta^{13}CO_2$ ‰
CH-1	2014/8/9	-110.48093	44.65255	2014/9/4	nd	nd	0.925	20.81	1.31	76.96	-2.48
CH-4	2014/8/9	-110.48319	44.65495	2014/9/4	nd	nd	0.932	20.97	0.59	77.51	-2.95
CH-6	2014/8/9	-110.48302	44.65289	2014/9/4	nd	nd	0.933	21.01	0.42	77.64	-4.27

nd: not detected

6. Discussion

6.1 CO_2 emission

In the following discussion the previously measured Crater Hills diffuse CO_2 data in 2007 is used for comparison with the current 2014 data. The sampling locations for both datasets are shown in Figure 26. The comparison between the 2007 and 2014 dataset offer insight into whether annual variance exists. The CO_2 flux of 2007 ranged from 2 to 11,501 g m^{-2} d^{-1}, with a mean of 493 g m^{-2} d^{-1}, and the total emission of 15.5 t d^{-1} in the area of 0.043 km^2. The box-whisker plots in Figure 27 (last two columns) compares the population distribution of the 2007 dataset and the 2014 data measured at the same area. Though the 2014 data had a higher mean from the box-whisker plot, the z-test for these two dataset indicates that the difference is not significant. Thus, the comparison between the two dataset from different years implies insignificant temporal variation in the diffuse degassing between 2007 and 2014.

Measurements for diffuse soil CO_2 flux have also been performed at other hydrothermal areas within or near the Yellowstone caldera: Mud Volcano (Werner et al., 2000), Hot Spring Basins (Werner et al., 2008), and Brimstone Basin (Bergfeld et al., 2012). The Mud Volcano and Hot Spring Basin areas, like Crater Hills, are located inside the caldera. In fact, the Mud Volcano area is only 5km away from Crater Hills, and both are situated at the eastern edge of the resurgent dome (Figure 2). Hot Spring Basin, Mud Volcano and Crater Hills also experienced a similar volcanic eruption history and, thereby, are located within similar lithologies. The area averaged CO_2 flux for Crater Hills was 212 g m^{-2} d^{-1}, while the area averages for Hot Spring Basin and Mud Volcano were 410 and 330 g m^{-2} d^{-1} (Werner and Brantley, 2003; Werner et al., 2000), which were 1.5-2 times larger than the areal averaged CO_2 emission at Crater Hills. Only if considering the active areas at Crater Hills, defined as flux > 30 g m^{-2} d^{-1}, the area averaged CO_2 flux would be of the same magnitude as

Mud Volcano and Hot Spring Basin, ~355 g m^{-2} d^{-1}. The difference in CO_2 emission can also be seen from the box-whisker plot (Figure 27), indicating a similar population distribution for Hot Spring Basin and Mud Volcano, but a slightly lower-valued population for Crater Hills compared to Hot Spring Basin and Mud Volcano.

The three hydrothermal regions can be further examined with respect to their location and other distinctive features. Mud Volcano and Crater Hills are both located around the Sour Creek resurgent dome, which was formed due to the intrusion of magma, which may indicate a shared branch of shallow magma intruded in the region. The Hot Spring Basin and Mud Volcano have water chemistry of high acid, high sulfate and low chloride, the typical characteristics of an acid-sulfate hydrothermal area. The pool water at Crater Hills (Sulfur Spring), on the other hand, showed high acid and sulfate, but was also high in chloride (Fournier, 1989) and had the highest calculated temperature of any reservoir in Yellowstone (270-300 °C) (Fournier, 1989) - a characteristic of neutral-chloride systems. The thermal water from Crater Hills is considered to represent the most direct upward discharge of deep parent fluid in the hydrothermal system based on its water chemistry (Fournier, 1989);

Based on the available data, the origin of the lower CO_2 emissions at Crater Hills could be related to several different processes. First, the hydrothermal reservoir right beneath Crater Hills, which is derived from a deeper parent reservoir could be smaller than those at Mud Volcano and Hot Spring Basin. Second, the hydrothermal waters beneath Crater Hills, which has the highest chloride concentration and highest temperature (270~300 °C) at Yellowstone, might have a much deeper source than the other hydrothermal systems, so that more gases and steams interact with the surrounding bedrock during ascent. Third, the mechanism of the hydrothermal system beneath Crater Hills and Mud Volcano/Hot Spring Basin might be different. Indicated by water chemistry, the Sulfur Spring at Crater Hills, originated from the liquid-dominated system and is a mixture of the steam-heated acid water and the deeply-derived neutral chloride water (Guo et al., 2014). Thus, more CO_2 and H_2S would be captured in the hydrothermal system and less released to the overlying vapor-dominated system and later released out through soil. Unlike Crater Hills, the liquid-dominated system at Mud Volcano and Hot Spring Basin which is depleted in acid released more CO_2 and H_2S into a vapor phase. Therefore, more CO_2 released from Mud Volcano and Hot Spring Basin.

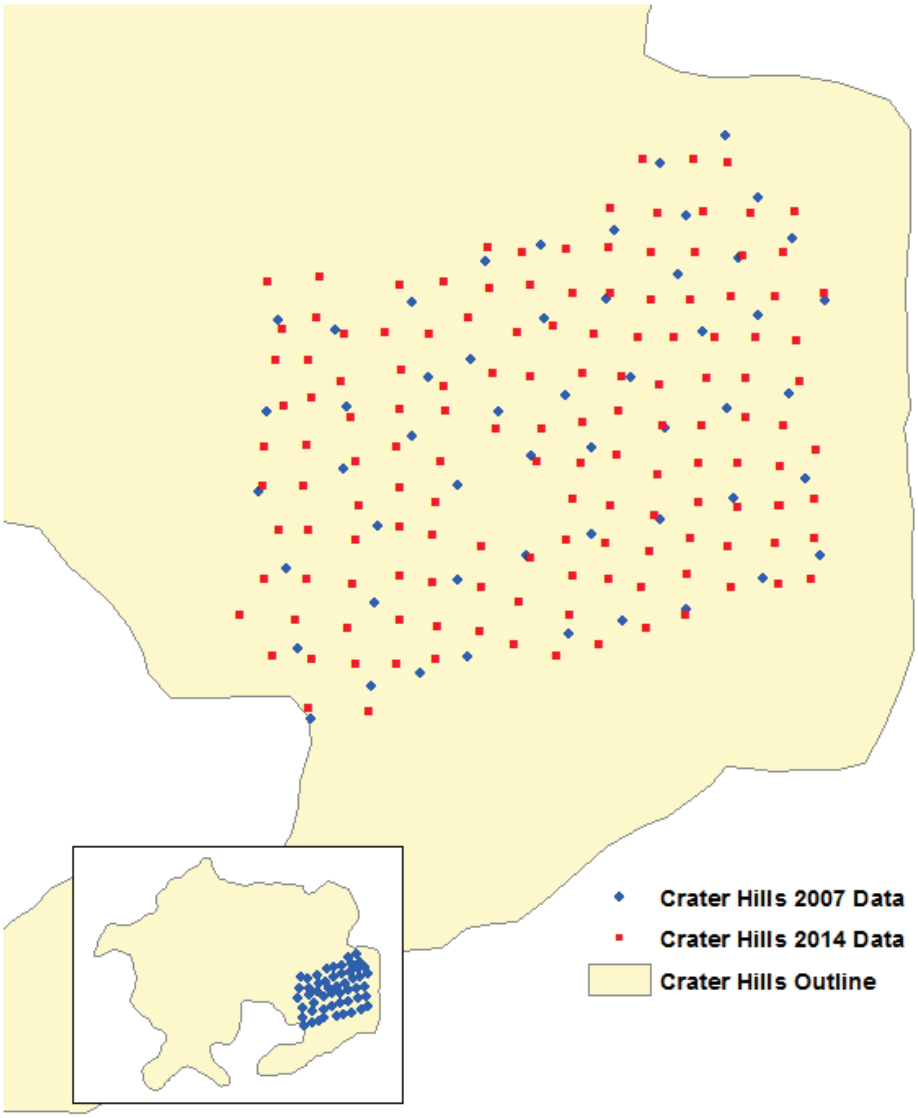

Figure 26. The small inset map shows the location of the CO_2 measured in 2007, which is located in the southeast. The blue points represent the 2007 data, with the spacing of 25-30 meters. The red points are the 2014 data collected in the same area (extracted from the complete 2014 dataset), with the spacing of ~15 meters.

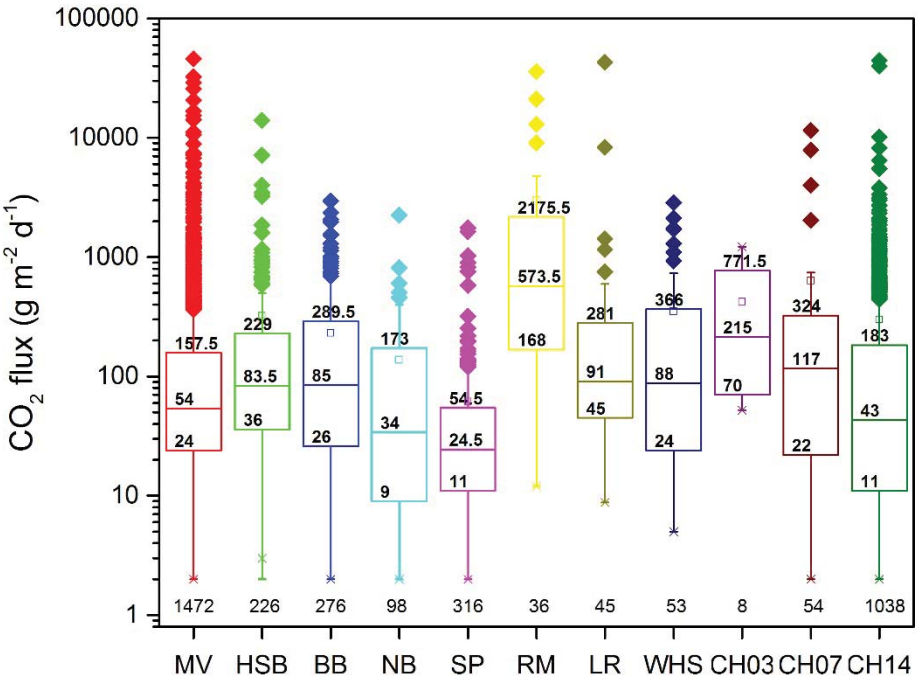

Figure 27. Box-whisker plot for the CO2 flux released from thermal areas in Yellowstone. The box represents the 25th and 75th percentile of the data, and the horizontal line inside the box represents the median value. The horizontal bar (whisker) indicates the range of the data, and the points outside the whiskers are considered outliers. The numbers on the line of range and median are the values for the range and the median. The number over the x-axis is the number of points (all points have the flux value > 2 g m-2 d-, which is the detection limit1) used for making the box-whisker plot. Data from Roaring Mountain (RM), Lamar Valley (LV), Washburn Hot Spring (WHS) and Crater Hills 2003 (CH03)are from Werner and Brantley (2003). Data from Hot Spring Basin (HSB) are from Werner et al. (2008), and the data from Brimstone Basin (BB) are from Bergfeld et al. (2012). Mud Volcano (MV) data include the data previously published in Werner and Brantley (2003) identified as GU97, GU98, GO97, GO98 and from unpublished data collected in 2008 and 2010. Data from Crater Hills2007 (CH07), Norris Geyser Basin (NB), Solfatara Plateau (SP) are unpublished data provided by Cynthia A. Werner (U.S. Geological Survey, written communication, 2015). The Crater Hills 2014 data were collected by our 2014 field campaign.

6.2 Spatial Variation of CO_2 flux

From the CO_2 flux map overlaid on the satellite image (Figure 28), it is clear from the uneven distribution of CO_2 flux that high flux was clustered to several areas, rather than randomly or

dispersedly distributed. Based on field observations and analysis of satellite imagery, most of these high flux clusters are related to topographical variability. Area 2, the largest high flux region in Crater Hills, is situated on the hill, where the elevation rises rapidly from south to north with a slope angle of approximately 30 degrees. Fumaroles were widespread on the slope, and obvious steam ascending from the soil on the slope could be seen in the morning, evidence of its significant activity. These areas are comparably dry, with few mud pots. The characteristics of the elevation rise and the widespread fumaroles on the slope were also shared by Area 3, Area 6 and the northern part of Area 1. Rather than experiencing an elevation rise, Areas 4 and 5 are located in valleys, where the elevation is about 10 meters lower than the surrounding areas. These areas were comparably wet areas with muddy floors, abundant mud pots, few fumaroles around the mud pots, and a discharging hot spring located at Area 5. Consequently, the high CO_2 flux clusters related to elevation change are categorized into two groups: one is identified by elevation rise with comparably dry thermal features; another group is related to lowered elevations with wet thermal features.

The flat areas at Crater Hills were mostly less-active, low-to-median CO_2 flux areas, except for Area 7 and the southern part of Area 1. The characteristics of the southern part of Area 1 were similar to the lower elevation regions of Areas 4 and 5 with muddy floors, abundant mud pots and a discharging pool, which indicates the similar processes control fluid discharge in these two regions. The small region of Area7 at the western edge of Crater Hills is special, as the edges near vegetation are normally low flux. A nearby small bubbling water pool at Area 7 (Figure 28 & Figure 31) indicates the existence of small fractures and might serve to explain this point-source elevated flux area.

Although no faults were indicated to transverse the Crater Hills area based on the 1977 geological map for Yellowstone (Richmond, 1977) , faults or fractures must exist to provide pathway for the upflow of the fluid and are likely covered by the thick alluvium (Christiansen, 2001). As the high flux regions are controlled by faults (Jolie et al., 2015) those at Crater Hills are also likely controlled by crustal structures. The trends in high flux clusters relative to valleys and high elevation areas (Figure 29) offers insight to the location of hidden faults or fractures. It is noteworthy that both trends of high-flux within the valleys happen to pass over other high flux areas: the hypothesized fault 1, the SE-NW trend of one valley perched high flux Area 5, also crosses high flux Area 7; the hypothesized fault 2, the SW-NE trend of another valley for high flux Area 4, traverses high flux Area 2, 3 and 6 as well. The hypothesized fault 3 would connect the most active regions at higher elevation. In addition, the hypothesized faults or fractures are consistent with trends of major fault groups at the Sour Creek resurgent dome region (Figure 30). The Crater Hill, one of the most active regions with plenty of fumaroles, happens to intersect hypothesized faults 2

and 3. Therefore, the high activity and permeability indicated by the high flux and the existence of fumaroles at Crater Hill could be explained if there is an intersection of two faults. The formation of the Crater Hill might be due to its highly fractured character, under which the upward steam and gas would concentrated to raise the elevation of this region.

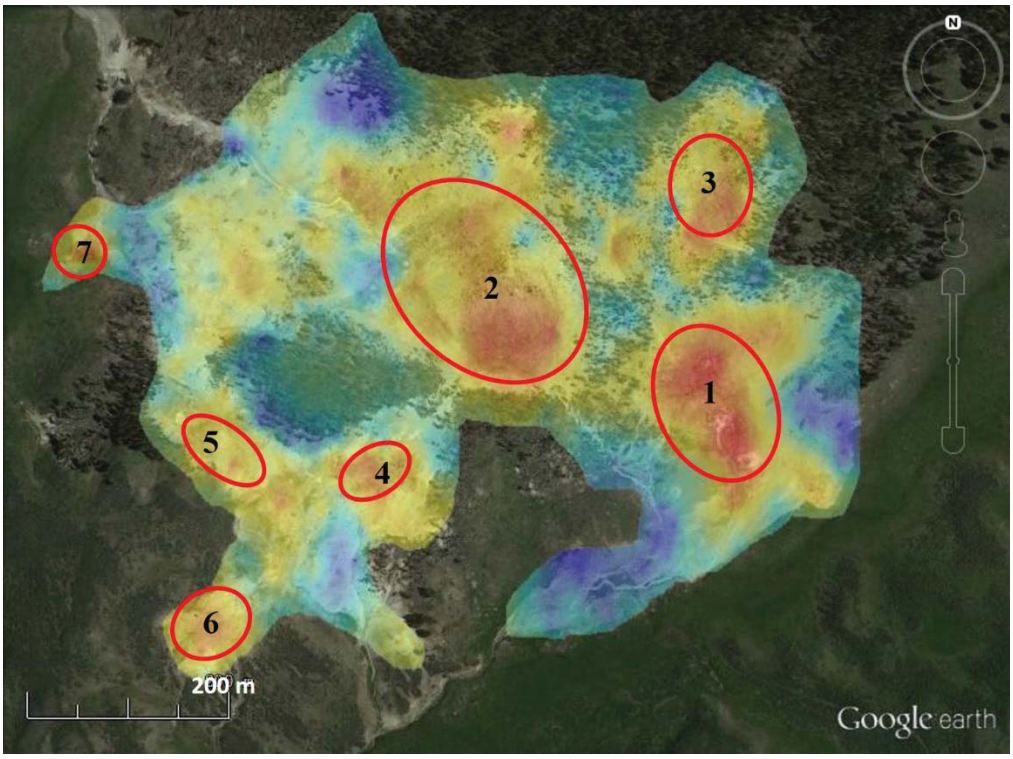

Figure 28. CO_2 flux data overlaid on the satellite image, showing the uneven distribution of CO_2 flux.. Source: Google earth V 7.1.2.2041. (June 18, 2013). Crater Hills, Yellowstone National Park. 44.653751°, -110.481026°, Eye alt 3.24 km. DigitalGlobe 2015. http://www.earth.google.com [July 23, 2015].

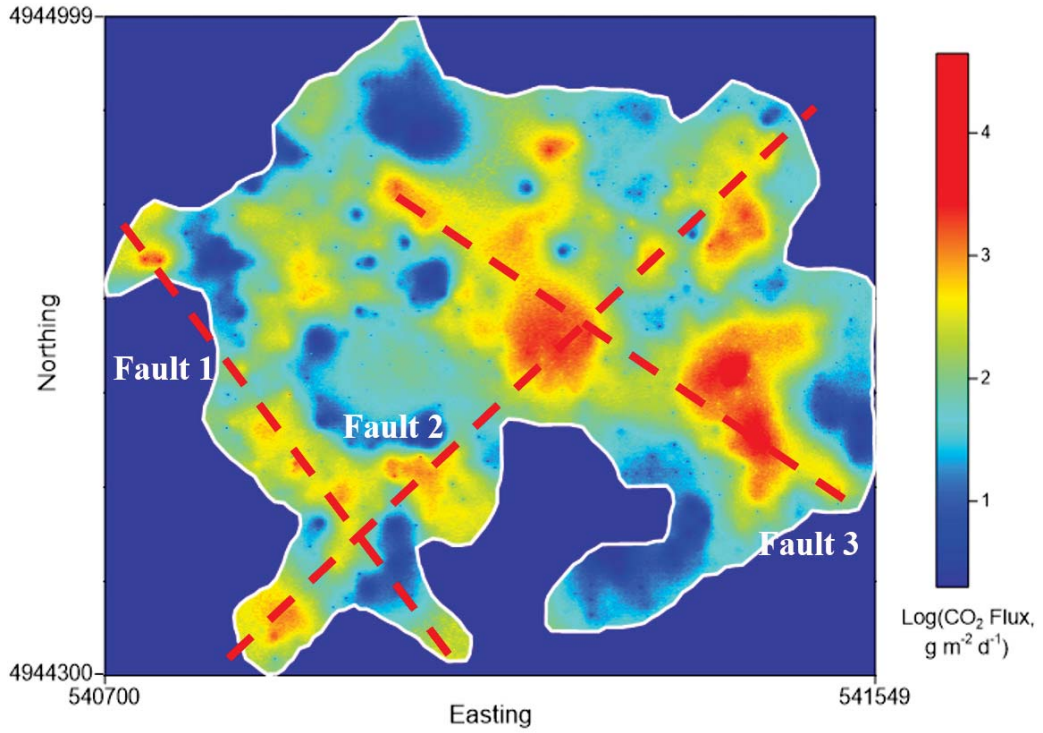

Figure 29. The hypothesized faults based on the relationship between topography and high flux regions at Crater Hills.

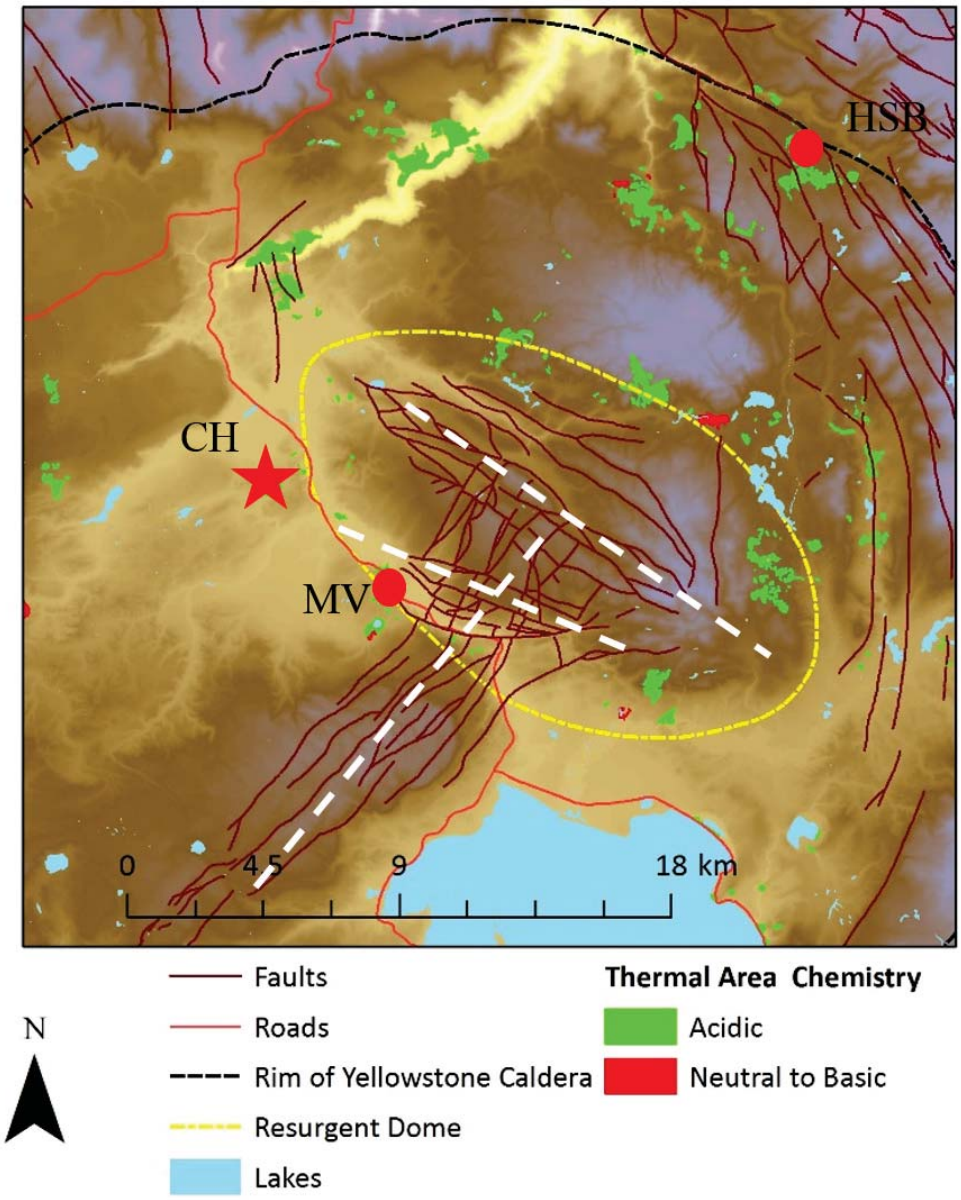

Figure 30. Map of regional faults for Sour Creek resurgent dome region. The white dashed line is the trend of major faults groups

Figure 31. The small bubbling pool at the western edge of the Crater Hills. The CO2 measured at the vicinity of this pool had a high emission rate.

6.3 CO_2 Source

Volatile gases are primarily derived from magmas generated in the mantle and emplaced within the crust; however, during the rising of fluids, the reactions with rocks (generally limestone and organic-rich sedimentary rocks) also contribute sedimentary components to the volatiles emitted at the surface. The question remains regarding the proportion of the gases derived from the magma and sedimentary rocks. Analysis of the fumarole gases and diffuse soil gases can be used to help determine the relative proportions.

The $\delta^{13}C$-CO_2 and $CO_2/^3He$ relation (equation) of each component proposed by Sano and Marty (1995) is one common method used for the estimation of the amount of each end-member – including magma, limestone and organic-rich sediment. Indicated by Bergfeld et al. (2011), the $\delta^{13}C$-CO_2 and $CO_2/^3He$ value were given (Table 4).Using the end-member values of $\delta^{13}C$-CO_2 and $CO_2/^3He$ used by Sano and Marty (1995) except the $\delta^{13}C$-CO_2 of -3.4 per mil (Lowenstern et al., 2015) for Yellowstone mantle end-member (Table 4), the proportion of mantle, limestone and sediment component are 58%, 39% and 3%, respectively.

$$(^{13}C/^{12}C)_{obs} = M \cdot (^{13}C/^{12}C)_{Magma} + L \cdot (^{13}C/^{12}C)_{Lim} + S \cdot (^{13}C/^{12}C)_{Sed} \quad (9)$$

$$1/(^{12}CO_2/\ ^3He)_{obs} = M/(^{12}CO_2/\ ^3He)_{Magma} + L/(^{12}CO_2/\ ^3He)_{Lim} + S/(^{12}CO_2/\ ^3He)_{Sed} \quad (10)$$

$$M + L + S = 1 \quad (11)$$

Werner and Brantley (2003) also applied the $\delta^{13}C$-CO_2 and $CO_2/^3He$ method to determine the source of CO_2, but they set the lowest measured $CO_2/^3He$ value from Yellowstone as the magmatic end-member as well as the $\delta^{13}C$ for limestone and sediment end-members from previous studies at Yellowstone (Des Marais and Truesdell, 1991; Friedman, 1970) (Table 4). By setting the lowest $CO_2/^3He$ value as the magmatic end-member, the maximum contribution from limestone and organic-rich sediment could be determined. Friedman (1970a) investigated travertine from hot springs and implied the range of $\delta^{13}C$ for the limestone as the potential source of CO_2; and the average of the range was used for calculation. Des Marais (1991) analyzed the $\delta^{13}C$ of hydrocarbons collected from springs and fumaroles at Yellowstone, which indicates the $\delta^{13}C$ for organic-rich sediments; the median of -26 per mil was used for calculation. Based on previous assumptions, the calculated minimum contribution from magma is 32% as well as 56% and 12% from limestone and sediment separately. However, the contribution from limestone and sediment must be overestimated by using the minimum $\delta^{13}C$ for magmatic end-member as indicated by hydrocarbons; because the amount of hydrocarbons, mainly derived from the organic-rich sediment (Des Marais et al., 1981), in the sampled fumarole at Crater Hills was quite low, among the Yellowstone sites with the lowest

hydrocarbon emission. Thus, the magmatic-sourced CO_2 must be much higher than 32%. The previous calculated magmatic end-member of 58% is much more reasonable when considering the low input from a sedimentary end-member. The improper estimation calculated from the lowest $CO_2/^3He$ of 8.2×10^8 for magmatic end-member as well indicates a much higher $CO_2/^3He$ of the magma at Yellowstone; the $CO_2/^3He$ value used by Sano and Marty (1995) of 1.5×10^9 is, therefore, more reasonable.

The estimated magmatic component for diffuse CO_2 at Mud Volcano ranged from 65% to 83% (Werner and Brantley, 2003). However, the estimation calculated using higher $CO_2/^3He$ value for magmatic end-member, resulted in a higher portion of the magmatic component. If the Sano and Marty (1995) $CO_2/^3He$ end-member values for the CO_2 source estimation are used for Mud Volcano, only 47%~53% are derived from magma, similar to, but a slightly less than, the proportion estimated for Crater Hills using the same $CO_2/^3He$ value. Using the same $CO_2/^3He$ end-member values, most of the CO_2, 90%-100%, released from diffused soil at Hot Spring Basin was magma-derived. Among these three locations, Hot Spring Basin has the highest magmatic component and lowest contribution from crust.The data of Hot Spring Basin provided in Bergfeld et al. (2011) has three fumarole data; but one of them is largely different with the other two, so that to be treated as an outlier.

Although previous calculations used fumarole gas data, the gas diffused from soil is likely to share a similar CO_2 source as that of the fumaroles. The $\delta^{13}C$ measured from diffused soil (Table 3) was consistent with the fumarole data except sample No. 3, which has a much lower $\delta^{13}C$. The differences between the abnormal sample No. 3 and the other two samples are that the sample No. 3 located on a slope, which is down along the edge of a vegetated area that is enclosed by thermally-altered regions; the schematic location of the sample No. 6 is shown Figure 32. It is likely that the contribution from organics increased ^{13}C in the gases, which lowered the $\delta^{13}C$.

Table 4 *$\delta^{13}C$ and $CO_2/^3He$ values used for CO_2 source estimation*

	Crater Hills [a]	Magma	Limestone	Sediment
Sano and Marty values				
$\delta^{13}C$ (per mil)	-2.9	-3.4 [b]	0	-30
$CO_2/^3He$	2.6×10^9	1.5×10^9	1×10^{13}	1×10^{13}
Multi-source values				
$\delta^{13}C$ (per mil)	-2.9	-3.4 [b]	-2.3 ~ 3.3 [d]	-41 ~ -20 [e]
$CO_2/^3He$	2.6×10^9	8.2×10^8 [c]	1×10^{13}	1×10^{13}

[a] This data is a fumarole gas data of Crater Hills measured in 2007, Bergfeld et al., 2011.

[b] This data is from Lowenstern et al., 2015.

[c] The lowest $CO_2/^3He$ measured from Yellowstone, Bergfeld et al., 2011.

[d] The carbon isotope of Madison limestone at Yellowstone, which was thought to be a possible source for CO_2 released from Yellowstone proposed by Friedman, 1970

[e] The carbon isotope of individual hydrocarbons in springs and fumaroles at Yellowstone indicated by Des Marais , 1991

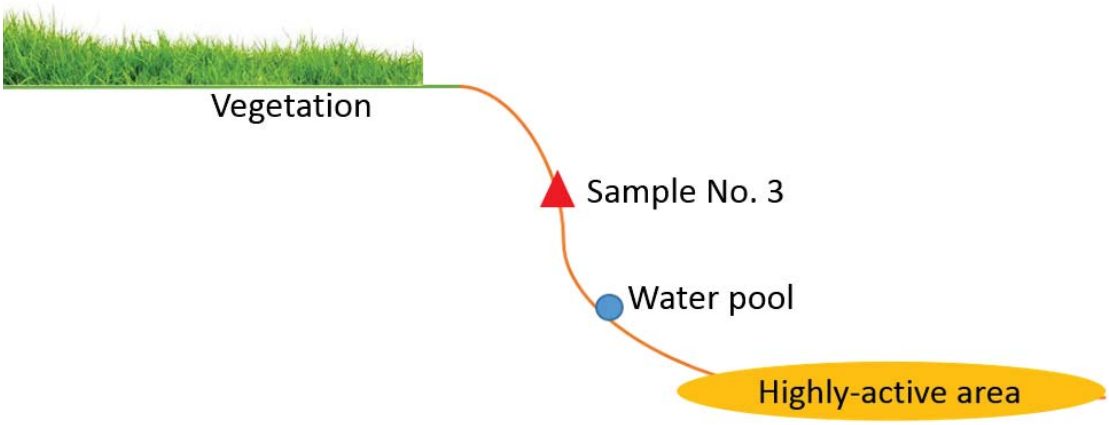

Figure 32 Schematic diagram for the location of diffused soil sample No.6

6.4 Reservoir temperature

An early estimation of the reservoir temperature at Crater Hills was made by Fournier (1989), indicating a high reservoir temperature of 270-300 ^{0}C. This estimation was based on the chloride-enthalpy relation -chloride geothermometer (Fournier et al., 1976) and silica-geothermometer (Fournier and Potter, 1982) applied to thermal waters collected at Crater Hills (unpublished USGS data). Fournier (1989) explained that the hot spring at Crater Hills comprising the highest chloride concentration and highest geothermometer temperature compared to other thermal water at Yellowstone National Park –including Gibbon, Geyser Hill, Heart Lake Basin, Hillside Springs, Lower Basin high chloride/bicarbonate water, Midway Basin, Mammoth Hot Springs, Madison Junction, Norris Basin, Shoshone Basin high-chloride water, Sylvan Springs, represented the most direct upward leakage from the deep reservoir. This leakage was produced from an adiabatic cooling and the evolved steam encountering residual liquid during ascent.

The fumarole gas geochemistry data (Bergfeld et al., 2011) were also used for estimating temperatures of the underlying reservoir. The empirical CO_2-CH_4-H_2-H_2S geothermometer proposed by D'Amore and Panichi (1980) assumed that the relative concentration of CO_2-CH_4-H_2-H_2S is controlled by reservoir temperature, according to the gas chemical analysis for 34 thermal systems; assuming that the interaction between the up-flow fluid and the surrounding environment is insignificant (Tassi et al., 2007). The reservoir temperature estimated using D'Amore's geothermometer was 213^{0}C. The temperature calculated by the H_2/Ar geothermometer of Giggenbach et al. (1994), another empirical geothermometer, was 217 ^{0}C. The temperature estimates derived from these two independent geothermometers are similar and together suggest the existence of a comparably shallow reservoir.

The difference between the reservoir temperature derived from thermal water, 270-300^{0}C, and the fumarole, 213-217^{0}C, do not conflict with each other; rather, this difference supports the bi-layered - the existence of deeper liquid-dominated system and the shallower vapor-dominated system - structure of the hydrothermal system proposed by Fournier (1989). It illustrates two different processes governing discharge at the pool and soil. The pool is charged by a deep high-temperature parent reservoir, which has experienced adiabatic cooling through rising. The adiabatic cooling of the rising fluid and the boiling of the hot water reservoir both contribute gas components to a vapor-dominated reservoir located over the hot water reservoir. The lower-temperature vapor-dominated reservoir was the origin for fumarole gases and diffused soil gases.

6.5 Heat Flux

As indicated by Chiodini (2005) and Chiodini et al. (2001), the diffuse CO_2 flux could be used to estimate the steam output, by assuming that the H_2O/CO_2 ratio measured at fumaroles represents the original fluid components of the reservoir without considering the condensation of steam while rising. The flux of steam could thus be calculated using the following equation:

$$F_{steam} = F_{CO_2} \cdot \frac{[H_2O]}{[CO_2]} \quad (12)$$

where F_{CO_2} is the mass flow of CO_2 in g d^{-1}, $\frac{[H_2O]}{[CO_2]}$ is the mass ratio measured at fumaroles, and F_{steam} is the mass flow of steam in g d^{-1}. The heat flow (H_s in watt) is thus calculated by multiplying the steam mass flow by the enthalpy of boiling water ($h_{s,boiling}$) (equation 9).

$$H_s = F_{steam} \cdot h_{s,boiling} \quad (13)$$

At Crater Hills, there exists one gas geochemistry datum for a fumarole measured in 2007 (Bergfeld et al., 2011). Previous CO_2 flux comparison showed a 20% elevation of CO_2 flux measured in 2014 compared to that of 2007, which indicates annual variation. Here we assume that this annual variation is related to the variation of some physical conditions throughout the reservoir, while the chemical composition of the fluid in the reservoir incurs few changes. Furthermore, previous condensation was experienced via steam, as the temperature measured at the fumarole was 90.9 ^{0}C (under the boiling point of 92^{0}C at the elevation of 2388 meters). The previous condensation would reduce the amount of steam and thus impact the H_2O/CO_2 ratio. Fumarole and diffuse gas data were collected at a different time than this study and previous condensation experienced by steam--were ignored for heat estimation, but inevitably would affect the accuracy of the heat estimation. The fumarole with the gas/steam ratio (Xg) of 3% and 98.4 mol% CO_2 in the gas phase derived the mass ratio of 13.44. Based on the total CO_2 emission of 84 t d^{-1} and the H_2O/CO_2 ratio,

the steam output was calculated to be 1129 t d^{-1}. As the boiling point of 92 ^{0}C corresponding to the enthalpy of 2663 J g^{-1}, the estimated total heat flow was ~35 MW for Crater Hills. If considering the size of Crater Hills, the heat flux at Crater Hills was ~100 W m^{-2}. The heat contribution from Crater Hills is also less than that from Hot Spring Basins which is estimated to be 140-370 MW. However, when considering the size of these two areas, the heat flux of Crater Hills, though slightly lower than that of Hot Spring Basin - 140 to 370 MW m^{-2}, would be much higher than the heat flux for Yellowstone as a whole - 2000 mW m^{-2} (Fournier, 1989).

6.6 Comparison between Crater Hills and Yellowstone

The proportion of CO_2 emitted from Crater Hills is about 2% of the total CO_2 emission from Yellowstone, 45±16 kt d^{-1} (Werner and Brantley, 2003).The heat flow from Crater Hills takes near 1% of the total heat flow from the Yellowstone hydrothermal system, 4.6-6 GW indicated by Friedman and Norton (2007).

The area of Crater Hills is only 0.34 km^2, about 0.004% the size of Yellowstone. However, it releases ~2% CO_2 and near 1% heat, which are much higher than area percentage of Crater Hills. The uneven distribution of heat flux at Yellowstone reinforces the heat as well as CO_2, are focused in localized areas that are likely structure controlled.

6.7 Sulfur budget

Sulfur is a significant, but unstable element in magma-related hydrothermal systems, which originally arrive in the form of H_2S and are oxidized to native sulfur or SO_4^- during ascent. The question is how much sulfur is released through diffuse soil in the form of H_2S and how much is converted to another form. The CO_2/H_2S mass ratio measured from the fumarole in 2007 is 100, which is assumed to represent the reservoir's original component without oxidization. In the 2014 campaign, the CO_2/H_2S mass ratio for three diffuse degassing samples around the fumarole ranged from 350 to 730 with an average of 500, which means 72% - 87% (0.28 – 0.34 t d^{-1}) of H_2S in the diffuse emission was lost, most likely oxidized into a native sulfur deposit and SO_4^-. In field observations, the native sulfur deposit was widespread at Crater Hills, especially around active areas; the yellow sulfur mud pot could also be seen inside the active areas.

7. Conclusion

The mean CO_2 flux for the diffused soil Crater Hills was 212 g m^{-2} d^{-1} and its total CO_2 emission was estimated to be 84 t d^{-1}. The total emission of H_2S was estimated to be 0.39 t d^{-1}. The CO_2 emission at the surface is a mixture of a magmatic and crustal component. The proportion of CO_2 from magma and crust were determined by using the $CO_2/^3He$ value for the magmatic end-member. No significant annual variation was observed in a comparison between data collected in 2007 and 2014. Crater Hills had less CO_2 emission – both in total emission and area averaged flux - compared to Mud Volcano and Hot Spring Basin in Yellowstone. There are several possible explanations for this based on the available information: 1) The lower emission at Crater Hills might be due to a smaller hydrothermal reservoir for Crater Hills, 2) A deeper source hydrothermal system feeding the Crater Hills, or 3) More gases were trapped into the hydrothermal system beneath Crater Hills. The difference between the reservoir temperatures calculated using water from Sulfur Spring and those gases collected from fumaroles suggest a two-layer hydrothermal system – the liquid-dominated system underlying the vapor-dominated system as proposed by Fournier (1989). Hidden faults or fracture is likely to exist at Crater Hills and to be covered by overlying alluvium based on the consistence between trend of regional fracture and the connected indicated by high flux areas. The high heat flux at the relatively small area encompassed by Crater Hills, ~100 W m^{-2}, compared to that for Yellowstone as a whole, 2000 mW m^{-2}, indicates a focused release of mass and heat.

8. Acknowledgements

Without invaluable counselling I received from my supervisors, I would be unable to finish this work. Firstly, I would like to thank my advisor Chad Deering for offering this precious research opportunity at Yellowstone National Park to quantify the gas emission there, as well as his patience, kindness and wise advice both in field, in the later data analysis and in my thesis writing. I would also like to thank Chad's wife, Heather Deering for her help in polishing the language of my thesis. I am also thankful for the helpful advices and data provided by Cynthia Werner, and for her patience to respond my questions as possible as she can during her busy works. My field work partner, Christie Torres, offered helps to collect gas flux and to measure other supplementary data at fields. I would also like to thank my committee member Simon Carn for giving advices for my thesis writing.

I am really thankful for the support and encouragements I gained at GMES department. The people here are so united and always supportive of other people. I would also like to thank my family members and friends for their love, support and kindness. I am grateful for my mom and

dad’s support for my decisions to do volcanology in U.S.

9. References

Allen, E.T., Day, A.L., 1935. Hot springs of the Yellowstone National Park. Carnegie Inst. Washingt. Publ. 466, 525.

Bergfeld, D., Evans, W.C., Lowenstern, J.B., Hurwitz, S., 2012. Carbon dioxide and hydrogen sulfide degassing and cryptic thermal input to Brimstone Basin, Yellowstone National Park, Wyoming. Chem. Geol. 330-331, 233–243. doi:10.1016/j.chemgeo.2012.09.001

Bergfeld, J.B., Hunt, A.G., Shanks, Wcp., Evans, W., 2011. Gas and isotope chemistry of thermal features in Yellowstone National Park, Wyoming.

Chiodini, G., 2005. Carbon dioxide diffuse degassing and estimation of heat release from volcanic and hydrothermal systems. J. Geophys. Res. 110, 204. doi:10.1029/2004JB003542

Chiodini, G., Cioni, R., Guidi, M., Raco, B., Marini, L., 1998. Soil CO2 flux measurements in volcanic and geothermal areas. Appl. Geochemistry 13, 543–552. doi:10.1016/S0883-2927(97)00076-0

Chiodini, G., Frondini, F., Cardellini, C., Granieri, D., Marini, L., Ventura, G., 2001. CO 2 degassing and energy release at Solfatara volcano, Campi Flegrei, Italy. J. Geophys. Res. 106, 16213. doi:10.1029/2001JB000246

Christiansen, R.L., 2001. The quaternary and pliocene Yellowstone Plateau volcanic field of Wyoming, Idaho, and Montana. U.S. Geological Survey Reston, VA, USA.

Christiansen, R.L., Lowenstern, J.B., Smith, R.B., Heasler, H., Morgan, L.A., Nathenson, M., Mastin, L.G., Muffler, Ljp., Robinson, J.E., 2007. Preliminary assessment of volcanic and hydrothermal hazards in Yellowstone National Park and vicinity. US Geological Survey.

Chu, R., Helmberger, D. V, Sun, D., Jackson, J.M., Zhu, L., 2010. Mushy magma beneath Yellowstone. Geophys. Res. Lett. 37.

D’Amore, F., Panichi, C., 1980. Evaluation of deep temperatures of hydrothermal systems by a new gas geothermometer. Geochim. Cosmochim. Acta 44, 549–556. doi:10.1016/0016-7037(80)90051-4

David, M., 1977. Geostatistical ore reserve estimation (Developments in geomathematics 2). Elsevie, New York.

Des Marais, D.J., Donchin, J.H., Nehring, N.L., Truesdell, A.H., 1981. Molecular carbon isotopic evidence for the origin of geothermal hydrocarbons.

Des Marais, D.J., Truesdell, A.H., 1991. Carbon isotope geochemistry of individual hydrocarbons in springs and fumaroles of Yellowstone National Park, Wyoming. Abstr. with Programs – Geol. Soc. Am. 23, 19.

Deutch, C. V, Journel, A.G., 1992. GSLIB: geostatistical software library and user’s guide.

Farrell, J., Smith, R.B.R., Husen, S., Diehl, T., 2014. Tomography from 26 years of seismicity revealing that the spatial extent of the Yellowstone crustal magma reservoir extends well beyond the Yellowstone caldera. Geophys. Res. Lett. 41, 3068–3073. doi:10.1002/2014GL059588

Fournier, R.O., 1989. Geochemistry and dynamics of the Yellowstone National Park hydrothermal system. Annu. Rev. Earth Planet. Sci. 13–53.

Fournier, R.O., Potter, R.W., 1982. An equation correlating the solubility of quartz in water from 25 to 900 C at pressures up to 10,000 bars. Geochim. Cosmochim. Acta 46, 1969–1973.

Fournier, R.O., White, D.E., Truesdell, A.H., 1976. Convective heat flow in Yellowstone National Park, in: Proceedings of the 2nd UN Symposium on the Development and Use of Geothermal Resources, San Francisco. pp. 731–739.

Friedman, I., 1970. Some investigations of the deposition of travertine from Hot Springs—I. The isotopic chemistry of a travertine-depositing spring. Geochim. Cosmochim. Acta 34, 1303–1315. doi:10.1016/0016-7037(70)90043-8

Friedman, I., Norton, D.R., 2007. Is Yellowstone Losing Its Steam?—Chloride Flux out of Yellowstone National Park.

Gansecki, C.A., Mahood, G.A., McWilliams, M.O., 1996. 40Ar39Ar geochronology of rhyolites erupted following collapse of the Yellowstone caldera, Yellowstone Plateau volcanic field: implications for crustal contamination. Earth Planet. Sci. Lett. 142, 91–107.

Geostatistics, I.A. for M.G.C. on, 1991. Geostatistical Glossary and Multilingual Dictionary. Oxford University Press.

Giggenbach, W., Sheppard, D., Robinson, B., Stewart, M., Lyon, G., 1994. Geochemical structure and position of the Waiotapu geothermal field, New Zealand. Geothermics 23, 599–644. doi:10.1016/0375-6505(94)90022-1

Giggenbach, W.F., 1988. Geothermal solute equilibria. Derivation of Na-K-Mg-Ca geoindicators. Geochim. Cosmochim. Acta 52, 2749–2765. doi:10.1016/0016-7037(88)90143-3

Goovaerts, P., 2001. Geostatistical modelling of uncertainty in soil science. Geoderma 103, 3–26. doi:http://dx.doi.org/10.1016/S0016-7061(01)00067-2

Guo, Q., Nordstrom, D.K., McCleskey, R.B., 2014. Towards understanding the puzzling lack of acid geothermal springs in Tibet (China): Insight from a comparison with Yellowstone (USA) and some active volcanic hydrothermal systems. J. Volcanol. Geotherm. Res. 288, 94–104.

Hurwitz, S., Hunt, A.G., Evans, W.C., 2012. Temporal variations of geyser water chemistry in the Upper Geyser Basin, Yellowstone National Park, USA. Geochemistry, Geophys. Geosystems 13.

Husen, S., Smith, R.B., Waite, G.P., 2004. Evidence for gas and magmatic sources beneath the Yellowstone volcanic field from seismic tomographic imaging. J. Volcanol. Geotherm. Res. 131, 397–410.

Jaworowski, C., Heasler, H.P., Neale, C.M.U., Sivarajan, S., 2010. Using thermal infrared imagery and LiDAR in Yellowstone geyser basins. Yellowstone Sci. 18, 8–19.

Jolie, E., Klinkmueller, M., Moeck, I., 2015. Diffuse surface emanations as indicator of structural permeability in fault-controlled geothermal systems. J. Volcanol. Geotherm. Res. 290, 97–113. doi:10.1016/j.jvolgeores.2014.11.003

Kharaka, Y.K., Sorey, M.L., Thordsen, J.J., 2000. Large-scale hydrothermal fluid discharges in the Norris–Mammoth corridor, Yellowstone National Park, USA. J. Geochemical Explor. 69-70, 201–205. doi:10.1016/S0375-6742(00)00025-X

Lanphere, M.A., Champion, D.E., Christiansen, R.L., Izett, G.A., Obradovich, J.D., 2002. Revised ages for tuffs of the Yellowstone Plateau volcanic field: Assignment of the Huckleberry Ridge Tuff to a new geomagnetic polarity event. Geol. Soc. Am. Bull. 114, 559–568.

Lowenstern, J.B., Bergfeld, D., Evans, W.C., Hunt, A.G., 2015. Origins of geothermal gases at Yellowstone. J. Volcanol. Geotherm. Res. 302, 87–101. doi:10.1016/j.jvolgeores.2015.06.010

Lowenstern, J.B., Hurwitz, S., 2008. Monitoring a supervolcano in repose: Heat and volatile flux at the yellostone caldera. Elements 4, 35–40. doi:10.2113/GSELEMENTS.4.1.35

Miller, D.S., Smith, R.B., 1999. P and S velocity structure of the Yellowstone volcanic field from local earthquake and controlled-source tomography. J. Geophys. Res. Solid Earth 104, 15105–15121.

Morgan, L.A., Shanks, W.C., 2005. Influences of rhyolitic lava flows on hydrothermal processes in Yellowstone Lake and on the Yellowstone Plateau, in: Geothermal Biology and Geochemistry in Yellowstone National Park. Proceeding of the Thermal Biology Institute Workshop. pp. 31–52.

Morgan, L.A., Shanks, W.C.P., Pierce, K.L., 2009. Hydrothermal processes above the Yellowstone magma chamber: Large hydrothermal systems and large hydrothermal explosions. Geol. Soc. Am. Spec. Pap. 459, 1–95.

Pierce, K.L., Morgan, L. a., 2009. Is the track of the Yellowstone hotspot driven by a deep mantle plume? - Review of volcanism, faulting, and uplift in light of new data. J. Volcanol. Geotherm. Res. 188, 1–25. doi:10.1016/j.jvolgeores.2009.07.009

Pierce, K.L., Morgan, L.A., 1992. The track of the Yellowstone hot spot: Volcanism, faulting, and uplift. Geol. Soc. Am. Mem. 179, 1–54.

Porritt, R.W., Allen, R.M., Pollitz, F.F., 2014. Seismic imaging east of the Rocky Mountains with USArray. Earth Planet. Sci. Lett. 402, 16–25.

Pyrcz, M.J., Deutsch, C. V., 2014. Geostatistical Reservoir Modeling. Oxford University Press.

Richmond, G.M., 1977. Surficial geologic map of the Canyon Village Quadrangle, Yellowstone National Park, Wyoming. I-0652. US Geol. Surv. Rest.

Rodman, A., Shovic, H., Thomas, D., 1996. Soils of Yellowstone National Park: Yellowstone Center for Resources, Yellowstone National Park, Wyoming. YCR-NRSR-96-2.

Sano, Y., Marty, B., 1995. Origin of carbon in fumarolic gas from island arcs. Chem. Geol. doi:10.1016/0009-2541(94)00097-R

Schmandt, B., Humphreys, E., 2010. Complex subduction and small-scale convection revealed by body-wave tomography of the western United States upper mantle. Earth Planet. Sci. Lett. 297, 435–445. doi:10.1016/j.epsl.2010.06.047

Sinclair, A.J., 1974. Selection of threshold values in geochemical data using probability graphs. J. Geochemical Explor. 3, 129–149. doi:http://dx.doi.org/10.1016/0375-6742(74)90030-2

Smith, R.B., Jordan, M., Steinberger, B., Puskas, C.M., Farrell, J., Waite, G.P., Husen, S., Chang, W.-L., O'Connell, R., 2009. Geodynamics of the Yellowstone hotspot and mantle plume: Seismic and GPS imaging, kinematics, and mantle flow. J. Volcanol. Geotherm. Res. 188, 26–56.

Sorey, M.L., Colvard, E.M., 1997. Hydrologic investigations in the Mammoth Corridor, Yellowstone National Park and vicinity, U.S.A. Geothermics 26, 221–249. doi:10.1016/S0375-6505(96)00041-7

Tassi, F., Vaselli, O., Capaccioni, B., Montegrossi, G., Barahona, F., Caprai, A., 2007. Scrubbing process and chemical equilibria controlling the composition of light hydrocarbons in natural

gas discharges: An example from the geothermal fields of El Salvador. Geochemistry, Geophys. Geosystems 8. doi:10.1029/2006GC001487

Truesdell, A.H., Fournier, R.O., 1976. Conditions in the deeper parts of the hot spring systems of Yellowstone National Park, Wyoming. US Geological Survey,.

Truesdell, A.H., Nathenson, M., Rye, R.O., 1977. The effects of subsurface boiling and dilution on the isotopic compositions of Yellowstone thermal waters. J. Geophys. Res. 82, 3694–3704. doi:10.1029/JB082i026p03694

Werner, C., Brantley, S., 2003. CO2 emissions from the Yellowstone volcanic system. Geochemistry, Geophys. Geosystems 4, n/a–n/a. doi:10.1029/2002GC000473

Werner, C., Brantley, S.L., Boomer, K., 2000. CO2 emissions related to the Yellowstone volcanic system: 2. Statistical sampling, total degassing, and transport mechanisms. J. Geophys. Res. Solid Earth 105, 10831–10846.

Werner, C., Hurwitz, S., Evans, W.C., Lowenstern, J.B., Bergfeld, D., Heasler, H., Jaworowski, C., Hunt, A., 2008. Volatile emissions and gas geochemistry of Hot Spring Basin, Yellowstone National Park, USA. J. Volcanol. Geotherm. Res. 178, 751–762. doi:10.1016/j.jvolgeores.2008.09.016

White, D.E., Muffler, L.J.P., Truesdell, A.H., 1971. Vapor-dominated hydrothermal systems compared with hot-water systems. Econ. Geol. 66, 75–97. doi:10.2113/gsecongeo.66.1.75

Appendix I: Sample Data

Table notes:

n.a.: no data measured

BD: have bad shape for the concentration-time relation, indicating the flux of 0.

UD: have a good shape for the concentration-time relation but the value is under detection limit

The absent air temperature calculated based on the existing temperature values for the determination of A.C.K is assumed to follow the arithmetic sequence.

Table 5 Summary of gas data collected from diffused soil in 2014

Date: 2014/7/23
Weather: little rainfall, only several drops around 8:00am, then sunny
Pressure: 1024.40 hPa
Data Collector: Peipei Lin

POINT	LONGITUDE	LATITUDE	UTM ZONE	UTM LONGITUDE	UTM LATITUDE	AIR TEMP.	AIR RH	WIND SPEED	SOIL TEMP	ACK	H_2S			H_2S R^2	CO_2			CO_2 R^2
						(°C)	(%)	(km/h)	(°C)		(ppm s^{-1})	(mol m^{-2} d^{-1})	(g m^{-2} d^{-1})		(ppm s^{-1})	(mol m^{-2} d^{-1})	(g m^{-2} d^{-1})	
1	-110.4845230	44.6511554	12	540874.88	4944347.00	22.9	34.2	10.3	21.8	0.7083	UD				3.04	2.15	94.71	0.999
2	-110.4843630	44.6512600	12	540885.88	4944340.50	27.0	28.0	2.0	55.4	0.6987	1.12	0.79	26.70	0.987	279.20	195.06	8582.78	0.960
3	-110.4842750	44.6513700	12	540892.75	4944352.50	23.4	24.7	2.1	38.2	0.7071	UD				24.58	17.38	764.78	0.999
4	-110.4841496	44.6514983	12	540902.62	4944366.87	25.3	24.1	2.2	83.2	0.7026	UD				55.82	39.22	1725.75	n.a.
5	-110.4840448	44.6515891	12	540910.34	4944379.47	25.8	23.7	2.6	33.7	0.7015	UD				9.34	6.55	288.33	0.999
6	-110.4839170	44.6517180	12	540920.88	4944391.50	26.0	21.0	2.3	n.a.	0.7010	UD				1.87	1.31	57.77	0.997
7	-110.4837630	44.6518220	12	540933.06	4944403.00	28.1	25.0	2.0	24.2	0.6961	UD				0.38	0.26	11.51	0.965

8	-110.4836610	44.6519410	12	540941.06	4944416.50				17.9	0.6961	UD				0.59	0.41	18.17	0.992
9	-110.4835240	44.6519778	12	540951.88	4944420.45	28.7	32.7	1.9	20.6	0.6947	UD				75.81	52.66	2317.23	n.a.
10	-110.4831850	44.6519200	12	540978.81	4944414.00	26.7	20.5	1.9	26.8	0.6993	UD				2.55	1.78	78.47	0.397
11	-110.4830430	44.6520860	12	540989.94	4944432.50	25.8	19.0	2.0	20.9	0.7015	UD				1.05	0.73	32.28	0.994
12	-110.4828830	44.6521320	12	541002.63	4944438.00	26.6	27.5	2.1	16.0	0.6996	UD				0.24	0.17	7.48	0.875
13	-110.4827860	44.6522020	12	541010.25	4944445.50				13.6	0.6996	UD				0.23	0.16	7.12	0.885
14	-110.4826680	44.6523180	12	541019.50	4944458.50	27.2	23.1	2.1	16.6	0.6982	UD				UD			
15	-110.4827790	44.6523800	12	541010.69	4944465.50				16.9	0.6982	UD				0.18	0.13	5.52	0.959
16	-110.4828750	44.6524930	12	541003.00	4944478.00				39.4	0.6982	UD				24.48	17.09	752.03	0.965
17	-110.4825940	44.6525050	12	541025.25	4944479.50	27.3	20.7	2.2	16.0	0.6980	UD				0.46	0.32	14.18	0.026
18	-110.4824320	44.6526340	12	541038.00	4944494.00	27.0	22.0	2.3	23.2	0.6987	UD				10.82	7.56	332.61	0.993
19	-110.4826170	44.6526600	12	541023.31	4944496.50				31.7	0.6993	UD				0.18	0.12	5.41	0.920
20	-110.4827650	44.6527110	12	541011.56	4944502.50				30.0	0.6998	0.08	0.05	1.78	0.986	0.48	0.33	14.71	0.956
21	-110.4826680	44.6527840	12	541019.19	4944510.50				43.8	0.7005	UD				135.10	94.64	4164.16	0.988
22	-110.4824320	44.6527740	12	541037.94	4944509.50				30.3	0.7012	UD				13.76	9.65	424.55	0.999
23	-110.4820470	44.6527520	12	541068.44	4944507.00	24.7	25.7	2.4	58.8	0.7040	UD				12.31	8.67	381.34	0.998
24	-110.4820880	44.6528100	12	541065.19	4944513.50				35.6	0.7033	0.46	0.32	11.00	0.998	36.46	25.64	1128.32	0.998
25	-110.4820670	44.6529450	12	541066.75	4944528.50				61.5	0.7026	UD				3.65	2.56	112.84	0.999
26	-110.4819050	44.6530120	12	541079.50	4944536.00				47.1	0.7022	UD				91.05	63.93	2812.99	0.999
27	-110.4818590	44.6530960	12	541083.13	4944545.50				60.6	0.7040	UD				3.14	2.21	97.24	0.998
28	-110.4816100	44.6530610	12	541102.88	4944541.50	26.1	20.8	2.7	18.3	0.7008	UD				3.07	2.15	94.63	0.990
29	-110.4814960	44.6531600	12	541111.88	4944553.00	27.5	20.1	2.3	15.0	0.6975	UD				0.18	0.13	5.57	0.972
30	-110.4814320	44.6532840	12	541116.81	4944566.50	26.2	17.6	2.2	14.9	0.7005	UD				0.52	0.36	16.00	0.989
31	-110.4812390	44.6533870	12	541132.06	4944578.00				15.0	0.7005	UD				1.87	1.31	57.64	0.998
32	-110.4812060	44.6535250	12	541134.56	4944593.50				14.9	0.7008	UD				2.09	1.46	64.35	0.983
33	-110.4812740	44.6528710	12	541129.69	4944521.00				19.2	0.7008	UD				0.29	0.20	8.99	0.112

34	-110.4814660	44.6527670	12	541114.50	4944509.00				17.0	0.7010	UD				8.07	5.66	249.03	0.973
35	-110.4816090	44.6526750	12	541103.25	4944499.00				22.1	0.7010	UD				7.72	5.41	238.14	0.998
36	-110.4817140	44.6525660	12	541095.00	4944486.50				21.5	0.7011	UD				0.95	0.67	29.38	0.989
37	-110.4819165	44.6525601	12	541074.31	4944483.00				29.3	0.7012	UD				4.19	2.94	129.36	0.999
38	-110.4820484	44.6524722	12	541070.06	4944479.00	26.0	12.9	2.2	39.2	0.7010	UD				9.65	6.76	297.61	0.985
39	-110.4822360	44.6523880	12	541053.75	4944466.50				53.3	0.7004	UD				37.70	26.41	1161.85	0.994
40	-110.4823660	44.6523190	12	541043.44	4944459.00				15.3	0.6998	UD				0.12	0.08	3.66	0.628
41	-110.4825370	44.6521840	12	541030.00	4944444.00				14.4	0.6993	UD				0.12	0.08	3.70	0.103
42	-110.4827380	44.6520180	12	541014.19	4944425.50				16.1	0.6987	UD				0.29	0.20	8.83	0.937
43	-110.4828240	44.6519330	12	541007.44	4944416.00				16.0	0.6981	UD				0.25	0.18	7.75	0.759
44	-110.4829320	44.6518220	12	540998.94	4944403.50				19.0	0.6976	UD				0.14	0.10	4.26	0.914
45	-110.4830600	44.6517270	12	540988.88	4944393.00				19.5	0.6970	UD				UD			
46	-110.4829066	44.6516363	12	540999.00	4944383.00				n.a.	0.6964	UD				0.24	0.17	7.26	0.929
47	-110.4835780	44.6521080	12	540947.50	4944435.00	28.2	21.3	6.7	29.9	0.6959	UD				2.35	1.64	71.95	0.998
48	-110.4834150	44.6523010	12	540960.31	4944456.50				35.7	0.6966	0.15	0.10	3.49	0.988	9.36	6.52	286.76	0.999
49	-110.4833240	44.6523550	12	540967.50	4944462.50				38.7	0.6973	UD				22.01	15.35	675.31	0.830
50	-110.4830960	44.6524980	12	540985.44	4944478.50				41.7	0.6980	UD				1.18	0.83	36.30	0.945
51	-110.4827820	44.6527220	12	541010.19	4944503.50				30.2	0.6988	UD				2.86	2.00	87.87	0.997
52	-110.4826000	44.6528290	12	541024.56	4944515.50				39.2	0.6995	UD				4.52	3.16	138.96	0.998
53	-110.4825220	44.6528580	12	541030.69	4944518.50				35.1	0.7002	0.09	0.06	2.07	0.997	39.71	27.81	1223.46	0.915
54	-110.4823040	44.6529760	12	541047.94	4944532.00				26.5	0.7010	UD				178.60	125.19	5508.40	0.993
55	-110.4822050	44.6531060	12	541055.69	4944546.50				17.7	0.7017	UD				UD			
56	-110.4820870	44.6531700	12	541065.00	4944553.50				15.6	0.7024	UD				UD			
57	-110.4819090	44.6533330	12	541079.00	4944572.00	25.7	18.3	2.2	n.a.	0.7017	UD				1.69	1.18	52.09	0.998

Date: 2014/7/23

Weather: little rainfall, only several drops around 8:00am, then sunny

Pressure: 1024.40 hPa

Data Collector: Christie E. Torres

POINT	LONGITUDE	LATITUDE	UTM ZONE	UTM LONGITUDE	UTM LATITUDE	AIR TEMP.	AIR RH	WIND SPEED	SOIL TEMP	ACK	H_2S	H_2S R^2	CO_2			CO_2 R^2
						(°C)	(%)	(km/h)	(°C)		(ppm s^{-1})	(mol m^{-2} d^{-1})	(g m^{-2} d^{-1})	(ppm s^{-1})	(mol m^{-2} d^{-1})	(g m^{-2} d^{-1})	
1	-110.4843709	44.6510603	12	540886.60	4944318.00	22.9	34.2	10.3	18.0	0.7083	n.a.		0.61	0.430	19.05	0.99
2	-110.4843709	44.6510603	12	540891.40	4944334.00	27.0	28.0	2.0	22.2	0.6987	n.a.		5.32	3.720	163.48	1.00
3	-110.4843709	44.6510603	12	540910.90	4944336.00	23.4	24.7	2.1	18.9	0.7071	n.a.		1.07	0.750	33.14	1.00
4	-110.4843709	44.6510603	12	540920.10	4944353.50	25.3	24.1	2.2	59.2	0.7026	n.a.		23.36	16.410	722.19	1.00
5	-110.4843709	44.6510603	12	540937.00	4944362.00	25.8	23.7	2.6	19.4	0.7015	n.a.		3.90	2.740	120.46	1.00
6	-110.4843709	44.6510603	12	540951.30	4944371.50	26.0	21.0	2.3	19.8	0.7010	n.a.		0.30	0.210	9.27	0.99
7	-110.4843709	44.6510603	12	540966.20	4944382.00	28.1	25.0	2.0	17.2	0.6961	n.a.		0.26	0.180	8.06	0.99
9	-110.4843709	44.6510603	12	540972.00	4944395.00				19.2	0.6954	n.a.		3.41	2.370	104.31	0.99
10	-110.4843709	44.6510603	12	540979.60	4944408.00	28.7	32.7	1.9	18.1	0.6947	n.a.		0.12	0.090	3.77	0.89
11	-110.4843709	44.6510603	12	540995.60	4944419.50	26.7	20.5	1.9	16.2	0.6993	n.a.		12.43	8.690	382.49	1.00
12	-110.4843709	44.6510603	12	541015.10	4944427.50	25.8	19.0	2.0	13.6	0.7015	n.a.		0.18	0.130	5.55	0.95
13	-110.4843709	44.6510603	12	541023.20	4944445.00	26.6	27.5	2.1	13.6	0.6996	n.a.		0.14	0.100	4.27	0.92
14	-110.4843709	44.6510603	12	541031.40	4944467.00	27.2	23.1	2.1	14.9	0.6982	n.a.		0.20	0.140	6.09	0.96
15	-110.4843709	44.6510603	12	541041.10	4944480.00	27.3	20.7	2.2	20.8	0.6980	n.a.		4.09	2.850	125.60	1.00
16	-110.4843709	44.6510603	12	541058.50	4944486.50	27.2	23.0	2.3	25.3	0.6982	n.a.		19.09	13.330	586.45	0.98
17	-110.4843709	44.6510603	12	541072.60	4944498.00	25.9	22.0	2.3	40.6	0.7012	n.a.		24.92	17.470	768.87	1.00
18	-110.4843709	44.6510603	12	541083.30	4944502.50	24.7	25.7	2.4	24.3	0.7040	n.a.		0.45	0.320	13.98	0.01
19	-110.4843709	44.6510603	12	541094.80	4944508.50	25.1	26.4	2.5	47.6	0.7031	n.a.		28.92	20.330	894.68	0.99
20	-110.4843709	44.6510603	12	541102.20	4944526.00	26.8	21.4	2.6	27.8	0.6991	n.a.		0.73	0.510	22.38	0.03

21	-110.4843709	44.6510603	12	541118.90	4944528.00	26.1	20.8	2.7	15.0	0.7008	n.a.		0.22	0.150	6.72	0.93
22	-110.4843709	44.6510603	12	541121.70	4944527.00	27.4	20.1	2.3	15.2	0.6977	n.a.		0.21	0.150	6.42	0.93
23	-110.4843709	44.6510603	12	541138.80	4944538.50	27.5	17.6	2.2	17.2	0.6975	n.a.		0.15	0.110	4.72	0.96
24	-110.4843709	44.6510603	12	541107.00	4944487.00	26.2	16.3	2.2	26.8	0.7005	n.a.		7.22	5.050	222.42	1.00
25	-110.4843709	44.6510603	12	541092.80	4944474.00				38.4	0.7007	n.a.		18.83	13.190	580.52	1.00
26	-110.4843709	44.6510603	12	541102.00	4944447.00				29.0	0.7008	n.a.		4.57	3.200	140.83	1.00
27	-110.4843709	44.6510603	12	541063.70	4944457.00	26.0	12.9	2.2	22.3	0.7010	n.a.		3.98	2.790	122.73	1.00
28	-110.4843709	44.6510603	12	541045.50	4944442.00				18.5	0.7010	n.a.		1.96	1.370	60.39	1.00
29	-110.4843709	44.6510603	12	541036.70	4944428.50				17.0	0.7010	n.a.		0.08	0.050	2.41	0.77
30	-110.4843709	44.6510603	12	541020.10	4944418.50				15.7	0.7010	n.a.		UD			
31	-110.4843709	44.6510603	12	541026.60	4944399.50				14.3	0.7010	n.a.		0.20	0.140	6.32	0.07
32	-110.4843709	44.6510603	12	541037.80	4944385.00				14.0	0.7010	n.a.		0.26	0.180	8.11	0.07
33	-110.4843709	44.6510603	12	541020.70	4944390.00				14.3	0.7010	n.a.		0.16	0.110	4.83	0.88

Date: 2014/7/24

Weather: sunny & Windy

Pressure: 1024.4 hPa

Data Collector: Christie E. Torres, Peipei Lin

POINT	**LONGITUDE**	**LATITUDE**	**UTM ZONE**	**UTM LONGITUDE**	**UTM LATITUDE**	**AIR TEMP.**	**AIR RH**	**WIND SPEED**	**SOIL TEMP**	**ACK**	**H_2S**	**H_2S R^2**	**CO_2**		**CO_2 R^2**
						(°C)	(%)	(km/h)	(°C)		($ppm\ s^{-1}$) ($mol\ m^{-2}\ d^{-1}$) ($g\ m^{-2}\ d^{-1}$)		($ppm\ s^{-1}$) ($mol\ m^{-2}\ d^{-1}$) ($g\ m^{-2}\ d^{-1}$)		
1	-110.4820000	44.6534000	12	541072.00	4944579.00	20.0	32.1	10.8	15.1	0.7153	UD		0.84	0.60	26.30	0.942
2	-110.4821800	44.6532900	12	541058.00	4944567.00				13.9	0.7146	UD		UD			
3	-110.4823000	44.6532300	12	541048.00	4944560.00				18.0	0.7139	UD		0.20	0.14	6.19	0.956
4	-110.4824300	44.6531500	12	541038.00	4944551.00				16.1	0.7132	UD		UD			
5	-110.4825300	44.6530200	12	541030.00	4944537.00				22.5	0.7125	UD		1.44	1.03	45.10	0.988

6	-110.4827200	44.6529300	12	541015.00	4944527.00				66.8	0.7118	3.29	2.34	79.50	0.990	106.00	75.10	3300.00	0.999
7	-110.4830100	44.6529100	12	540992.00	4944524.00				24.4	0.7111	BD				3.74	2.66	117.00	0.997
8	-110.4833000	44.6524200	12	540969.00	4944470.00				21.2	0.7104	UD				2.34	1.66	73.00	0.995
9	-110.4835200	44.6522700	12	540952.00	4944452.00				25.9	0.7097	UD				1.24	0.88	38.60	0.985
10	-110.4836100	44.6521100	12	540945.00	4944436.00	22.6	31.4	5.6	20.6	0.7090	UD				5.32	3.77	166.00	0.998
11	-110.4837700	44.6520400	12	540932.00	4944428.00				17.4	0.7093	UD				0.37	0.26	11.60	0.985
12	-110.4838500	44.6521300	12	540926.00	4944437.00				17.8	0.7095	UD				0.26	0.19	8.25	0.946
13	-110.4835600	44.6521900	12	540949.00	4944444.00				21.9	0.7097	UD				4.23	3.00	132.00	0.995
14	-110.4837100	44.6523500	12	540937.00	4944462.00				19.5	0.7099	UD				UD			
15	-110.4836700	44.6524700	12	540940.00	4944475.00				22.8	0.7101	UD				1.63	1.16	50.90	0.996
16	-110.4834200	44.6525900	12	540960.00	4944489.00				45.8	0.7103	UD				87.20	62.00	2730.00	0.998
17	-110.4831700	44.6529400	12	540979.00	4944528.00				20.0	0.7106	UD				2.05	1.46	64.20	0.998
18	-110.4829800	44.6530800	12	540994.00	4944543.00				20.5	0.7108	UD				0.06	0.04	1.83	0.684
19	-110.4832890	44.6531020	12	540969.75	4944545.50				18.2	0.7110	UD				0.07	0.05	2.28	0.699
20	-110.4834100	44.6529400	12	540961.00	4944528.00	21.7	28.4	6.2	27.5	0.7112	UD				23.90	17.00	747.00	0.995
21	-110.4835800	44.6528100	12	540947.00	4944513.00				33.6	0.7109	UD				1.24	0.88	38.90	0.997
22	-110.4837700	44.6527000	12	540932.00	4944501.00				24.4	0.7107	UD				19.00	13.50	593.00	0.999
23	-110.4839900	44.6527300	12	540915.00	4944504.00				n.a.	0.7104	UD				4.07	2.89	127.00	0.992
24	-110.4839440	44.6528120	12	540918.00	4944513.00				19.3	0.7101	UD				6.23	4.42	195.00	0.993
25	-110.4841000	44.6528800	12	540906.00	4944520.00				17.8	0.7099	UD				1.64	1.16	51.20	0.995
26	-110.4842600	44.6529800	12	540893.00	4944531.00				20.5	0.7096	UD				2.40	1.71	75.10	0.999
27	-110.4844400	44.6530800	12	540878.00	4944542.00				33.3	0.7094	UD				11.70	8.27	364.00	0.999
28	-110.4846000	44.6532400	12	540866.00	4944560.00				24.5	0.7091	0.25	0.18	5.98	1.000	28.00	19.80	873.00	0.994
29	-110.4849400	44.6533100	12	540839.00	4944568.00				21.9	0.7088	0.18	0.13	4.31	0.998	44.90	31.80	1400.00	0.999
30	-110.4850400	44.6535000	12	540830.00	4944589.00	22.8	28.0	0.9	17.9	0.7086	BD				0.51	0.36	15.70	0.988
31	-110.4849900	44.6535800	12	540835.00	4944598.00				20.0	0.7086	UD				0.18	0.13	5.57	0.893

32	-110.4848800	44.6535400	12	540843.00	4944593.00				25.7	0.7087	UD	0.64	0.45	19.80	0.948
33	-110.4849600	44.6539500	12	540837.00	4944639.00				17.0	0.7087	UD	0.67	0.47	20.80	0.990
34	-110.4847800	44.6538300	12	540851.00	4944626.00				18.7	0.7088	UD	41.50	29.40	1290.00	0.995
35	-110.4847800	44.6538300	12	540851.00	4944625.00				20.4	0.7088	BD	11.50	8.16	359.00	0.925
36	-110.4845300	44.6535900	12	540871.00	4944599.00				26.0	0.7089	UD	0.46	0.33	14.30	0.988
37	-110.4844200	44.6534700	12	540880.00	4944586.00				39.3	0.7089	UD	4.42	3.13	138.00	0.987
38	-110.4842600	44.6533500	12	540892.00	4944572.00				26.6	0.7089	UD	10.60	7.50	330.00	0.968
40	-110.4841400	44.6532200	12	540902.00	4944558.00				19.3	0.7090	UD	2.77	1.96	86.40	0.998
41	-110.4839900	44.6531200	12	540914.00	4944547.00	22.6	29.0	1.6	24.6	0.7090	UD	15.00	10.60	468.00	0.999
42	-110.4838700	44.6530400	12	540924.00	4944538.00				25.0	0.7092	UD	2.86	2.02	89.10	0.976
43	-110.4836900	44.6529400	12	540938.00	4944527.00				22.7	0.7093	UD	2.09	1.48	65.20	0.983
44	-110.4838200	44.6527600	12	540928.00	4944507.00				21.6	0.7095	UD	5.13	3.64	160.00	0.998
45	-110.4839400	44.6526900	12	540919.00	4944499.00				19.0	0.7096	UD	2.57	1.82	80.20	0.928
46	-110.4840500	44.6529200	12	540910.00	4944525.00				25.8	0.7098	UD	1710.00	1220.00	53500.00	0.928
47	-110.4840740	44.6528510	12	540907.69	4944517.00				n.a.	0.7099	UD	59.40	42.10	1850.00	0.998
48	-110.4840900	44.6529900	12	540906.00	4944532.00				19.3	0.7101	UD	1.27	0.90	39.60	0.958
49	-110.4841600	44.6532400	12	540900.00	4944560.00				21.4	0.7102	UD	18.70	13.30	586.00	0.997
50	-110.4834900	44.6531500	12	540954.00	4944551.00				18.5	0.7103	UD	1.05	0.74	32.80	0.065
51	-110.4835700	44.6530800	12	540948.00	4944543.00				20.5	0.7105	UD	5.01	3.56	157.00	0.999
52	-110.4837000	44.6531800	12	540937.00	4944554.00	22.0	19.4	1.8	31.6	0.7105	UD	15.20	10.80	476.00	1.000
53	-110.4838300	44.6533000	12	540927.00	4944568.00				20.2	0.7102	UD	2.24	1.59	69.80	0.997
54	-110.4840500	44.6534400	12	540909.00	4944582.00				22.2	0.7100	UD	4.15	2.95	130.00	0.992
55	-110.4841300	44.6535800	12	540903.00	4944598.00				22.6	0.7097	UD	90.30	64.00	2820.00	0.988
56	-110.4843200	44.6537200	12	540888.00	4944613.00				16.7	0.7094	UD	2.29	1.63	71.60	0.998
57	-110.4846000	44.6537400	12	540865.00	4944616.00				16.4	0.7092	UD	0.17	0.12	5.38	0.680
58	-110.4847000	44.6539000	12	540857.00	4944634.00				18.0	0.7089	UD	1.61	1.14	50.30	0.998

59	-110.4847800	44.6540700	12	540851.00	4944652.00				15.9	0.7086	UD				0.07	0.05	2.18	0.855
60	-110.4847900	44.6541600	12	540850.00	4944663.00				18.7	0.7084	UD				0.53	0.38	16.60	0.974
61	-110.4846300	44.6540800	12	540863.00	4944653.00				21.7	0.7081	UD				6.38	4.52	199.00	0.999
62	-110.4843900	44.6541100	12	540882.00	4944657.00	23.1	23.2	1.6	21.5	0.7078	UD				11.80	8.35	368.00	0.989
63	-110.4841700	44.6541100	12	540899.00	4944657.00				41.1	0.7076	0.12	0.08	2.85	1.000	16.70	11.80	520.00	0.999
64	-110.4843100	44.6539500	12	540888.00	4944639.00				14.3	0.7074	BD				0.80	0.56	24.70	0.994
65	-110.4845100	44.6539600	12	540872.00	4944640.00				15.2	0.7072	UD				2.90	2.05	90.10	0.995
66	-110.4843600	44.6538400	12	540884.00	4944627.00				14.7	0.7070	UD				1.31	0.92	40.60	0.998
67	-110.4842900	44.6536600	12	540890.00	4944607.00				19.7	0.7068	UD				0.31	0.22	9.67	0.970
68	-110.4840400	44.6535800	12	540910.00	4944598.00				22.3	0.7066	UD				0.13	0.09	4.04	0.916
69	-110.4838500	44.6534700	12	540925.00	4944586.00				20.7	0.7063	UD				0.90	0.64	27.90	0.994
70	-110.4837000	44.6533400	12	540937.00	4944571.00				19.8	0.7061	UD				0.09	0.06	2.77	0.884
71	-110.4836700	44.6533200	12	540939.00	4944569.00	24.0	21.0	1.4	22.4	0.7057	UD				UD			

Date: 2014/7/26

Weather: sunny

Pressure: 1026.75 hPa

Data Collector: Christie E. Torres, Peipei Lin

POINT	**LONGITUDE**	**LATITUDE**	**UTM ZONE**	**UTM LONGITUDE**	**UTM LATITUDE**	**AIR TEMP.**	**AIR RH**	**WIND SPEED**	**SOIL TEMP**	**ACK**	**H_2S**		**H_2S R^2**	**CO_2**		**CO_2 R^2**
						(°C)	(%)	(km/h)	(°C)		($ppm\ s^{-1}$)	($mol\ m^{-2}\ d^{-1}$) ($g\ m^{-2}\ d^{-1}$)		($ppm\ s^{-1}$)	($mol\ m^{-2}\ d^{-1}$) ($g\ m^{-2}\ d^{-1}$)	
1	44.6541600	-110.4833400	12	540964.38	4944662.50	23.4	224.0	1.1	14.5	0.7088	UD			0.12	0.08	3.63	0.922
2	44.6541300	-110.4837600	12	540931.88	4944659.00				14.0	0.7087	UD			UD			
3	44.6541500	-110.4848800	12	540843.38	4944661.50				11.2	0.7087	BD			0.20	0.14	6.11	0.761
4	44.6542400	-110.4851000	12	540825.13	4944671.00				15.5	0.7087	UD			0.41	0.29	12.90	0.980
5	44.6542500	-110.4848000	12	540848.88	4944672.50				14.9	0.7086	UD			3.99	2.83	124.00	0.988

6	44.6542500	-110.4845900	12	540865.75	4944672.50				15.4	0.7086	UD	0.45	0.32	14.10	0.990
7	44.6542600	-110.4843500	12	540884.44	4944673.50				25.9	0.7086	UD	4.03	2.85	126.00	0.998
8	44.6542500	-110.4841600	12	540899.75	4944673.00				27.4	0.7086	UD	5.32	3.77	166.00	0.999
9	44.6542300	-110.4839400	12	540917.00	4944670.50				18.5	0.7085	UD	1.47	1.04	45.80	0.998
10	44.6543700	-110.4838600	12	540923.25	4944686.50	23.5	48.0	0.2	13.0	0.7085	UD	3.18	2.25	99.20	0.995
11	44.6543500	-110.4840900	12	540903.94	4944684.00				27.1	0.7102	UD	0.52	0.37	16.20	0.993
12	44.6543600	-110.4843700	12	540883.13	4944684.50				29.9	0.7119	UD	3.27	2.33	102.00	0.998
13	44.6543400	-110.4845800	12	540866.38	4944682.50				17.5	0.7136	UD	4.24	3.03	133.00	0.993
14	44.6543700	-110.4848200	12	540847.56	4944685.00				14.8	0.7153	UD	UD			
15	44.6543700	-110.4850400	12	540829.50	4944686.50				14.2	0.7170	UD	0.18	0.13	5.77	0.947
16	44.6545100	-110.4850760	12	540825.88	4944700.50				15.6	0.7187	UD	0.10	0.07	3.23	0.827
17	44.6544810	-110.4848230	12	540847.13	4944698.00				22.1	0.7204	UD	0.53	0.38	16.60	0.983
18	44.6544800	-110.4848500	12	540865.13	4944699.00				17.8	0.7221	UD	0.23	0.17	7.29	0.968
19	44.6544900	-110.4846000	12	540883.00	4944699.00				24.6	0.7239	UD	7.23	5.23	230.00	0.999
20	44.6544900	-110.4843700	12	540901.06	4944698.50	16.5	21.4	2.2	16.8	0.7256	UD	16.90	12.20	539.00	0.997
21	44.6544800	-110.4841400	12	540918.81	4944699.00				18.7	0.7254	UD	11.20	8.14	358.00	0.990
22	44.6544900	-110.4839100	12	540938.13	4944697.50				23.8	0.7251	UD	40.00	29.00	1280.00	1.000
23	44.6544700	-110.4836700	12	540956.19	4944698.00				17.5	0.7249	UD	3.04	2.20	96.80	0.999
24	44.6544800	-110.4834500	12	540970.94	4944696.00				17.4	0.7246	UD	3.84	2.78	122.00	0.999
25	44.6544600	-110.4832600	12	540969.19	4944710.00				16.4	0.7244	UD	2.82	2.04	89.70	0.999
26	44.6545800	-110.4832800	12	540952.50	4944708.50				17.0	0.7241	UD	1.64	1.19	52.20	0.998
27	44.6545700	-110.4835000	12	540937.75	4944709.00				25.5	0.7239	UD	8.89	6.44	283.00	0.971
28	44.6545700	-110.4836900	12	540919.19	4944709.50				24.9	0.7236	UD	35.00	25.40	1120.00	0.999
29	44.6545700	-110.4839100	12	540904.75	4944710.50				16.9	0.7234	UD	11.00	7.96	350.00	0.999
30	44.6545900	-110.4841000	12	540885.81	4944711.50	17.5	26.0	0.9	52.0	0.7231	UD	2.38	1.72	75.80	0.999
31	44.6546000	-110.4843400	12	540871.50	4944709.50				19.1	0.7220	UD	0.11	0.08	3.58	0.963

32	44.6545800	-110.4845200	12	540854.38	4944709.50				16.7	0.7209	UD	0.92	0.66	29.00	0.997
33	44.6545800	-110.4847300	12	540836.50	4944712.50				21.4	0.7197	UD	3.65	2.63	116.00	0.999
34	44.6546100	-110.4849500	12	540817.69	4944711.50				18.9	0.7186	UD	0.07	0.05	2.31	0.837
35	44.6546000	-110.4851900	12	540782.81	4944727.50				16.6	0.7175	UD	1.25	0.90	39.50	0.933
36	44.6547500	-110.4856300	12	540803.25	4944731.00				18.4	0.7163	UD	0.18	0.13	5.51	0.890
37	44.6547800	-110.4853700	12	540817.63	4944728.00				17.6	0.7152	UD	0.07	0.05	2.27	0.744
38	44.6547500	-110.4851900	12	540832.25	4944728.00				17.8	0.7141	UD	0.34	0.24	10.70	0.961
39	44.6547500	-110.4850100	12	540849.06	4944729.50				18.0	0.7130	UD	0.27	0.19	8.46	0.973
40	44.6547500	-110.4847900	12	540865.94	4944728.00	22.1	21.0	2.0	23.7	0.7119	UD	2.92	2.08	91.60	0.999
41	44.6547400	-110.4845800	12	540881.69	4944725.50				15.5	0.7124	UD	1.73	1.23	54.20	0.998
42	44.6547200	-110.4843700	12	540900.06	4944726.00				17.4	0.7129	UD	1.56	1.11	48.90	0.998
43	44.6547300	-110.4841500	12	540915.06	4944723.00				18.5	0.7135	UD	7.95	5.67	250.00	0.999
44	44.6547000	-110.4839600	12	540932.06	4944724.00				25.5	0.7140	UD	22.40	16.00	705.00	0.991
45	44.6547100	-110.4837500	12	540946.63	4944724.00				20.3	0.7145	UD	3.16	2.25	99.20	0.999
46	44.6547200	-110.4835500	12	540962.94	4944722.50				18.2	0.7151	UD	1.68	1.20	52.80	0.997
47	44.6546900	-110.4833600	12	540978.31	4944718.00				20.2	0.7156	UD	0.83	0.60	26.20	0.994
48	44.6546600	-110.4831600	12	540978.75	4944736.00				22.8	0.7161	UD	3.76	2.69	119.00	0.999
49	44.6548100	-110.4831600	12	540960.38	4944738.50				16.8	0.7167	UD	0.09	0.07	2.92	0.879
50	44.6548400	-110.4833900	12	540944.56	4944739.00	19.9	16.5	1.0	16.5	0.7172	UD	3.66	2.62	115.00	0.999
51	44.6548400	-110.4835900	12	540929.50	4944739.50				17.2	0.7166	UD	8.51	6.10	268.00	0.999
52	44.6548500	-110.4837800	12	540912.63	4944741.00				23.2	0.7160	UD	13.50	9.63	424.00	0.999
53	44.6548700	-110.4839900	12	540895.69	4944740.50				30.6	0.7154	UD	22.40	16.00	705.00	0.999
54	44.6548600	-110.4842100	12	540878.31	4944738.50				18.8	0.7148	UD	2.64	1.88	82.90	0.996
55	44.6548400	-110.4844300	12	540862.38	4944737.50				17.5	0.7142	UD	0.75	0.54	23.60	0.994
56	44.6548400	-110.4846300	12	540845.63	4944739.00				19.7	0.7136	UD	0.14	0.10	4.51	0.171
57	44.6548500	-110.4848400	12	540828.75	4944739.50				18.8	0.7130	UD	UD			

58	44.6548600	-110.4850500	12	540812.63	4944740.00				20.7	0.7124	UD				UD			
59	44.6548700	-110.4852500	12	540795.88	4944740.00				19.1	0.7118	UD				UD			
60	44.6548600	-110.4854600	12	540776.88	4944737.50	22.4	44.2	1.4	19.4	0.7112	0.08	0.06	2.00	0.931	1.01	0.72	31.50	0.955
61	44.6548400	-110.4857000	12	540759.94	4944740.00				18.0	0.7110	UD				3.75	2.67	117.00	0.991
62	44.6548600	-110.4859100	12	540742.13	4944741.00				14.6	0.7108	0.17	0.12	4.11	0.996	433.00	307.00	13500.00	0.999
63	44.6548700	-110.4861400	12	540742.31	4944740.50					0.7106	0.11	0.08	2.63	0.986	349.00	248.00	10900.00	0.997
64	44.6547200	-110.4860400	12	540750.75	4944725.50				14.6	0.7104	BD				0.23	0.16	7.16	0.901
65	44.6546900	-110.4862700	12	540734.31	4944721.50				13.7	0.7102	UD				1.39	0.99	43.60	0.998
66	44.6546100	-110.4864000	12	540727.31	4944711.50				19.7	0.7100	UD				0.40	0.29	12.60	0.986
67	44.6545600	-110.4865000	12	540715.25	4944708.50				16.1	0.7098	UD				0.46	0.33	14.40	0.961
68	44.6549800	-110.4861800	12	540739.56	4944752.50				21.5	0.7096	BD				1.29	0.91	40.10	0.998
69	44.6549900	-110.4859000	12	540760.81	4944754.00				16.7	0.7094	UD				7.18	5.09	224.00	0.978
70	44.6550000	-110.4856800	12	540778.94	4944755.00	23.2	20.9	1.2	19.1	0.7092	UD				4.72	3.35	147.00	0.985
71	44.6549900	-110.4854500	12	540796.94	4944753.50				19.6	0.7091	UD				0.25	0.18	7.68	0.970
72	44.6550100	-110.4852600	12	540811.69	4944755.00				21.3	0.7090	UD				0.21	0.15	6.44	0.986
73	44.6550100	-110.4851000	12	540824.00	4944756.00				20.1	0.7089	UD				UD			
74	44.6550000	-110.4848700	12	540843.00	4944755.00				21.4	0.7088	UD				2.28	1.61	71.00	0.999
75	44.6550100	-110.4846500	12	540858.25	4944756.00				23.6	0.7086	UD				1.11	0.78	34.50	0.998
76	44.6550200	-110.4844500	12	540876.19	4944758.00				21.8	0.7085	UD				7.01	4.97	219.00	0.999
77	44.6549900	-110.4842300	12	540893.75	4944756.00				23.6	0.7084	UD				6.57	4.65	205.00	0.997
78	44.6550100	-110.4840200	12	540909.25	4944756.00				24.6	0.7083	UD				1.41	1.00	43.80	0.960
79	44.6549900	-110.4838300	12	540925.38	4944755.00				19.3	0.7082	UD				12.30	8.74	385.00	0.999
80	44.6549700	-110.4836600	12	540938.50	4944753.50	23.7	15.5	1.2	18.7	0.7080	UD				0.56	0.40	17.50	0.981
81	44.6549800	-110.4834600	12	540952.88	4944753.50				21.5	0.7084	UD				0.37	0.26	11.40	0.983
82	44.6549800	-110.4832500	12	540971.63	4944755.00				24.2	0.7087	UD				1.62	1.15	50.50	0.997
83	44.6551500	-110.4833100	12	540966.75	4944772.50				45.2	0.7090	UD				8.69	6.16	271.00	0.987

84	44.6551200	-110.4835300	12	540949.13	4944769.00				19.3	0.7094	UD		4.19	2.97	131.00	0.999
85	44.6551400	-110.4837700	12	540929.56	4944772.00				21.3	0.7097	UD		4.50	3.19	140.00	0.990
86	44.6551600	-110.4839700	12	540913.88	4944773.00				26.6	0.7100	UD		5.73	4.07	179.00	0.997
87	44.6551500	-110.4842200	12	540894.19	4944772.00				22.5	0.7104	UD		2.28	1.62	71.40	0.999
88	44.6551600	-110.4844600	12	540875.25	4944773.00				25.2	0.7107	UD		2.04	1.45	63.90	0.998
89	44.6551500	-110.4846700	12	540858.31	4944772.00				36.2	0.7111	UD		2.59	1.84	81.10	0.999
90	44.6551400	-110.4848800	12	540841.81	4944771.00	22.3	16.3	1.1	27.8	0.7114	UD		1.50	1.06	46.90	0.998
91	44.6551500	-110.4851200	12	540823.06	4944772.50				22.9	0.7107	UD		5.57	3.96	174.00	0.999
92	44.6551600	-110.4853500	12	540805.56	4944773.00				21.8	0.7100	UD		0.21	0.15	6.41	0.960
93	44.6551300	-110.4855500	12	540789.13	4944769.50				22.5	0.7094	UD		0.10	0.07	3.23	0.916
94	44.6551600	-110.4857700	12	540771.31	4944772.50				19.9	0.7087	UD		0.27	0.19	8.45	0.892
95	44.6551700	-110.4860300	12	540750.81	4944773.50				22.9	0.7080	UD		1.77	1.25	55.10	0.998
96	44.6553600	-110.4859400	12	540757.63	4944795.00				17.2	0.7074	UD		26.90	19.00	838.00	0.992
97	44.6553100	-110.4857400	12	540772.31	4944788.50				17.8	0.7067	UD		3.42	2.42	106.00	0.986
98	44.6553000	-110.4855600	12	540789.44	4944788.50				20.2	0.7060	UD		0.42	0.29	12.90	0.988
99	44.6552900	-110.4853100	12	540807.00	4944789.50				24.4	0.7054	BD		0.13	0.09	4.00	0.917
100	44.6552800	-110.4851200	12	540822.50	4944788.00	25.1	14.0	1.2	23.4	0.7047	UD		0.27	0.19	8.28	0.974
101	44.6552900	-110.4849000	12	540840.25	4944788.00				28.2	0.7047	UD		0.53	0.37	16.40	0.986

Date: 2014/7/27

Weather: sunny

Pressure: 961.73 hPa

Data Collector: Christie E. Torres, Peipei Lin

POINT	**LONGITUDE**	**LATITUDE**	**UTM ZONE**	**UTM LONGITUDE**	**UTM LATITUDE**	**AIR TEMP.**	**AIR RH**	**WIND SPEED**	**SOIL TEMP**	**ACK**	**H_2S**	**H_2S R^2**	**CO_2**	**CO_2 R^2**
						(°C)	(%)	(km/h)	(°C)		(ppm s^{-1}) (mol m^{-2} d^{-1}) (g m^{-2} d^{-1})		(ppm s^{-1}) (mol m^{-2} d^{-1}) (g m^{-2} d^{-1})	

1	44.6569900	-110.4823100	12	541045.00	4944978.00	19.2	73.8	0.1	14.9	0.6734	UD	0.48	0.32	14.20	0.988
2	44.6568600	-110.4824800	12	541031.00	4944963.00				18.5	0.6730	UD	0.24	0.16	7.09	0.930
3	44.6567600	-110.4826000	12	541022.00	4944952.00				19.9	0.6726	UD	4.12	2.77	122.00	0.998
4	44.6567300	-110.4823500	12	541041.00	4944949.00				14.8	0.6722	UD	0.20	0.14	5.94	0.952
5	44.6567300	-110.4828500	12	541002.00	4944948.00				17.3	0.6718	UD	0.79	0.53	23.50	0.982
6	44.6566300	-110.4823400	12	541042.00	4944938.00				14.3	0.6714	UD	0.09	0.06	2.57	0.806
7	44.6565900	-110.4825900	12	541023.00	4944933.00				13.7	0.6710	UD	0.22	0.15	6.45	0.880
8	44.6565600	-110.4828700	12	541001.00	4944930.00				13.5	0.6706	UD	0.08	0.05	2.35	0.308
9	44.6565400	-110.4830700	12	540985.00	4944928.00				14.7	0.6701	UD	0.17	0.12	5.09	0.535
10	44.6565200	-110.4832800	12	540968.00	4944925.00	20.8	34.0	0.1	18.4	0.6697	UD	0.79	0.53	23.20	0.994
11	44.6564400	-110.4837200	12	540934.00	4944916.00				19.6	0.6696	UD	2.24	1.50	65.80	0.978
12	44.6563900	-110.4834800	12	540952.00	4944911.00				21.2	0.6694	UD	3.26	2.18	96.00	0.998
13	44.6563800	-110.4832400	12	540971.00	4944909.00				17.7	0.6693	UD	0.89	0.60	26.30	0.995
14	44.6563900	-110.4830000	12	540991.00	4944911.00				14.0	0.6691	UD	0.69	0.46	20.30	0.990
15	44.6564000	-110.4828200	12	541004.00	4944912.00				14.5	0.6689	UD	0.11	0.07	3.20	0.825
16	44.6563900	-110.4826000	12	541022.00	4944911.00				15.1	0.6688	UD	0.15	0.10	4.41	0.940
17	44.6564100	-110.4823700	12	541040.00	4944914.00				14.2	0.6686	UD	0.12	0.08	3.37	0.747
18	44.6562200	-110.4821500	12	541058.00	4944893.00				14.5	0.6685	UD	0.12	0.08	3.54	0.905
19	44.6562600	-110.4825000	12	541030.00	4944897.00				14.2	0.6683	UD	0.09	0.06	2.59	0.826
20	44.6562700	-110.4827600	12	541009.00	4944897.00	21.5	37.3	0.1	13.9	0.6682	UD	UD			
21	44.6562600	-110.4829500	12	540995.00	4944896.00				14.4	0.6682	UD	0.14	0.10	4.24	0.920
22	44.6562500	-110.4831400	12	540980.00	4944896.00				13.9	0.6682	UD	0.39	0.26	11.50	0.988
23	44.6562500	-110.4834600	12	540954.00	4944895.00				16.3	0.6683	UD	1.16	0.77	34.00	0.997
24	44.6562500	-110.4836800	12	540936.00	4944895.00				21.2	0.6683	UD	2.94	1.96	86.40	0.999
25	44.6562600	-110.4839100	12	540919.00	4944896.00				18.1	0.6684	UD	0.65	0.44	19.20	0.992
26	44.6561400	-110.4841700	12	540898.00	4944882.00				16.8	0.6684	UD	1.92	1.28	56.40	0.984

27	44.6561500	-110.4839400	12	540916.00	4944884.00				22.2	0.6685	UD	5.58	3.73	164.00	0.999
28	44.6561100	-110.4837300	12	540933.00	4944880.00				23.1	0.6685	UD	5.63	3.76	166.00	0.999
29	44.6561300	-110.4835000	12	540951.00	4944881.00				16.9	0.6686	UD	1.49	0.99	43.70	0.997
30	44.6561000	-110.4832900	12	540967.00	4944879.00	21.3	19.6	0.9	15.5	0.6686	UD	0.21	0.14	6.30	0.966
31	44.6561100	-110.4830900	12	540983.00	4944879.00				14.2	0.6675	UD	0.46	0.31	13.50	0.984
32	44.6561000	-110.4829200	12	540997.00	4944878.00				13.5	0.6664	UD	0.13	0.09	3.74	0.897
33	44.6560800	-110.4827400	12	541011.00	4944876.00				12.9	0.6654	UD	UD			
34	44.6560800	-110.4825800	12	541024.00	4944876.00				14.6	0.6643	UD	0.12	0.08	3.47	0.079
35	44.6560900	-110.4823400	12	541043.00	4944878.00				14.5	0.6632	UD	UD			
36	44.6560800	-110.4820800	12	541064.00	4944877.00				12.5	0.6621	UD	UD			
37	44.6559700	-110.4824000	12	541038.00	4944865.00				14.8	0.6611	UD	UD			
38	44.6559900	-110.4825700	12	541025.00	4944867.00				12.9	0.6600	UD	0.26	0.17	7.53	0.956
39	44.6559800	-110.4827300	12	541012.00	4944865.00				12.8	0.6589	UD	0.33	0.22	9.54	0.962
40	44.6560000	-110.4829300	12	540996.00	4944867.00	26.1	21.9	0.9	14.8	0.6579	UD	0.83	0.55	24.10	0.995
41	44.6559800	-110.4831300	12	540980.00	4944866.00				14.4	0.6582	UD	2.77	1.82	80.20	0.998
42	44.6560000	-110.4833200	12	540965.00	4944867.00				14.5	0.6585	UD	0.72	0.48	21.00	0.996
43	44.6560200	-110.4835300	12	540949.00	4944869.00				16.5	0.6588	UD	0.24	0.16	6.96	0.962
44	44.6559900	-110.4837200	12	540934.00	4944866.00				28.2	0.6591	UD	1.76	1.16	51.10	0.998
45	44.6560000	-110.4839600	12	540915.00	4944867.00				44.4	0.6594	UD	1.96	1.30	57.00	0.996
46	44.6560200	-110.4842100	12	540895.00	4944870.00				24.4	0.6597	UD	0.13	0.09	3.85	0.948
47	44.6560300	-110.4844800	12	540873.00	4944871.00				21.7	0.6600	UD	UD			
48	44.6558800	-110.4840700	12	540906.00	4944853.00				19.4	0.6604	UD	UD			
49	44.6558700	-110.4838700	12	540922.00	4944852.00				22.3	0.6607	UD	0.15	0.10	4.24	0.926
50	44.6558700	-110.4836500	12	540939.00	4944852.00	24.7	21.2	5.9	21.3	0.6610	UD	2.45	1.62	71.30	0.997
51	44.6558400	-110.4834700	12	540953.00	4944850.00				18.5	0.6609	UD	0.28	0.19	8.17	0.962
52	44.6558500	-110.4833200	12	540965.00	4944850.00				18.8	0.6608	UD	2.35	1.55	68.40	0.998

53	44.6558300	-110.4831300	12	540980.00	4944849.00				18.6	0.6608	UD	1.85	1.22	53.70	0.998
54	44.6558500	-110.4829700	12	540993.00	4944851.00				22.0	0.6607	UD	0.20	0.13	5.86	0.961
55	44.6558400	-110.4828000	12	541007.00	4944850.00				24.4	0.6606	UD	2.18	1.44	63.20	0.998
56	44.6558400	-110.4826800	12	541016.00	4944849.00				25.5	0.6606	UD	2.15	1.42	62.50	0.999
57	44.6557300	-110.4825900	12	541023.00	4944837.00					0.6605	UD	5.77	3.81	168.00	0.977
58	44.6557300	-110.4827600	12	541009.00	4944837.00				44.0	0.6604	UD	13.40	8.85	389.00	0.990
59	44.6557000	-110.4829500	12	540995.00	4944834.00				40.0	0.6604	UD	1.16	0.77	33.60	0.990
60	44.6557000	-110.4831600	12	540978.00	4944834.00	25.0	22.0	1.2	23.5	0.6603	UD	0.61	0.40	17.60	0.973
61	44.6557100	-110.4833500	12	540963.00	4944836.00				21.3	0.6604	UD	3.03	2.00	88.00	0.995
62	44.6557100	-110.4835400	12	540948.00	4944835.00				18.2	0.6606	UD	0.15	0.10	4.26	0.915
63	44.6557100	-110.4837400	12	540932.00	4944835.00				26.2	0.6607	UD	1.13	0.75	32.90	0.997
64	44.6557300	-110.4839600	12	540915.00	4944836.00				18.6	0.6608	UD	0.48	0.32	14.10	0.996
65	44.6557100	-110.4841700	12	540898.00	4944835.00				17.7	0.6610	UD	1.62	1.07	47.20	0.992
66	44.6555700	-110.4846200	12	540862.00	4944818.00				23.4	0.6611	UD	UD			
67	44.6555700	-110.4843500	12	540884.00	4944820.00				21.5	0.6612	UD	1.51	1.00	44.00	0.996
68	44.6555700	-110.4841500	12	540900.00	4944819.00				21.8	0.6614	UD	0.90	0.60	26.20	0.996
69	44.6555700	-110.4839600	12	540915.00	4944819.00				20.4	0.6615	UD	2.67	1.76	77.60	0.999
70	44.6555800	-110.4837500	12	540931.00	4944821.00	24.4	16.4	1.0	21.2	0.6616	UD	1.19	0.79	34.60	0.998
71	44.6555800	-110.4835900	12	540944.00	4944821.00				25.5	0.6613	UD	1.82	1.20	52.90	0.999
72	44.6555800	-110.4833800	12	540961.00	4944821.00				23.0	0.6609	UD	4.66	3.08	136.00	0.995
73	44.6555900	-110.4832100	12	540974.00	4944822.00				39.3	0.6606	UD	4.15	2.74	121.00	0.996
74	44.6555900	-110.4830100	12	540990.00	4944822.00				34.8	0.6602	UD	0.42	0.28	12.20	0.980
75	44.6555900	-110.4827700	12	541009.00	4944822.00				58.8	0.6599	BD	17.80	11.70	515.00	0.949
76	44.6555500	-110.4826000	12	541022.00	4944818.00				33.4	0.6595	UD	117.00	77.00	3390.00	0.994
77	44.6554400	-110.4827500	12	541011.00	4944806.00				47.0	0.6592	BD	12.70	8.34	367.00	0.999
78	44.6554100	-110.4829600	12	540994.00	4944802.00				37.2	0.6588	BD	17.80	11.70	515.00	0.985

79	44.6554300	-110.4832300	12	540973.00	4944804.00				44.5	0.6585	UD				2.26	1.49	65.40	0.998
80	44.6554400	-110.4834200	12	540958.00	4944805.00	26.0	17.2	1.2	27.2*	0.6581	UD				7.82	5.14	226.00	0.993
81	44.6554300	-110.4836600	12	540939.00	4944804.00				28.1	0.6576	UD				0.23	0.15	6.54	0.962
82	44.6554300	-110.4838500	12	540924.00	4944804.00				22.5	0.6572	UD				4.16	2.73	120.00	0.999
83	44.6554300	-110.4840200	12	540910.00	4944804.00				24.7	0.6567	UD				4.39	2.88	127.00	0.998
84	44.6554200	-110.4842600	12	540891.00	4944803.00				25.8	0.6563	UD				1.65	1.08	47.50	0.999
85	44.6554300	-110.4844600	12	540875.00	4944803.00				25.3	0.6558	UD				1.68	1.10	48.40	0.999
86	44.6554400	-110.4846800	12	540858.00	4944804.00				37.4	0.6553	UD				6.91	4.53	199.00	0.999
87	44.6554400	-110.4848800	12	540842.00	4944804.00				29.3	0.6549	UD				2.91	1.90	83.80	0.999
88	44.6552800	-110.4847200	12	540855.00	4944787.00				28.2	0.6544	UD				15.80	10.40	456.00	0.999
89	44.6553000	-110.4845100	12	540872.00	4944789.00				36.5	0.6540	UD				8.26	5.40	238.00	0.999
90	44.6553000	-110.4843300	12	540885.00	4944789.00	28.1	15.1	1.2	54.1	0.6535	UD				7.92	5.17	228.00	0.999
91	44.6553100	-110.4841500	12	540900.00	4944790.00				23.3	0.6536	UD				2.46	1.61	70.60	0.998
92	44.6553100	-110.4839700	12	540914.00	4944790.00				23.0	0.6536	UD				0.47	0.31	13.50	0.988
93	44.6553000	-110.4837500	12	540931.00	4944789.00				28.2*	0.6537	0.08	0.05	1.72	0.991	2.53	1.65	72.70	0.998
94	44.6553000	-110.4835800	12	540945.00	4944789.00				32.5*	0.6537	UD				4.45	2.91	128.00	0.999
95	44.6552900	-110.4834000	12	540960.00	4944788.00				47.6*	0.6538	UD				1.89	1.24	54.50	0.998
96	44.6552900	-110.4831800	12	540977.00	4944789.00					0.6538	UD				UD			
97	44.6553100	-110.4830100	12	540991.00	4944791.00				53.7*	0.6539	UD				0.66	0.43	19.10	0.991
98	44.6551800	-110.4830300	12	540989.00	4944777.00				65.6	0.6539	UD				2.08	1.36	59.80	0.995
99	44.6551700	-110.4828000	12	541007.00	4944775.00	27.9	20.8	1.2	40*	0.6539	UD				2.89	1.89	83.20	0.958

Date: 2014/7/31

Weather: Sunny

Pressure: 1027.77 hPa

Data Collector: Christie E. Torres, Peipei Lin

POINT	LONGITUDE	LATITUDE	UTM ZONE	UTM LONGITUDE	UTM LATITUDE	AIR TEMP.	AIR RH	WIND SPEED	SOIL TEMP	ACK	H_2S			H_2S R^2	CO_2			CO_2 R^2
						(°C)	(%)	(km/h)	(°C)		(ppm s^{-1})	(mol m^{-2} d^{-1})	(g m^{-2} d^{-1})		(ppm s^{-1})	(mol m^{-2} d^{-1})	(g m^{-2} d^{-1})	
1	44.6549800	-110.4831000	12	540983.00	4944754.00	22.1	47.7	2.0	24.3	0.7126	UD				13.70	9.76	430.00	0.999
2	44.6550000	-110.4828800	12	541001.00	4944757.00				68.6	0.7118	BD				18.70	13.30	586.00	0.558
3	44.6550000	-110.4827000	12	541015.00	4944757.00				35.6	0.7110	BD				2.97	2.11	92.80	0.999
4	44.6550200	-110.4825000	12	541031.00	4944759.00				28.9	0.7102	BD				UD			
5	44.6550300	-110.4823500	12	541043.00	4944760.00				35.2	0.7094	BD				1.34	0.95	41.80	0.990
6	44.6550700	-110.4821400	12	541060.00	4944765.00				27.4	0.7086	BD				1.90	1.35	59.20	0.998
7	44.6551000	-110.4819900	12	541071.00	4944768.00				21.6	0.7078	BD				4.68	3.31	146.00	0.999
8	44.6551500	-110.4825700	12	541026.00	4944773.00					0.7070	BD				0.29	0.21	9.00	0.053
9	44.6551600	-110.4823500	12	541043.00	4944774.00				37.5	0.7062	BD				30.30	21.40	941.00	0.999
10	44.6551700	-110.4822000	12	541054.00	4944776.00	25.1	43.1	0.1	76.1	0.7054	0.11	0.07	2.54	0.976	39.10	27.60	1210.00	0.999
11	44.6551900	-110.4821100	12	541061.00	4944778.00				45.3	0.7063	BD				23.40	16.50	726.00	0.967
12	44.6548500	-110.4829900	12	540992.00	4944739.00				45.6	0.7072	BD				UD			
13	44.6548600	-110.4827900	12	541008.00	4944741.00				52.8	0.7081	0.07	0.05	1.72	0.960	2.54	1.80	79.00	0.083
14	44.6549000	-110.4825800	12	541025.00	4944746.00				40.1	0.7090	0.11	0.08	2.62	0.953	1.18	0.84	36.80	0.997
15	44.6549100	-110.4824000	12	541039.00	4944747.00				19.3	0.7099	UD				3.55	2.52	111.00	0.998
16	44.6549300	-110.4822000	12	541055.00	4944749.00				18.4	0.7108	UD				7.47	5.31	234.00	0.972
17	44.6549700	-110.4820300	12	541068.00	4944754.00				15.3	0.7118	UD				0.57	0.41	17.90	0.993
18	44.6547600	-110.4820700	12	541065.00	4944730.00				26.0	0.7127	UD				UD			
19	44.6547500	-110.4822800	12	541049.00	4944728.00				27.2	0.7136	UD				0.08	0.06	2.51	0.741
20	44.6547400	-110.4825000	12	541031.00	4944727.00	21.3	43.6	0.1	18.0	0.7145	UD				0.23	0.17	7.29	0.949
21	44.6547300	-110.4826700	12	541017.00	4944727.00				20.6	0.7129	UD				0.70	0.50	21.90	0.994
22	44.6547200	-110.4829000	12	540999.00	4944725.00				19.6	0.7113	UD				3.07	2.18	96.00	0.998
23	44.6547000	-110.4831300	12	540982.00	4944723.00				17.5	0.7097	UD				4.04	2.87	126.00	1.000

24	44.6545700	-110.4831800	12	540977.00	4944708.00				18.8	0.7082	UD	2.80	1.98	87.30	0.999
25	44.6545900	-110.4829300	12	540997.00	4944711.00				18.0	0.7066	UD	6.41	4.53	199.00	0.954
26	44.6546000	-110.4827700	12	541010.00	4944712.00				17.8	0.7050	UD	1.01	0.71	31.40	0.995
27	44.6546200	-110.4825700	12	541025.00	4944715.00				20.1	0.7035	UD	0.13	0.09	3.94	0.871
28	44.6546300	-110.4823900	12	541040.00	4944716.00				51.4	0.7019	UD	0.67	0.47	20.70	0.989
29	44.6546400	-110.4822100	12	541054.00	4944717.00				34.4	0.7004	UD	UD			
30	44.6546500	-110.4819900	12	541072.00	4944718.00	27.9	28.3	0.0	24.5	0.6989	UD	0.15	0.10	4.57	0.644
31	44.6546300	-110.4818000	12	541087.00	4944715.00				55.1	0.6997	BD	1.11	0.78	34.30	0.996
32	44.6546700	-110.4816200	12	541101.00	4944721.00				57.8	0.7006	BD	28.10	19.70	867.00	0.999
33	44.6546800	-110.4814900	12	541111.00	4944722.00				28.9	0.7015	BD	2.86	2.00	88.19	0.991
34	44.6545500	-110.4813400	12	541123.00	4944707.00				22.0	0.7024	BD	0.84	0.59	25.89	0.991
35	44.6545200	-110.4815100	12	541110.00	4944704.00				30.3	0.7033	BD	4.27	3.00	132.07	0.998
36	44.6545400	-110.4816500	12	541099.00	4944706.00				68.1	0.7042	BD	39.64	27.91	1228.21	0.997
37	44.6545100	-110.4817900	12	541087.00	4944703.00				81.5	0.7051	BD	46.48	32.77	1441.98	0.999
38	44.6545300	-110.4819900	12	541071.00	4944705.00					0.7060	BD	UD			
39	44.6545000	-110.4822100	12	541054.00	4944701.00					0.7069	BD	0.22	0.16	6.98	0.946
40	44.6544800	-110.4823900	12	541040.00	4944699.00	24.1	31.4	0.2	29.4	0.7078	BD	0.09	0.06	2.82	0.684
41	44.6544700	-110.4825900	12	541024.00	4944698.00				35.3	0.7083	BD	5.94	4.21	185.08	0.999
42	44.6544900	-110.4827800	12	541009.00	4944700.00				18.9	0.7087	BD	6.06	4.30	189.07	0.998
43	44.6545000	-110.4829700	12	540994.00	4944700.00				17.3	0.7092	UD	5.71	4.05	178.22	0.983
44	44.6544700	-110.4831200	12	540982.00	4944697.00				25.6	0.7097	UD	15.51	11.01	484.33	0.994
45	44.6544200	-110.4832700	12	540970.00	4944692.00				19.3	0.7102	UD	2.57	1.82	80.21	0.997
46	44.6543600	-110.4835400	12	540949.00	4944685.00				20.4	0.7107	UD	2.74	1.95	85.61	0.998
47	44.6543700	-110.4833300	12	540966.00	4944686.00				20.8	0.7111	UD	6.37	4.53	199.22	0.999
48	44.6543800	-110.4831500	12	540980.00	4944687.00				19.6	0.7116	UD	UD			
49	44.6543400	-110.4829300	12	540998.00	4944683.00				18.3	0.7121	UD	0.17	0.12	5.45	0.926

50	44.6543900	-110.4827300	12	541013.00	4944689.00	22.1	25.6	0.3	22.5	0.7126	UD		0.38	0.27	11.82	0.976
51	44.6543700	-110.4825300	12	541029.00	4944687.00				23.0	0.7104	UD		0.94	0.66	29.23	0.996
52	44.6543700	-110.4823200	12	541046.00	4944687.00				29.3	0.7082	UD		0.38	0.27	11.92	0.972
53	44.6543900	-110.4821400	12	541060.00	4944689.00					0.7061	UD		0.25	0.17	7.65	0.936
54	44.6543900	-110.4819500	12	541075.00	4944690.00				68.0	0.7039	UD		33.29	23.43	1031.05	0.998
55	44.6543700	-110.4817600	12	541090.00	4944688.00				50.2	0.7018	BD		0.54	0.38	16.75	0.984
56	44.6543800	-110.4815900	12	541104.00	4944688.00				50.0	0.6996	UD		6.91	4.83	212.57	0.999
57	44.6544100	-110.4814400	12	541116.00	4944691.00				32.9	0.6975	BD		6.86	4.78	210.39	0.999
58	44.6544000	-110.4813000	12	541127.00	4944691.00				34.5	0.6954	UD		4.65	3.23	142.32	0.997
59	44.6542700	-110.4812300	12	541132.00	4944676.00				42.8	0.6933	UD		5.24	3.64	159.95	0.993
60	44.6542400	-110.4814600	12	541114.00	4944673.00	31.2	21.6	0.1	75.0	0.6913	UD		25.59	17.69	778.35	0.998
61	44.6542500	-110.4816600	12	541098.00	4944673.00				39.7	0.6935	UD		10.73	7.44	327.43	0.999
62	44.6542400	-110.4818600	12	541083.00	4944673.00				59.4	0.6958	UD		10.08	7.01	308.60	0.999
63	44.6542600	-110.4820500	12	541067.00	4944675.00				52.3	0.6981	UD		13.94	9.73	428.18	0.995
64	44.6542600	-110.4822500	12	541051.00	4944675.00				44.0	0.7004	UD		9.49	6.64	292.30	0.997
65	44.6542600	-110.4824800	12	541033.00	4944674.00				24.9	0.7027	UD		2.07	1.45	63.85	0.998
66	44.6542500	-110.4826800	12	541017.00	4944673.00				24.4	0.7050	UD		0.28	0.20	8.71	0.971
67	44.6542300	-110.4828800	12	541001.00	4944671.00				20.8	0.7074	UD		0.92	0.65	28.74	0.997
68	44.6542300	-110.4831300	12	540981.00	4944671.00				18.4	0.7097	UD		3.02	2.14	94.31	0.999
69	44.6542500	-110.4833700	12	540962.00	4944673.00				22.2	0.7121	UD		2.16	1.54	67.62	0.998
70	44.6542500	-110.4835700	12	540946.00	4944672.00	21.3	46.5	0.9	18.3	0.7145	UD		0.48	0.35	15.24	0.987
71	44.6541200	-110.4825700	12	541026.00	4944659.00				24.0	0.7136	UD		0.55	0.39	17.31	0.995
72	44.6541000	-110.4822900	12	541048.00	4944657.00				22.2	0.7127	UD		0.27	0.19	8.39	0.946
73	44.6541200	-110.4820800	12	541065.00	4944659.00				25.4	0.7118	UD		0.70	0.50	22.00	0.996
74	44.6541100	-110.4818900	12	541080.00	4944658.00				32.9	0.7108	UD		6.51	4.63	203.62	0.999
75	44.6541100	-110.4817100	12	541094.00	4944659.00				23.9	0.7099	UD		1.48	1.05	46.29	0.998

76	44.6541100	-110.4815200	12	541109.00	4944658.00				51.2	0.7090	UD				17.48	12.39	545.33	0.996
77	44.6541100	-110.4813300	12	541124.00	4944659.00				37.6	0.7081	UD				17.70	12.53	551.48	0.978
78	44.6541200	-110.4811600	12	541138.00	4944659.00				41.8	0.7072	UD				6.93	4.90	215.74	0.995
79	44.6541900	-110.4810700	12	541145.00	4944667.00				56.6	0.7063	UD				37.35	26.38	1160.76	0.998
80	44.6540000	-110.4824500	12	541036.00	4944646.00	25.1	19.9	1.6	18.0	0.7054	UD				1.14	0.80	35.26	0.997
81	44.6539700	-110.4822200	12	541054.00	4944643.00				25.2	0.7047	UD				0.75	0.53	23.17	0.997
82	44.6539900	-110.4820000	12	541072.00	4944645.00				24.5	0.7040	UD				0.63	0.45	19.61	0.997
83	44.6539700	-110.4818100	12	541086.00	4944643.00				37.6	0.7033	UD				4.72	3.32	146.06	0.998
84	44.6539800	-110.4815900	12	541104.00	4944643.00				26.5	0.7026	UD				0.99	0.69	30.47	0.996
85	44.6539800	-110.4814000	12	541119.00	4944644.00				25.8	0.7019	UD				5.73	4.02	177.08	0.999
86	44.6540000	-110.4811800	12	541136.00	4944646.00				37.3	0.7012	UD				1.34	0.94	41.19	0.996
87	44.6539900	-110.4809900	12	541151.00	4944645.00				64.2	0.7005	0.16	0.11	3.80	1.000	18.27	12.80	563.10	0.983
88	44.6539900	-110.4807700	12	541169.00	4944645.00				78.7	0.6998	UD				72.21	50.53	2223.38	0.997
89	44.6540200	-110.4806100	12	541182.00	4944648.00				59.1	0.6991	UD				28.58	19.98	879.11	0.998
90	44.6537500	-110.4805900	12	541183.00	4944619.00	28.1	25.1	0.1	63.8	0.6984	UD				21.06	14.71	647.16	0.999
91	44.6537600	-110.4808200	12	541165.00	4944619.00				47.9	0.6999	UD				4.28	3.00	131.86	0.999
92	44.6537600	-110.4810400	12	541148.00	4944620.00				50.1	0.7014	UD				29.35	20.59	905.75	0.999
93	44.6537500	-110.4812100	12	541134.00	4944619.00				35.1	0.7029	UD				0.39	0.27	11.92	0.989
94	44.6537600	-110.4814400	12	541116.00	4944619.00				23.9	0.7044	UD				1.86	1.31	57.71	0.999
95	44.6536200	-110.4812100	12	541134.00	4944604.00				20.0	0.7059	UD				3.92	2.77	121.72	1.000
96	44.6536000	-110.4810000	12	541151.00	4944602.00				29.9	0.7074	UD				3.92	2.77	121.95	0.999
97	44.6536200	-110.4807700	12	541169.00	4944604.00				27.2	0.7089	UD				9.06	6.42	282.48	0.999
98	44.6536100	-110.4805400	12	541187.00	4944603.00				48.6	0.7105	UD				25.95	18.44	811.21	0.996
99	44.6536100	-110.4803300	12	541204.00	4944603.00				39.6	0.7120	UD				5.24	3.73	164.07	0.999
100	44.6536000	-110.4801300	12	541220.00	4944602.00	21.7	24.2	1.2	25.2	0.7135	UD				39.65	28.29	1244.86	0.998
101	44.6536100	-110.4799200	12	541236.00	4944603.00				24.0	0.7135	UD				2.59	1.85	81.19	0.999

102	44.6536200	-110.4797500	12	541250.00	4944605.00				29.9	0.7135	UD		5.37	3.83	168.50	0.998
103	44.6536100	-110.4795400	12	541267.00	4944604.00				33.8	0.7135	UD		5.50	3.93	172.71	0.999
104	44.6536400	-110.4793300	12	541283.00	4944607.00				29.8	0.7135	UD		3.31	2.36	104.05	0.978

Date: 2014/8/3

Weather: Sunny, became cloudy at 13:00, rained yesterday but the ground already dry

Pressure: 1025.06 hPa

Data Collector: Christie E. Torres, Peipei Lin

POINT	**LONGITUDE**	**LATITUDE**	**UTM ZONE**	**UTM LONGITUDE**	**UTM LATITUDE**	**AIR TEMP.** (°C)	**AIR RH** (%)	**WIND SPEED** (km/h)	**SOIL TEMP** (°C)	**ACK**	**H_2S** ($ppm\ s^{-1}$)	**H_2S R^2** ($mol\ m^{-2}\ d^{-1}$)	**CO_2** ($g\ m^{-2}\ d^{-1}$)	**CO_2** ($ppm\ s^{-1}$)	**CO_2 R^2** ($mol\ m^{-2}\ d^{-1}$)	($g\ m^{-2}\ d^{-1}$)
1	44.6557200	-110.4806600	12	541176.00	4944838.00	21.3	55.2	3.8	37.3	0.7126	BD			6.35	4.52	199.00	0.999
2	44.6557500	-110.4804200	12	541195.00	4944841.00				38.5	0.7118	UD			11.10	7.89	347.00	0.999
3	44.6558000	-110.4802800	12	541206.00	4944846.00				23.9	0.7110	UD			4.13	2.94	129.00	0.999
4	44.6558400	-110.4801100	12	541219.00	4944851.00				22.1	0.7102	UD			3.37	2.39	105.00	0.999
5	44.6558300	-110.4799000	12	541236.00	4944851.00				22.0	0.7094	UD			2.12	1.50	66.00	0.997
6	44.6558600	-110.4797200	12	541251.00	4944853.00				13.7	0.7086	UD			0.39	0.28	12.20	0.988
7	44.6558800	-110.4795500	12	541265.00	4944855.00				13.5	0.7078	UD			0.37	0.26	11.60	0.988
8	44.6559000	-110.4793100	12	541283.00	4944858.00				15.3	0.7070	BD			0.50	0.35	15.60	0.971
9	44.6559600	-110.4801600	12	541216.00	4944865.00				39.1	0.7062	BD			41.70	29.40	1290.00	0.986
10	44.6559200	-110.4803400	12	541202.00	4944860.00	24.3	35.2	1.1	50.1	0.7054	BD			32.90	23.20	1020.00	0.987
11	44.6558900	-110.4804900	12	541190.00	4944857.00				44.7	0.7053	UD			163.00	115.00	5060.00	0.998
12	44.6560900	-110.4802000	12	541212.00	4944879.00				27.1	0.7052	UD			11.90	8.37	368.00	0.999
13	44.6560700	-110.4804000	12	541197.00	4944876.00				25.9	0.7051	UD			7.41	5.23	230.00	0.999
14	44.6560700	-110.4806000	12	541181.00	4944876.00				46.5	0.7050	UD			11.30	7.97	351.00	0.999
15	44.6562300	-110.4802400	12	541209.00	4944894.00				22.8	0.7049	UD			0.84	0.59	26.10	0.989

16	44.6562200	-110.4804400	12	541193.00	4944894.00				19.9	0.7047	UD	0.29	0.21	9.02	0.979
17	44.6563900	-110.4805000	12	541188.00	4944912.00				16.2	0.7046	UD	0.64	0.45	19.70	0.992
18	44.6562700	-110.4800900	12	541221.00	4944899.00				18.5	0.7045	UD	0.69	0.49	21.40	0.964
19	44.6563200	-110.4798600	12	541239.00	4944905.00				14.7	0.7044	UD	0.46	0.33	14.40	0.985
20	44.6563200	-110.4796700	12	541255.00	4944904.00	24.8	38.0	1.0	15.8	0.7043	UD	0.65	0.46	20.10	0.988
21	44.6561500	-110.4800100	12	541228.00	4944886.00				17.6	0.7037	UD	0.28	0.19	8.51	0.969
22	44.6562200	-110.4798100	12	541243.00	4944894.00				18.5	0.7031	UD	0.31	0.22	9.51	0.971
23	44.6562300	-110.4796500	12	541256.00	4944895.00				16.9	0.7025	UD	0.31	0.22	9.66	0.981
24	44.6562900	-110.4794700	12	541270.00	4944902.00				15.0	0.7019	UD	0.19	0.14	5.94	0.947
25	44.6563200	-110.4792800	12	541285.00	4944904.00				13.6	0.7013	UD	0.26	0.19	8.14	0.970
26	44.6561200	-110.4793800	12	541278.00	4944882.00				21.4	0.7007	UD	0.62	0.44	19.10	0.987
27	44.6562000	-110.4791300	12	541297.00	4944892.00				14.9	0.7002	UD	0.11	0.07	3.25	0.883
28	44.6561100	-110.4795900	12	541261.00	4944881.00				20.2	0.6996	UD	1.05	0.73	32.20	0.985
29	44.6560800	-110.4797300	12	541250.00	4944878.00				17.3	0.6990	UD	0.31	0.22	9.52	0.981
30	44.6560200	-110.4799100	12	541235.00	4944872.00	27.3	8.3	0.9	17.0	0.6984	UD	0.37	0.26	11.50	0.984
31	44.6555200	-110.4808000	12	541166.00	4944816.00				21.4	0.6991	UD	UD			
32	44.6555800	-110.4805100	12	541188.00	4944822.00				35.6	0.6998	UD	4.53	3.17	139.00	0.999
33	44.6556300	-110.4803200	12	541204.00	4944827.00				25.6	0.7005	UD	6.57	4.60	202.00	0.999
34	44.6556300	-110.4800800	12	541222.00	4944828.00				21.6	0.7012	UD	7.73	5.42	238.00	0.999
35	44.6556600	-110.4799100	12	541236.00	4944832.00				22.0	0.7019	UD	0.13	0.09	4.09	0.931
36	44.6556900	-110.4797200	12	541251.00	4944834.00				19.4	0.7026	UD	0.32	0.22	9.79	0.953
37	44.6557400	-110.4795500	12	541264.00	4944840.00				15.7	0.7033	UD	0.69	0.49	21.40	0.971
38	44.6555700	-110.4795900	12	541261.00	4944822.00				20.4	0.7040	UD	0.63	0.44	19.40	0.985
39	44.6555600	-110.4797900	12	541245.00	4944820.00				17.6	0.7047	UD	0.24	0.17	7.33	0.939
40	44.6555500	-110.4800000	12	541229.00	4944819.00	24.3	39.4	0.1	19.6	0.7054	UD	1.00	0.71	31.20	0.985
41	44.6554900	-110.4801900	12	541214.00	4944813.00				37.8	0.7056	BD	10.60	7.44	328.00	0.999

42	44.6554600	-110.4803700	12	541199.00	4944809.00				39.8	0.7057	BD	12.20	8.57	377.00	0.993
43	44.6554200	-110.4806000	12	541181.00	4944805.00				38.4	0.7059	BD	8.24	5.82	256.00	0.997
44	44.6553800	-110.4808500	12	541161.00	4944799.00				46.3	0.7060	BD	10.30	7.27	320.00	0.995
45	44.6553100	-110.4810200	12	541148.00	4944791.00				38.4	0.7062	BD	12.90	9.10	400.00	0.997
46	44.6552000	-110.4811300	12	541139.00	4944779.00				57.7	0.7063	UD	6.35	4.49	197.00	0.970
47	44.6552300	-110.4808700	12	541160.00	4944783.00				54.0	0.7064	BD	20.00	14.10	622.00	0.999
48	44.6552900	-110.4806600	12	541177.00	4944789.00				90.1	0.7066	BD	24.90	17.60	773.00	0.997
49	44.6553000	-110.4804800	12	541191.00	4944791.00				53.2	0.7067	UD	14.90	10.50	462.00	0.998
50	44.6553700	-110.4802900	12	541206.00	4944799.00	23.7	32.6	0.9	36.3	0.7069	BD	15.60	11.00	486.00	0.999
51	44.6553700	-110.4801200	12	541220.00	4944799.00				32.5	0.7065	BD	5.12	3.62	159.00	0.999
52	44.6554100	-110.4799700	12	541231.00	4944803.00				20.7	0.7062	UD	3.24	2.29	101.00	0.999
53	44.6554200	-110.4798100	12	541244.00	4944805.00				24.2	0.7059	UD	5.83	4.12	181.00	0.999
54	44.6554300	-110.4796700	12	541255.00	4944806.00				19.4	0.7055	UD	0.41	0.29	12.70	0.986
55	44.6553600	-110.4795300	12	541266.00	4944798.00				19.1	0.7052	UD	0.55	0.39	16.90	0.990
56	44.6552700	-110.4797400	12	541249.00	4944788.00				32.0	0.7049	UD	18.60	13.10	576.00	0.994
57	44.6552500	-110.4799500	12	541233.00	4944786.00				23.1	0.7045	UD	1.37	0.97	42.50	0.998
58	44.6552300	-110.4801500	12	541217.00	4944783.00				31.9	0.7042	UD	2.27	1.60	70.30	0.999
59	44.6551800	-110.4803700	12	541200.00	4944778.00				39.5	0.7039	UD	12.50	8.80	387.00	0.999
60	44.6551500	-110.4805800	12	541183.00	4944774.00	25.1	36.8	1.0	35.6	0.7036	UD	7.11	5.00	220.00	0.998
61	44.6551400	-110.4807500	12	541170.00	4944773.00				34.2	0.7037	UD	7.70	5.42	238.00	0.999
62	44.6550800	-110.4809400	12	541154.00	4944766.00				57.2	0.7038	UD	41.30	29.00	1280.00	0.993
63	44.6549800	-110.4808200	12	541164.00	4944756.00				44.0	0.7040	UD	11.80	8.32	366.00	0.999
64	44.6550200	-110.4806600	12	541177.00	4944760.00				40.2	0.7041	UD	21.70	15.30	673.00	0.997
65	44.6550400	-110.4804800	12	541191.00	4944762.00				29.5	0.7043	UD	1.98	1.40	61.50	0.994
66	44.6550700	-110.4802600	12	541208.00	4944766.00				22.8	0.7044	UD	1.16	0.82	36.00	0.995
67	44.6550900	-110.4800800	12	541223.00	4944768.00				26.0	0.7045	UD	1.26	0.89	38.90	0.997

68	44.6551200	-110.4798800	12	541239.00	4944771.00				24.4	0.7047	UD	2.60	1.83	80.70	0.999
69	44.6551500	-110.4796700	12	541255.00	4944774.00				30.2	0.7048	UD	6.55	4.62	203.00	0.998
70	44.6551500	-110.4794900	12	541270.00	4944775.00	24.5	40.2	0.9	20.8	0.7050	UD	0.37	0.26	11.50	0.990
71	44.6551900	-110.4793400	12	541281.00	4944780.00				35.0	0.7038	UD	58.70	41.30	1820.00	0.997
72	44.6552700	-110.4791700	12	541295.00	4944789.00				21.8	0.7027	UD	0.56	0.39	17.20	0.993
73	44.6550500	-110.4793600	12	541280.00	4944764.00				32.0	0.7016	UD	0.15	0.11	4.77	0.913
74	44.6550400	-110.4795300	12	541267.00	4944762.00				24.9	0.7005	BD	0.98	0.69	30.30	0.996
75	44.6549900	-110.4797400	12	541250.00	4944757.00				24.2	0.6993	UD	1.01	0.71	31.10	0.990
76	44.6549800	-110.4799300	12	541234.00	4944756.00				27.3	0.6982	UD	5.04	3.52	155.00	0.999
77	44.6549600	-110.4801300	12	541219.00	4944753.00				22.3	0.6971	UD	0.47	0.32	14.30	0.915
78	44.6549300	-110.4803100	12	541204.00	4944750.00				19.1	0.6960	UD	UD			
79	44.6548900	-110.4804900	12	541190.00	4944745.00				32.0	0.6949	UD	9.28	6.45	284.00	0.986
80	44.6547500	-110.4803300	12	541203.00	4944730.00	29.3	24.7	0.1	32.8	0.6938	UD	11.20	7.77	342.00	0.979
81	44.6547800	-110.4801300	12	541219.00	4944733.00				23.3	0.6943	UD	4.21	2.92	129.00	0.998
82	44.6548200	-110.4799500	12	541234.00	4944738.00				31.6	0.6948	UD	10.80	7.50	330.00	0.996
83	44.6548400	-110.4797500	12	541249.00	4944740.00				25.3	0.6953	UD	3.73	2.60	114.00	0.999
84	44.6548500	-110.4796200	12	541259.00	4944741.00				35.5	0.6958	UD	2.97	2.07	91.00	0.998
85	44.6547100	-110.4798000	12	541246.00	4944725.00				19.4	0.6963	UD	1.25	0.87	38.30	0.998
86	44.6546600	-110.4800500	12	541226.00	4944720.00				28.8	0.6968	UD	6.61	4.60	203.00	0.999
87	44.6545800	-110.4797400	12	541250.00	4944711.00				21.6	0.6973	UD	2.12	1.48	65.00	0.998
88	44.6549300	-110.4793700	12	541279.00	4944750.00				29.9	0.6978	UD	0.25	0.18	7.76	0.968
89	44.6549500	-110.4791700	12	541295.00	4944753.00				53.2	0.6984	UD	30.10	21.00	925.00	0.970
90	44.6548200	-110.4791200	12	541299.00	4944739.00	27.1	30.8	0.9	82.0	0.6989	UD	62.90	44.00	1930.00	0.998
91	44.6547800	-110.4793500	12	541281.00	4944734.00				31.2	0.6987	UD	2.07	1.45	63.70	0.999
92	44.6547600	-110.4795400	12	541266.00	4944731.00				26.5	0.6985	UD	1.45	1.01	44.60	0.999
93	44.6546100	-110.4795600	12	541264.00	4944714.00				22.9	0.6982	UD	0.80	0.56	24.50	0.996

94	44.6546300	-110.4793700	12	541280.00	4944717.00				30.2	0.6980	UD	6.14	4.29	189.00	0.999
95	44.6546900	-110.4791500	12	541297.00	4944723.00				35.1	0.6978	UD	5.51	3.84	169.00	0.999
96	44.6545200	-110.4789500	12	541313.00	4944705.00				26.2	0.6976	UD	2.91	2.03	89.20	0.999
97	44.6544900	-110.4791900	12	541294.00	4944701.00				22.8	0.6974	UD	0.98	0.68	30.10	0.997
98	44.6544600	-110.4793600	12	541281.00	4944698.00				24.9	0.6972	UD	0.59	0.41	18.20	0.993
99	44.6544700	-110.4795300	12	541267.00	4944699.00	27.9	30.2	0.9	24.2	0.6970	UD	0.63	0.44	19.20	0.988

Date: 2014/8/4

Weather: Cloudy, few rain drops and later rains. *Surface soil is dry but wet when goes deeper*

Pressure: 1026.75 hPa

Data Collector: Christie E. Torres, Peipei Lin

POINT	**LONGITUDE**	**LATITUDE**	**UTM ZONE**	**UTM LONGITUDE**	**UTM LATITUDE**	**AIR TEMP.** (°C)	**AIR RH** (%)	**WIND SPEED** (km/h)	**SOIL TEMP** (°C)	**ACK**	**H_2S** ($ppm\ s^{-1}$) ($mol\ m^{-2}\ d^{-1}$)	**H_2S R^2** ($g\ m^{-2}\ d^{-1}$)	**CO_2** ($ppm\ s^{-1}$)	($mol\ m^{-2}\ d^{-1}$)	**CO_2 R^2** ($g\ m^{-2}\ d^{-1}$)
1	44.6539000	-110.4788800	12	541319.00	4944636.00	12.9	99.9	1.1	24.4	0.7348	UD		8.53	6.27	276.00	0.999
2	44.6540600	-110.4789400	12	541314.00	4944653.00				16.1	0.7341	BD		3.04	2.23	98.20	0.999
3	44.6542000	-110.4789600	12	541312.00	4944670.00				17.6	0.7335	BD		0.11	0.08	3.46	0.341
4	44.6543400	-110.4789500	12	541313.00	4944686.00				17.9	0.7329	BD		0.23	0.17	7.46	0.926
5	44.6546700	-110.4789700	12	541311.00	4944722.00				32.3	0.7323	BD		4.40	3.22	142.00	0.907
6	44.6548400	-110.4789900	12	541310.00	4944741.00				35.2	0.7316	BD		10.90	7.95	350.00	0.992
7	44.6549700	-110.4789800	12	541310.00	4944756.00				53.7	0.7310	BD		15.50	11.30	498.00	0.999
8	44.6552800	-110.4790100	12	541307.00	4944790.00				26.9	0.7304	UD		0.21	0.15	6.65	0.431
9	44.6554800	-110.4790300	12	541306.00	4944812.00				19.3	0.7298	BD		0.61	0.45	19.70	0.992
10	44.6556400	-110.4790700	12	541302.00	4944830.00	15.1	70.1	3.7	18.5	0.7292	BD		0.25	0.19	8.16	0.962
11	44.6557100	-110.4789000	12	541316.00	4944837.00				20.5	0.7289	BD		0.82	0.60	26.30	0.993
12	44.6555500	-110.4788600	12	541319.00	4944819.00				19.2	0.7286	BD		0.11	0.08	3.63	0.735

13	44.6553900	-110.4788500	12	541320.00	4944802.00				47.6	0.7283	BD		25.30	18.40	810.00	0.999
14	44.6552500	-110.4788500	12	541320.00	4944786.00				23.9	0.7279	BD		3.06	2.23	98.10	0.890
15	44.6551300	-110.4788400	12	541321.00	4944772.00				23.4	0.7276	UD		0.58	0.42	18.60	0.788
16	44.6550000	-110.4788400	12	541321.00	4944758.00				33.4	0.7273	BD		5.46	3.97	175.00	0.761
17	44.6548900	-110.4787900	12	541325.00	4944746.00				37.8	0.7270	BD		10.50	7.63	336.00	0.993
18	44.6547500	-110.4787900	12	541325.00	4944731.00				30.1	0.7267	BD		0.49	0.36	15.70	0.291
19	44.6546100	-110.4787900	12	541326.00	4944715.00				22.8	0.7264	BD		9.93	7.21	317.00	0.999
20	44.6544800	-110.4787900	12	541325.00	4944701.00	16.3	63.2	1.3	17.9	0.7261	BD		0.08	0.06	2.52	0.275
21	44.6543500	-110.4787500	12	541329.00	4944686.00				20.6	0.7261	UD		1.45	1.05	46.30	0.951
22	44.6542200	-110.4787300	12	541330.00	4944671.00				19.3	0.7261	BD		0.90	0.65	28.60	0.994
23	44.6540700	-110.4787000	12	541333.00	4944655.00				18.4	0.7261	UD		0.89	0.65	28.60	0.992
24	44.6539300	-110.4787100	12	541332.00	4944640.00				22.7	0.7261	BD		4.78	3.47	153.00	0.999

Date: 2014/8/10

Weather: Sunny, surface of soil is dry, but the deep soil a litte wet.

Pressure: 1025.40 hPa

Data Collectore: Christie E. Torres, Peipei Lin

Notes: the air temperature, air relative humidity and wind speed are measured three times and the average was used for the calculation of ACK.

POINT	**LONGITUDE**	**LATITUDE**	**UTM ZONE**	**UTM LONGITUDE**	**UTM LATITUDE**	**AIR TEMP.**	**AIR RH**	**WIND SPEED**	**SOIL TEMP**	**ACK**	**H_2S**	**H_2S R^2**	**CO_2**		**CO_2 R^2**
						(°C)	(%)	(km/h)	(°C)		(ppm s^{-1}) (mol m^{-2} d^{-1}) (g m^{-2} d^{-1})		(ppm s^{-1}) (mol m^{-2} d^{-1}) (g m^{-2} d^{-1})		
1	44.6539800	-110.4785400	12	541344.00	4944663.00	27.5	24.6	0.9	34.0	0.6982	UD		6.96	4.86	214.00	0.999
2	44.6541400	-110.4785600	12	541344.00	4944679.00				32.8	0.6982	BD		8.64	6.03	265.00	0.999
3	44.6542800	-110.4785600	12	541343.00	4944696.00				23.9	0.6982	UD		1.48	1.03	45.50	0.998
4	44.6544400	-110.4785700	12	541342.00	4944711.00				24.3	0.6982	BD		0.08	0.06	2.52	0.794
5	44.6545700	-110.4785800	12	541341.00	4944728.00				20.5	0.6982	UD		0.34	0.24	10.40	0.976

6	44.6547300	-110.4785900	12	541339.00	4944747.00	22.6	0.6982	BD	0.83	0.58	25.40	0.996
7	44.6549000	-110.4786100	12	541339.00	4944763.00	22.9	0.6982	BD	5.66	3.95	174.00	0.999
8	44.6550400	-110.4786100	12	541338.00	4944779.00	23.9	0.6982	UD	0.76	0.53	23.20	0.997
9	44.6551900	-110.4786300	12	541334.00	4944796.00	29.9	0.6982	UD	7.72	5.39	237.00	0.999
10	44.6553400	-110.4786800	12	541332.00	4944814.00	36.2	0.6982	UD	16.00	11.20	491.00	0.999
11	44.6555000	-110.4787000	12	541331.00	4944830.00	48.9	0.6982	UD	14.90	10.40	457.00	0.998
12	44.6556400	-110.4787100	12	541349.00	4944841.00	26.1	0.6982	UD	0.43	0.30	13.30	0.993
13	44.6557400	-110.4784800	12	541365.00	4944852.00	29.2	0.6982	UD	5.77	4.03	177.00	0.998
14	44.6558400	-110.4782700	12	541377.00	4944864.00	31.6	0.6982	UD	6.38	4.46	196.00	0.999
15	44.6559500	-110.4781300	12	541394.00	4944882.00	31.5	0.6982	UD	6.90	4.82	212.00	0.999
16	44.6561000	-110.4779100	12	541407.00	4944892.00	33.6	0.6982	UD	6.62	4.62	203.00	0.999
17	44.6562000	-110.4777500	12	541430.00	4944889.00	27.2	0.6982	UD	UD			
18	44.6561700	-110.4774500	12	541414.00	4944877.00	61.3	0.6982	UD	20.30	14.20	625.00	0.994
19	44.6560600	-110.4776600	12	541402.00	4944865.00	39.5	0.6982	UD	0.47	0.33	14.40	0.978
20	44.6559500	-110.4778100	12	541388.00	4944854.00	36.1	0.6982	UD	11.70	8.18	360.00	0.999
21	44.6558600	-110.4779800	12	541376.00	4944845.00	25.1	0.6982	UD	3.38	2.36	104.00	0.999
22	44.6557800	-110.4781400	12	541361.00	4944835.00	36.9	0.6982	UD	14.30	9.96	438.00	0.983
23	44.6556800	-110.4783300	12	541347.00	4944823.00	28.3	0.6982	UD	3.57	2.49	110.00	0.999
24	44.6555800	-110.4785100	12	541346.00	4944823.00	26.6	0.6982	UD	0.56	0.39	17.30	0.992
25	44.6554000	-110.4785300	12	541353.00	4944810.00	47.3	0.6982	UD	25.30	17.70	777.00	0.999
26	44.6554600	-110.4784400	12	541370.00	4944821.00	22.7	0.6982	UD	3.12	2.18	95.80	0.999
27	44.6555600	-110.4782200	12	541385.00	4944832.00	24.9	0.6982	UD	2.61	1.82	80.10	0.998
28	44.6556600	-110.4780300	12	541398.00	4944842.00	43.0	0.6982	UD	21.10	14.70	648.00	0.979
29	44.6557500	-110.4778600	12	541411.00	4944854.00	32.5	0.6982	UD	2.91	2.03	89.30	0.998
30	44.6558600	-110.4777000	12	541425.00	4944862.00	38.0	0.6982	UD	8.39	5.86	258.00	0.999
31	44.6559300	-110.4775300	12	541437.00	4944874.00	57.8	0.6982	UD	31.90	22.30	981.00	0.999

32	44.6560300	-110.4773700	12	541420.00	4944791.00	50.6	0.6982	UD	26.70	18.60	819.00	0.999
33	44.6552900	-110.4775800	12	541424.00	4944769.00	65.6	0.6982	BD	81.20	56.70	2490.00	0.952
34	44.6550900	-110.4775400	12	541424.00	4944753.00	36.3	0.6982	BD	8.78	6.13	270.00	0.976
35	44.6549500	-110.4775400	12	541427.00	4944733.00	28.9	0.6982	UD	2.04	1.42	62.60	0.997
36	44.6547700	-110.4775100	12	541411.00	4944742.00	25.7	0.6982	UD	2.46	1.71	75.40	0.999
37	44.6548400	-110.4777100	12	541408.00	4944758.00	34.7	0.6982	UD	12.60	8.82	388.00	0.999
38	44.6549900	-110.4777400	12	541408.00	4944777.00	46.5	0.6982	UD	22.90	16.00	703.00	0.999
39	44.6551600	-110.4777400	12	541407.00	4944789.00	85.2	0.6982	BD	107.00	74.60	3280.00	0.999
40	44.6552700	-110.4777500	12	541407.00	4944804.00	60.1	0.6982	UD	20.40	14.30	628.00	0.998
41	44.6554000	-110.4777500	12	541394.00	4944787.00	50.2	0.6982	UD	17.90	12.50	549.00	0.988
42	44.6552500	-110.4779200	12	541394.00	4944773.00	40.2	0.6982	UD	6.95	4.85	214.00	0.911
43	44.6551300	-110.4779300	12	541395.00	4944757.00	55.9	0.6982	UD	27.40	19.10	841.00	0.998
44	44.6549900	-110.4779100	12	541392.00	4944742.00	49.1	0.6982	UD	24.00	16.70	736.00	0.999
45	44.6548500	-110.4779500	12	541380.00	4944752.00	46.8	0.6982	UD	19.00	13.20	582.00	0.991
46	44.6549400	-110.4780900	12	541382.00	4944768.00	60.4	0.6982	UD	102.00	70.90	3120.00	0.985
47	44.6550900	-110.4780700	12	541367.00	4944756.00	92.3	0.6982	UD	145.00	101.00	4450.00	0.999
48	44.6549800	-110.4782700	12	541368.00	4944744.00	51.4	0.6982	BD	34.60	24.10	1060.00	0.999
49	44.6548600	-110.4782500	12	541367.99	4944747.70	30.6	0.6982	UD	7.30	5.09	224.00	0.999
50	44.6546200	-110.4783800	12	541358.00	4944716.00	33.3	0.6982	UD	7.06	4.93	217.00	0.998
51	44.6546200	-110.4783800	12	541356.00	4944736.00	36.5	0.6982	UD	5.44	3.79	167.00	1.000
52	44.6547900	-110.4784000	12	541353.00	4944751.00	41.5	0.6982	UD	8.68	6.06	267.00	0.999
53	44.6549300	-110.4784400	12	541348.00	4944767.00	26.9	0.6982	UD	UD			
54	44.6550700	-110.4785000	12	541351.00	4944785.00	28.3	0.6982	UD	0.08	0.06	2.58	0.841
55	44.6552400	-110.4784600	12	541359.00	4944679.00	27.0	0.6982	UD	0.35	0.24	10.60	0.986
56	44.6542800	-110.4783600	12	541376.00	4944680.00	27.2	0.6982	UD	1.77	1.24	54.50	0.997
57	44.6542900	-110.4781500	12	541395.00	4944682.00	35.4	0.6982	UD	1.34	0.93	41.00	0.995

58	44.6543100	-110.4779100	12	541411.00	4944681.00			49.6	0.6982	UD	14.80	10.30	455.00	0.999
59	44.6542900	-110.4777100	12	541424.00	4944683.00			31.0	0.6982	UD	5.74	4.01	176.00	0.999
60	44.6543100	-110.4775500	12	541439.00	4944680.00			37.0	0.6982	UD	9.06	6.33	278.00	0.997
61	44.6542900	-110.4773500	12	541456.00	4944678.00			39.5	0.6982	UD	10.60	7.43	327.00	0.999
62	44.6542700	-110.4771500	12	541473.00	4944679.00			41.5	0.6982	UD	19.40	13.50	596.00	0.998
63	44.6542700	-110.4769300	12	541490.00	4944678.00			35.6	0.6982	UD	9.79	6.83	301.00	0.998
64	44.6542600	-110.4767200	12	541506.00	4944679.00			24.9	0.6982	UD	1.13	0.79	34.70	0.993
65	44.6542700	-110.4765200	12	541523.00	4944677.00			23.8	0.6982	UD	0.25	0.17	7.61	0.950

Date: 2014/8/11

Weather: Sunny

Pressure: 1029.46 hPa

Data Collector: Peipei Lin

Notes: the air temperature, air relative humidity and wind speed are measured by Christie at different locations compared to this dataset. Thus the average of Christie's air temperature, humidity and wind speed was used

POINT	**LONGITUDE**	**LATITUDE**	**UTM ZONE**	**UTM LONGITUDE**	**UTM LATITUDE**	**AIR TEMP.** (°C)	**AIR RH** (%)	**WIND SPEED** (km/h)	**SOIL TEMP** (°C)	**ACK**	**H_2S** (ppm s^{-1})	**H_2S R^2**	**CO_2** (mol m^{-2} d^{-1})	**CO_2** (ppm s^{-1})	**CO_2** (g m^{-2} d^{-1})	**CO_2 R^2**
1	44.6541300	-110.4763500	12	541519.00	4944663.00	26.0	33.8	1.8	15.6	0.7044	UD		0.20	0.14	6.20	0.956
2	44.6541400	-110.4765700	12	541502.00	4944664.00				16.1	0.7044	UD		1.00	0.70	30.90	0.985
3	44.6541300	-110.4767600	12	541487.00	4944663.00				24.0	0.7044	UD		1.32	0.93	40.90	0.992
4	44.6541400	-110.4769700	12	541470.00	4944664.00				35.0	0.7044	UD		13.80	9.74	428.00	0.999
5	44.6541500	-110.4771700	12	541454.00	4944664.00				47.7	0.7044	UD		28.00	19.70	868.00	0.998
6	44.6541600	-110.4773700	12	541438.00	4944666.00				40.6	0.7044	UD		15.80	11.10	489.00	0.999
7	44.6541500	-110.4775600	12	541423.00	4944665.00				40.9	0.7044	UD		13.40	9.43	415.00	0.999
8	44.6541500	-110.4777600	12	541407.00	4944664.00				45.1	0.7044	UD		16.60	11.70	513.00	0.999

9	44.6541600	-110.4779300	12	541394.00	4944666.00	54.6	0.7044	UD				48.10	33.90	1490.00	0.999
10	44.6541700	-110.4781300	12	541378.00	4944667.00	41.2	0.7044	UD				15.50	10.90	482.00	0.998
11	44.6541700	-110.4783700	12	541359.00	4944666.00	35.2	0.7044	UD				4.79	3.37	148.00	0.999
12	44.6540400	-110.4783300	12	541362.00	4944652.00	38.5	0.7044	UD				15.60	11.00	483.00	0.999
13	44.6540400	-110.4781300	12	541378.00	4944653.00	50.4	0.7044	UD				16.30	11.50	505.00	0.996
14	44.6540300	-110.4779200	12	541395.00	4944651.00	55.9	0.7044	UD				12.20	8.57	377.00	0.999
15	44.6540400	-110.4777300	12	541410.00	4944652.00	62.9	0.7044	UD				16.20	11.40	502.00	0.999
16	44.6540100	-110.4775400	12	541425.00	4944649.00	46.0	0.7044	UD				28.20	19.90	875.00	0.999
17	44.6540100	-110.4773600	12	541439.00	4944649.00	40.0	0.7044	UD				17.40	12.20	538.00	0.999
18	44.6539900	-110.4771800	12	541454.00	4944647.00	36.3	0.7044	UD				15.30	10.80	475.00	0.999
19	44.6539900	-110.4770000	12	541468.00	4944647.00	40.8	0.7044	UD				16.40	11.50	507.00	0.999
20	44.6540000	-110.4768000	12	541483.00	4944648.00	32.6	0.7044	UD				11.70	8.21	361.00	0.999
21	44.6539900	-110.4766100	12	541499.00	4944648.00	18.7	0.7044	UD				1.40	0.99	43.50	0.998
22	44.6540000	-110.4763800	12	541517.00	4944649.00	17.9	0.7044	UD				0.77	0.54	23.90	0.986
23	44.6538600	-110.4766900	12	541492.00	4944633.00	21.2	0.7044	UD				1.34	0.94	41.50	0.990
24	44.6538600	-110.4768800	12	541477.00	4944633.00	21.0	0.7044	UD				5.77	4.06	179.00	0.999
25	44.6538600	-110.4770700	12	541462.00	4944633.00	26.2	0.7044	UD				9.80	6.91	304.00	0.999
26	44.6538600	-110.4772400	12	541449.00	4944633.00	31.8	0.7044	UD				10.90	7.70	339.00	0.999
27	44.6538800	-110.4774400	12	541433.00	4944634.00	44.9	0.7044	UD				10.90	7.66	337.00	0.999
28	44.6539000	-110.4776300	12	541418.00	4944637.00	50.8	0.7044	UD				5.66	3.99	176.00	0.999
29	44.6538900	-110.4777900	12	541405.00	4944635.00	64.0	0.7044	0.23	0.16	5.41	0.999	129.00	90.50	3980.00	0.991
30	44.6539300	-110.4780200	12	541387.00	4944640.00	52.5	0.7044	0.16	0.11	3.74	0.798	42.00	29.60	1300.00	0.998
31	44.6538700	-110.4781900	12	541373.00	4944634.00	54.9	0.7044	0.08	0.06	1.96	0.922	29.70	20.90	919.00	0.999
32	44.6538900	-110.4784000	12	541357.00	4944635.00	45.8	0.7044	UD				16.50	11.70	513.00	0.999
33	44.6538700	-110.4785800	12	541342.00	4944634.00	32.0	0.7044	UD				7.61	5.36	236.00	0.999
34	44.6538000	-110.4789100	12	541317.00	4944625.00	29.6	0.7044	UD				4.81	3.39	149.00	0.999

35	44.6536500	-110.4788700	12	541320.00	4944608.00	20.8	0.7044	UD	1.71	1.20	52.90	0.998
36	44.6536700	-110.4787400	12	541330.00	4944611.00	24.4	0.7044	UD	6.94	4.89	215.00	0.999
37	44.6538000	-110.4787500	12	541329.00	4944625.00	24.8	0.7044	UD	1.25	0.88	38.70	0.997
38	44.6537300	-110.4786000	12	541341.00	4944617.00	55.8	0.7044	UD	37.00	26.10	1150.00	0.992
39	44.6536100	-110.4785700	12	541344.00	4944604.00	48.8	0.7044	UD	22.40	15.80	694.00	0.999
40	44.6534600	-110.4785500	12	541346.00	4944588.00	33.9	0.7044	UD	17.40	12.30	540.00	0.945
41	44.6533200	-110.4785200	12	541347.00	4944572.00	22.6	0.7044	UD	7.86	5.54	244.00	0.999
42	44.6532000	-110.4785400	12	541346.00	4944559.00	22.0	0.7044	UD	2.24	1.58	69.50	0.998
43	44.6530600	-110.4785600	12	541345.00	4944543.00	21.2	0.7044	UD	0.41	0.29	12.80	0.976
44	44.6529200	-110.4785800	12	541343.00	4944527.00	20.0	0.7044	UD	0.27	0.19	8.45	0.963
45	44.6528000	-110.4785400	12	541346.00	4944514.00	24.5	0.7044	UD	0.24	0.17	7.44	0.959
46	44.6528000	-110.4783500	12	541361.00	4944514.00	20.3	0.7044	UD	0.67	0.47	20.80	0.988
47	44.6529400	-110.4783500	12	541362.00	4944530.00	25.5	0.7044	UD	0.68	0.48	21.10	0.982
48	44.6530800	-110.4783500	12	541362.00	4944546.00	33.0	0.7044	UD	20.40	14.40	633.00	0.999
49	44.6532500	-110.4783400	12	541362.00	4944564.00	61.2	0.7044	UD	5.55	3.91	172.00	0.999
50	44.6533800	-110.4783400	12	541362.00	4944578.00	53.6	0.7044	UD	30.00	21.10	930.00	0.999
51	44.6535100	-110.4783500	12	541361.00	4944593.00	48.6	0.7044	UD	19.10	13.40	590.00	0.999
52	44.6536400	-110.4783300	12	541362.00	4944607.00	60.8	0.7044	UD	60.50	42.60	1870.00	0.992
53	44.6537600	-110.4783200	12	541363.00	4944621.00	60.0	0.7044	UD	43.20	30.40	1340.00	0.999
54	44.6542400	-110.4760900	12	541539.00	4944675.00	19.9	0.7044	UD	0.84	0.60	26.20	0.989
55	44.6541300	-110.4761200	12	541537.00	4944664.00	19.8	0.7044	UD	0.33	0.24	10.40	0.948
56	44.6540000	-110.4761200	12	541537.00	4944648.00	17.7	0.7044	UD	0.46	0.33	14.40	0.985
57	44.6538700	-110.4761400	12	541536.00	4944634.00	18.1	0.7044	UD	0.34	0.24	10.50	0.975
58	44.6537200	-110.4761300	12	541537.00	4944618.00	16.7	0.7044	UD	0.27	0.19	8.45	0.977
59	44.6535700	-110.4761500	12	541535.00	4944601.00	20.0	0.7044	UD	0.41	0.29	12.80	0.986
60	44.6534400	-110.4761700	12	541534.00	4944587.00	20.4	0.7044	UD	0.13	0.09	4.10	0.936

61	44.6533000	-110.4761800	12	541533.00	4944571.00	22.1	0.7044	UD	UD				
62	44.6531600	-110.4761700	12	541534.00	4944556.00	20.4	0.7044	UD	0.07	0.05	2.02	0.824	
63	44.6530400	-110.4762000	12	541532.00	4944542.00	19.6	0.7044	UD	UD				
64	44.6529200	-110.4762500	12	541528.00	4944528.00	17.1	0.7044	UD	0.11	0.07	3.29	0.834	
65	44.6527800	-110.4762700	12	541526.00	4944514.00	18.0	0.7044	UD	2.52	1.77	78.00	0.999	
66	44.6526500	-110.4762900	12	541525.00	4944498.00	18.4	0.7044	UD	4.93	3.47	153.00	0.992	
67	44.6525100	-110.4762700	12	541526.00	4944483.00	18.7	0.7044	UD	0.69	0.49	21.40	0.986	
68	44.6525000	-110.4764900	12	541509.00	4944482.00	20.6	0.7044	UD	0.76	0.54	23.70	0.993	
69	44.6526300	-110.4764800	12	541510.00	4944496.00	26.2	0.7044	UD	57.80	40.70	1790.00	0.998	
70	44.6527800	-110.4765100	12	541508.00	4944514.00	35.6	0.7044	UD	8.64	6.08	268.00	0.999	
71	44.6529300	-110.4764700	12	541511.00	4944530.00	19.7	0.7044	UD	1.72	1.21	53.40	0.997	
72	44.6530700	-110.4764600	12	541512.00	4944545.00	19.8	0.7044	UD	0.55	0.39	17.10	0.989	
73	44.6532000	-110.4764400	12	541513.00	4944560.00	21.4	0.7044	UD	0.65	0.46	20.30	0.992	
74	44.6533300	-110.4764300	12	541513.00	4944574.00	21.5	0.7044	UD	0.17	0.12	5.34	0.945	
75	44.6534900	-110.4764200	12	541514.00	4944592.00	21.4	0.7044	UD	0.16	0.11	4.84	0.898	
76	44.6537400	-110.4763200	12	541522.00	4944620.00	18.0	0.7044	UD	0.30	0.21	9.17	0.976	
77	44.6539000	-110.4763300	12	541521.00	4944637.00	20.9	0.7044	UD	0.34	0.24	10.50	0.980	
78	44.6538500	-110.4765000	12	541507.00	4944632.00	23.0	0.7044	UD	0.51	0.36	15.60	0.981	
79	44.6537200	-110.4765000	12	541508.00	4944617.00	22.4	0.7044	UD	0.40	0.28	12.40	0.976	
80	44.6535700	-110.4765700	12	541502.00	4944601.00	22.8	0.7044	UD	0.18	0.13	5.68	0.957	
81	44.6534300	-110.4765800	12	541501.00	4944586.00	22.2	0.7044	UD	0.08	0.06	2.58	0.869	
82	44.6533100	-110.4765900	12	541501.00	4944572.00	23.7	0.7044	UD	UD				
83	44.6533100	-110.4766000	12	541500.00	4944572.00	23.7	0.7044	UD	0.17	0.12	5.10	0.895	
84	44.6531800	-110.4766100	12	541499.00	4944558.00	24.5	0.7044	UD	0.42	0.30	13.00	0.989	
85	44.6530500	-110.4766000	12	541500.00	4944543.00	21.1	0.7044	UD	0.95	0.67	29.40	0.994	
86	44.6529100	-110.4766200	12	541499.00	4944528.00	21.8	0.7044	UD	10.50	7.40	326.00	0.999	

87	44.6527800	-110.4766300	12	541498.00	4944513.00				37.8	0.7044	UD		18.30	12.90	568.00	0.999
88	44.6526500	-110.4766800	12	541494.00	4944498.00				35.2	0.7044	UD		16.60	11.70	514.00	
89	44.6525400	-110.4767300	12	541490.00	4944486.00				23.5	0.7044	UD		0.60	0.42	18.50	0.962
90	44.6525500	-110.4769100	12	541476.00	4944487.00				22.9	0.7044	UD		0.43	0.31	13.40	0.972
91	44.6526700	-110.4768600	12	541480.00	4944501.00				22.1	0.7044	UD		4.57	3.22	141.00	0.992

Date: 2014/8/11

Data Collector: Christie E. Torres

POINT	**LONGITUDE**	**LATITUDE**	**UTM ZONE**	**UTM LONGITUDE**	**UTM LATITUDE**	**AIR TEMP.**	**AIR RH**	**WIND SPEED**	**SOIL TEMP**	**ACK**	**H_2S**	**H_2S R^2**	**CO_2**		**CO_2 R^2**
						(°C)	(%)	(km/h)	(°C)		(ppm s^{-1}) (mol m^{-2} d^{-1}) (g m^{-2} d^{-1})		(ppm s^{-1}) (mol m^{-2} d^{-1}) (g m^{-2} d^{-1})		
15	44.6562800	-110.4778400	12	541399.00	4944902.00	19.3	60.8	1.8	16.6	0.7206	n.a.		0.36	0.26	11.50	0.984
16	44.6561900	-110.4779700	12	541389.00	4944891.00				18.3	0.7180	n.a.		3.89	2.79	123.00	0.999
17	44.6561200	-110.4781200	12	541377.00	4944883.00				19.2	0.7154	n.a.		3.11	2.23	98.00	0.998
18	44.6560300	-110.4782500	12	541367.00	4944873.00				16.7	0.7128	n.a.		3.07	2.19	96.30	0.998
19	44.6559400	-110.4784100	12	541354.00	4944863.00				16.5	0.7102	n.a.		0.53	0.38	16.70	0.993
20	44.6558500	-110.4785600	12	541343.00	4944853.00				24.2	0.7077	n.a.		3.43	2.42	107.00	0.998
21	44.6557600	-110.4786900	12	541332.00	4944843.00				18.0	0.7052	n.a.		0.98	0.69	30.40	0.966
22	44.6561900	-110.4782700	12	541366.00	4944891.00				13.3	0.7026	n.a.		0.40	0.28	12.40	0.986
23	44.6562600	-110.4781200	12	541377.00	4944899.00				13.9	0.7002	n.a.		0.29	0.20	8.92	0.977
24	44.6563500	-110.4780300	12	541385.00	4944909.00	28.9	27.5	1.0	13.0	0.6977	n.a.		0.25	0.17	7.64	0.953
25	44.6564000	-110.4778500	12	541399.00	4944915.00				14.9	0.6977	n.a.		1.02	0.71	31.20	0.996
26	44.6563300	-110.4776600	12	541414.00	4944907.00				18.3	0.6977	n.a.		0.22	0.16	6.87	0.955
27	44.6562900	-110.4774800	12	541428.00	4944903.00				17.0	0.6977	n.a.		1.49	1.04	45.70	0.994
28	44.6562400	-110.4773300	12	541440.00	4944897.00				21.2	0.6977	n.a.		0.10	0.07	2.98	0.866
29	44.6561500	-110.4771300	12	541456.00	4944888.00				15.8	0.6977	n.a.		0.45	0.31	13.70	0.975

30	44.6560000	-110.4771900	12	541452.00	4944870.00				18.1	0.6977	n.a.	0.59	0.41	18.20	0.989
31	44.6559200	-110.4773100	12	541442.00	4944861.00				27.4	0.6977	n.a.	5.88	4.10	181.00	0.999
32	44.6558300	-110.4774600	12	541430.00	4944851.00				49.8	0.6977	n.a.	64.30	44.90	1970.00	0.972
33	44.6557200	-110.4775900	12	541419.00	4944839.00				36.5	0.6977	n.a.	7.95	5.55	244.00	0.998
34	44.6556200	-110.4775000	12	541427.00	4944828.00	28.9	26.1	2.4	22.1	0.6977	n.a.	2.04	1.42	62.70	0.998
35	44.6557100	-110.4773900	12	541436.00	4944838.00				30.0	0.6981	n.a.	10.60	7.38	325.00	0.998
36	44.6558100	-110.4772200	12	541449.00	4944849.00				20.9	0.6986	n.a.	1.05	0.74	32.40	0.993
37	44.6557000	-110.4771700	12	541453.00	4944837.00				17.0	0.6991	n.a.	0.22	0.16	6.85	0.969
38	44.6556000	-110.4773000	12	541442.00	4944826.00				20.6	0.6995	n.a.	0.45	0.32	13.90	0.986
39	44.6555100	-110.4774400	12	541431.00	4944816.00				19.5	0.7000	n.a.	0.26	0.18	7.96	0.970
40	44.6553800	-110.4773300	12	541440.00	4944801.00				21.6	0.7005	n.a.	2.09	1.47	64.50	0.997
41	44.6554800	-110.4771800	12	541452.00	4944813.00				27.3	0.7009	n.a.	0.56	0.39	17.20	0.942
42	44.6556000	-110.4770100	12	541466.00	4944826.00				22.5	0.7014	n.a.	0.63	0.44	19.40	0.992
43	44.6556800	-110.4768400	12	541479.00	4944836.00				17.8	0.7019	n.a.	0.60	0.42	18.50	0.989
44	44.6554000	-110.4771300	12	541457.00	4944803.00	26.9	20.6	1.8	20.6	0.7023	n.a.	0.41	0.29	12.70	0.974
45	44.6554700	-110.4769100	12	541474.00	4944812.00				21.7	0.7023	n.a.	0.55	0.39	17.00	0.990

Date: 2014/8/12

Weather: Sunny

Pressure: 1026.08 hPa

Data Collector: Peipei Lin

Notes: the air temperature, air relative humidity and wind speed are measured by Christie at different locations compared to this dataset. Thus the average of Christie's air temperature, humidity and wind speed was used

POINT	**LONGITUDE**	**LATITUDE**	**UTM ZONE**	**UTM LONGITUDE**	**UTM LATITUDE**	**AIR TEMP.**	**AIR RH**	**WIND SPEED**	**SOIL TEMP**	**ACK**	**H_2S**	**H_2S R^2**	**CO_2**	**CO_2 R^2**
						(°C)	(%)	(km/h)	(°C)		(ppm s^{-1}) (mol m^{-2} d^{-1}) (g m^{-2} d^{-1})		(ppm s^{-1}) (mol m^{-2} d^{-1}) (g m^{-2} d^{-1})	

1	44.6537300	-110.4767400	12	541488.00	4944618.00	29.4	29.4	1.6	17.9	0.6942	BD		0.15	0.10	4.42	0.384
2	44.6536000	-110.4767500	12	541488.00	4944604.00				16.6	0.6942	BD		0.09	0.06	2.65	0.647
3	44.6534400	-110.4767900	12	541485.00	4944587.00				17.0	0.6942	UD		0.10	0.07	3.17	0.860
4	44.6533000	-110.4767900	12	541485.00	4944571.00				16.9	0.6942	UD		0.18	0.13	5.63	0.956
5	44.6531700	-110.4768200	12	541482.00	4944557.00				16.7	0.6942	UD		0.60	0.42	18.20	0.983
6	44.6530500	-110.4768100	12	541483.00	4944542.00				19.0	0.6942	UD		3.21	2.23	98.00	0.999
7	44.6529200	-110.4768300	12	541482.00	4944528.00				31.3	0.6942	UD		14.20	9.82	432.00	0.998
8	44.6527900	-110.4768600	12	541480.00	4944514.00				21.8	0.6942	UD		12.00	8.36	368.00	0.999
9	44.6527100	-110.4768500	12	541481.00	4944505.00				18.9	0.6942	UD		1.85	1.28	56.40	0.998
10	44.6524000	-110.4770700	12	541463.00	4944470.00				16.6	0.6942	UD		0.41	0.29	12.70	0.977
11	44.6525800	-110.4770700	12	541463.00	4944490.00				17.9	0.6942	UD		0.21	0.14	6.34	0.944
12	44.6527000	-110.4770700	12	541463.00	4944504.00				18.9	0.6942	UD		2.11	1.46	64.30	0.996
13	44.6528100	-110.4770400	12	541465.00	4944516.00				19.1	0.6942	UD		6.16	4.28	188.00	0.999
14	44.6529500	-110.4770300	12	541466.00	4944532.00				21.8	0.6942	UD		8.92	6.19	272.00	0.999
15	44.6530900	-110.4770200	12	541467.00	4944547.00				20.9	0.6942	UD		8.44	5.86	258.00	0.999
16	44.6532000	-110.4770000	12	541468.00	4944560.00				18.8	0.6942	UD		2.62	1.82	80.10	0.996
17	44.6533200	-110.4769700	12	541471.00	4944573.00				19.6	0.6942	UD		1.21	0.84	37.10	0.992
18	44.6534500	-110.4769700	12	541471.00	4944587.00				18.6	0.6942	UD		0.40	0.27	12.10	0.975
19	44.6535700	-110.4769500	12	541472.00	4944601.00				18.8	0.6942	UD		0.59	0.41	18.10	0.977
20	44.6537300	-110.4769200	12	541474.00	4944618.00				20.2	0.6942	UD		1.18	0.82	36.00	0.994
21	44.6537100	-110.4771400	12	541457.00	4944616.00				20.2	0.6942	UD		1.60	1.11	48.70	0.992
22	44.6535700	-110.4771300	12	541458.00	4944601.00				20.0	0.6942	UD		0.94	0.65	28.70	0.989
23	44.6534100	-110.4771600	12	541456.00	4944583.00				19.7	0.6942	UD		0.87	0.60	26.50	0.986
24	44.6532800	-110.4771700	12	541455.00	4944568.00				19.5	0.6942	UD		2.14	1.48	65.30	0.999
25	44.6531600	-110.4771900	12	541453.00	4944555.00				21.2	0.6942	UD		8.32	5.77	254.00	0.998
26	44.6530400	-110.4772300	12	541450.00	4944542.00				19.3	0.6942	UD		9.24	6.41	282.00	0.999

27	44.6529100	-110.4772100	12	541452.00	4944527.00	22.5	0.6942	UD				13.90	9.66	425.00	0.988
28	44.6527800	-110.4772300	12	541450.00	4944513.00	22.0	0.6942	UD				14.80	10.30	452.00	0.999
29	44.6526500	-110.4772700	12	541447.00	4944498.00	22.5	0.6942	UD				13.80	9.59	422.00	0.999
30	44.6526900	-110.4774500	12	541433.00	4944503.00	31.6	0.6942	UD				14.90	10.30	454.00	0.991
31	44.6528600	-110.4774300	12	541435.00	4944521.00	28.2	0.6942	UD				25.30	17.50	772.00	0.990
32	44.6530700	-110.4773800	12	541438.00	4944545.00	39.8	0.6942	UD				51.60	35.80	1570.00	0.979
33	44.6531900	-110.4773900	12	541437.00	4944558.00	49.0	0.6942	BD				25.00	17.30	763.00	0.999
34	44.6533200	-110.4773700	12	541439.00	4944572.00	32.7	0.6942	UD				10.20	7.09	312.00	0.999
35	44.6534800	-110.4773500	12	541441.00	4944590.00	25.9	0.6942	UD				9.46	6.57	289.00	0.999
36	44.6536200	-110.4773300	12	541442.00	4944606.00	20.7	0.6942	UD				2.56	1.78	78.10	0.997
37	44.6537400	-110.4773100	12	541443.00	4944619.00	25.0	0.6942	UD				8.90	6.18	272.00	0.998
38	44.6537500	-110.4774900	12	541429.00	4944620.00	30.8	0.6942	UD				11.10	7.73	340.00	0.999
39	44.6535900	-110.4774900	12	541429.00	4944602.00	41.8	0.6942	UD				23.40	16.20	714.00	0.999
40	44.6534500	-110.4775100	12	541428.00	4944587.00	48.2	0.6942	UD				22.30	15.40	680.00	0.997
41	44.6533300	-110.4775500	12	541425.00	4944574.00	62.2	0.6942	UD				81.20	56.40	2480.00	0.880
42	44.6531900	-110.4775700	12	541423.00	4944559.00	78.4	0.6942	UD				86.60	60.10	2650.00	0.997
43	44.6530800	-110.4775500	12	541425.00	4944546.00	79.4	0.6942	UD				102.00	70.70	3110.00	0.980
44	44.6529600	-110.4775600	12	541424.00	4944532.00	46.4	0.6942	UD				51.00	35.40	1560.00	0.975
45	44.6528200	-110.4776200	12	541419.00	4944517.00	51.5	0.6942	UD				18.50	12.80	565.00	0.983
46	44.6527100	-110.4776500	12	541417.00	4944505.00	48.1	0.6942	UD				49.30	34.20	1500.00	0.999
47	44.6527200	-110.4778000	12	541405.00	4944506.00	32.7	0.6942	UD				8.30	5.76	253.00	0.999
48	44.6528600	-110.4778100	12	541404.00	4944521.00	25.0	0.6942	UD				1.13	0.79	34.50	0.998
49	44.6530000	-110.4777900	12	541405.81	4944536.90	42.5	0.6942	UD				44.00	30.50	1340.00	0.999
50	44.6531400	-110.4777400	12	541410.00	4944553.00	64.1	0.6942	UD				67.80	47.10	2070.00	0.996
51	44.6531900	-110.4779600	12	541392.00	4944557.00	50.5	0.6942	UD				11.10	7.68	338.00	0.999
52	44.6530400	-110.4779600	12	541392.00	4944542.00	70.1	0.6942	0.38	0.19	6.51	1.000	53.90	37.40	1650.00	0.997

53	44.6529000	-110.4779700	12	541391.00	4944526.00	24.2	0.6942	UD				1.44	1.00	44.00	0.998
54	44.6527700	-110.4779900	12	541390.00	4944511.00	26.3	0.6942	UD				0.84	0.58	25.60	0.993
55	44.6537100	-110.4781300	12	541378.00	4944615.00	64.1	0.6942	0.22	0.11	3.76	0.997	36.00	25.00	1100.00	0.997
56	44.6536300	-110.4781300	12	541379.00	4944606.00	77.4	0.6942	UD				45.70	31.80	1400.00	0.998
57	44.6534600	-110.4781500	12	541377.00	4944588.00	34.5	0.6942	UD				15.10	10.40	460.00	0.999
58	44.6533300	-110.4781800	12	541375.00	4944573.00	58.9	0.6942	UD				42.70	29.60	1300.00	0.993
59	44.6532200	-110.4781900	12	541374.00	4944561.00	62.1	0.6942	UD				0.36	0.25	11.00	0.975
60	44.6530700	-110.4781900	12	541374.00	4944544.00	44.3	0.6942	UD				13.40	9.29	409.00	0.998
61	44.6529300	-110.4781700	12	541376.00	4944528.00	29.6	0.6942	UD				0.43	0.30	13.10	0.977
62	44.6528200	-110.4781800	12	541375.00	4944516.00	23.3	0.6942	UD				0.82	0.57	25.00	0.982
63	44.6526600	-110.4787600	12	541329.00	4944498.00	25.3	0.6942	UD				0.42	0.29	12.70	0.130
64	44.6526500	-110.4784800	12	541351.00	4944497.00	26.2	0.6942	UD				0.58	0.40	17.70	0.955
65	44.6526300	-110.4783100	12	541365.00	4944495.00	24.0	0.6942	UD				0.75	0.52	23.00	0.987
66	44.6526000	-110.4781400	12	541378.00	4944492.00	24.2	0.6942	UD				0.54	0.37	16.30	0.985
67	44.6525900	-110.4779800	12	541391.00	4944492.00	30.5	0.6942	UD				2.71	1.88	82.70	0.998
68	44.6525600	-110.4778100	12	541405.00	4944488.00	31.6	0.6942	UD				7.22	5.01	220.00	0.999
69	44.6525700	-110.4776200	12	541420.00	4944489.00	39.3	0.6942	UD				61.80	42.90	1890.00	0.999
70	44.6525500	-110.4774500	12	541433.00	4944487.00	30.8	0.6942	UD				10.80	7.53	331.00	0.999
71	44.6525600	-110.4772600	12	541448.00	4944488.00	28.1	0.6942	UD				1.62	1.12	49.50	0.991
72	44.6524300	-110.4770400	12	541466.00	4944473.00	28.8	0.6942	UD				0.17	0.12	5.21	0.899
73	44.6524000	-110.4772400	12	541450.00	4944471.00	27.9	0.6942	UD				1.18	0.82	36.10	0.994
74	44.6524200	-110.4774200	12	541436.00	4944472.00	27.1	0.6942	UD				5.33	3.70	163.00	0.998
75	44.6524300	-110.4776200	12	541420.00	4944474.00	31.3	0.6942	UD				0.77	0.54	23.60	0.980
76	44.6524400	-110.4778000	12	541406.00	4944475.00	31.2	0.6942	UD				3.33	2.31	102.00	0.998
77	44.6524500	-110.4779800	12	541391.00	4944476.00	27.6	0.6942	UD				4.00	2.77	122.00	0.999
78	44.6524600	-110.4781600	12	541377.00	4944477.00	27.2	0.6942	UD				1.56	1.08	47.50	0.995

79	44.6524700	-110.4783400	12	541363.00	4944478.00			25.2	0.6942	UD		0.23	0.16	7.04	0.940
80	44.6524800	-110.4785300	12	541348.00	4944479.00				0.6942	UD		UD			
81	44.6525000	-110.4787000	12	541334.00	4944481.00			30.4	0.6942	UD		0.38	0.26	11.60	0.116
82	44.6523700	-110.4787500	12	541330.00	4944467.00			28.5	0.6942	UD		0.21	0.14	6.35	0.955
83	44.6523600	-110.4785300	12	541347.00	4944465.00			26.1	0.6942	UD		0.23	0.16	7.10	0.057
84	44.6523600	-110.4783600	12	541361.00	4944465.00			23.8	0.6942	UD		UD			
85	44.6523400	-110.4782000	12	541373.00	4944463.00			24.8	0.6942	UD		2.59	1.79	79.00	0.997
86	44.6523100	-110.4780300	12	541387.00	4944461.00			25.6	0.6942	UD		0.60	0.42	18.40	0.983
87	44.6523000	-110.4778500	12	541402.00	4944459.00			32.9	0.6942	UD		9.23	6.41	282.00	0.998
88	44.6523100	-110.4776600	12	541416.00	4944461.00			29.8	0.6942	UD		2.98	2.07	91.00	0.996
89	44.6522900	-110.4775000	12	541430.00	4944458.00			24.3	0.6942	UD		1.19	0.83	36.30	0.994
90	44.6522800	-110.4773300	12	541443.00	4944457.00			23.8	0.6942	UD		1.95	1.35	59.50	0.997
91	44.6521600	-110.4775400	12	541426.00	4944444.00			23.8	0.6942	UD		0.13	0.09	3.92	0.921
92	44.6521600	-110.4777200	12	541412.00	4944444.00			23.5	0.6942	UD		3.37	2.34	103.00	0.998
93	44.6521800	-110.4778900	12	541398.00	4944446.00			30.3	0.6942	UD		0.85	0.59	26.00	0.995
94	44.6521800	-110.4780700	12	541384.00	4944445.00			29.6	0.6942	UD		0.44	0.30	13.30	0.974
95	44.6522000	-110.4782700	12	541368.00	4944448.00			27.5	0.6942	UD		0.47	0.33	14.40	0.993
96	44.6522000	-110.4784200	12	541356.00	4944448.00			25.4	0.6942	UD		0.13	0.09	3.94	0.868
97	44.6522300	-110.4785800	12	541344.00	4944451.00			27.9	0.6942	UD		UD			
98	44.6522300	-110.4787900	12	541327.00	4944450.00			29.0	0.6942	UD		0.69	0.48	21.10	0.991

Date: 2014/8/12

Data Collector: Christie E. Torres

POINT	**LONGITUDE**	**LATITUDE**	**UTM ZONE**	**UTM LONGITUDE**	**UTM LATITUDE**	**AIR TEMP.**	**AIR RH**	**WIND SPEED**	**SOIL TEMP**	**ACK**	**H_2S**	**H_2S R^2**	**CO_2**	**CO_2 R^2**
						(°C)	(%)	(km/h)	(°C)		(ppm s^{-1}) (mol m^{-2} d^{-1}) (g m^{-2} d^{-1})		(ppm s^{-1}) (mol m^{-2} d^{-1}) (g m^{-2} d^{-1})	

1	44.6548400	-110.4773500	12	541440.00	4944741.00	25.2	48.2	1.2	15.9	0.7040	n.a.	0.88	0.62	27.20	0.992
2	44.6549600	-110.4773400	12	541440.00	4944755.00				20.1	0.7033	n.a.	1.44	1.01	44.50	0.997
3	44.6551100	-110.4773300	12	541441.00	4944772.00				19.6	0.7026	n.a.	1.14	0.80	35.30	0.995
4	44.6552800	-110.4773300	12	541441.00	4944791.00				18.7	0.7018	n.a.	1.44	1.01	44.40	0.995
5	44.6547400	-110.4773000	12	541444.00	4944730.00				15.2	0.7011	n.a.	0.16	0.11	4.97	0.887
6	44.6547300	-110.4774800	12	541430.00	4944729.00				14.5	0.7004	n.a.	0.69	0.49	21.40	0.994
7	44.6547200	-110.4776500	12	541415.00	4944728.00				16.7	0.6996	n.a.	0.91	0.64	28.10	0.996
8	44.6547000	-110.4778100	12	541403.00	4944726.00				16.8	0.6989	n.a.	0.53	0.37	16.40	0.986
9	44.6547100	-110.4779900	12	541389.00	4944727.00				21.3	0.6982	n.a.	7.49	5.23	230.00	0.999
10	44.6547100	-110.4781800	12	541374.00	4944727.00	28.0	48.5	0.1	27.5	0.6975	n.a.	4.19	2.92	128.00	0.999
11	44.6547200	-110.4783800	12	541358.00	4944727.00				33.0	0.6981	n.a.	10.60	7.39	325.00	0.999
12	44.6545700	-110.4781900	12	541373.00	4944711.00				46.6	0.6988	n.a.	28.20	19.70	867.00	0.999
13	44.6545900	-110.4779900	12	541389.00	4944713.00				20.6	0.6995	n.a.	0.42	0.29	12.90	0.992
14	44.6545700	-110.4778200	12	541403.00	4944711.00				19.0	0.7002	n.a.	0.38	0.27	11.80	0.983
15	44.6545900	-110.4776100	12	541419.00	4944714.00				19.9	0.7008	n.a.	0.19	0.13	5.79	0.943
16	44.6546000	-110.4774100	12	541435.00	4944715.00				22.9	0.7015	n.a.	0.19	0.13	5.76	0.363
17	44.6545900	-110.4772600	12	541446.00	4944714.00				26.7	0.7022	n.a.	0.12	0.08	3.57	0.905
18	44.6545800	-110.4770700	12	541461.00	4944713.00				18.5	0.7029	n.a.	1.43	1.01	44.30	0.997
19	44.6545900	-110.4768800	12	541477.00	4944714.00				19.2	0.7036	n.a.	1.34	0.94	41.30	0.997
20	44.6545900	-110.4766900	12	541492.00	4944714.00	25.1	23.2	3.2	21.8	0.7043	n.a.	0.78	0.55	24.20	0.993
21	44.6546000	-110.4764900	12	541507.00	4944715.00				18.2	0.7043	n.a.	0.41	0.29	12.60	0.989
22	44.6545900	-110.4763000	12	541523.00	4944714.00				16.9	0.7043	n.a.	0.48	0.34	14.90	0.983
23	44.6546000	-110.4761700	12	541533.00	4944716.00				16.6	0.7043	n.a.	0.53	0.37	16.30	0.992
24	44.6544600	-110.4760400	12	541544.00	4944700.00				15.3	0.7043	n.a.	0.40	0.28	12.30	0.963
25	44.6544400	-110.4762300	12	541528.00	4944698.00				17.9	0.7044	n.a.	0.80	0.56	24.80	0.989
26	44.6544600	-110.4764100	12	541514.00	4944700.00				19.3	0.7044	n.a.	0.94	0.66	29.10	0.992

27	44.6544400	-110.4766200	12	541498.00	4944698.00				19.9	0.7044	n.a.	1.38	0.97	42.70	0.996
28	44.6544400	-110.4768200	12	541482.00	4944697.00				20.0	0.7044	n.a.	0.30	0.21	9.13	0.931
29	44.6544500	-110.4769800	12	541469.00	4944698.00				18.5	0.7045	n.a.	1.56	1.10	48.30	0.996
30	44.6544500	-110.4772100	12	541451.00	4944698.00	25.0	23.6	0.9	23.9	0.7045	n.a.	1.21	0.85	37.50	0.996
31	44.6544500	-110.4774200	12	541434.00	4944698.00				22.3	0.7034	n.a.	0.13	0.09	4.04	0.909
32	44.6544500	-110.4776100	12	541419.00	4944698.00				21.3	0.7024	n.a.	0.60	0.42	18.60	0.990
33	44.6544400	-110.4778300	12	541402.00	4944696.00				30.6	0.7013	n.a.	10.60	7.40	326.00	0.998
34	44.6544300	-110.4780200	12	541387.00	4944696.00				22.7	0.7003	n.a.	0.64	0.45	19.80	0.988
35	44.6544300	-110.4782200	12	541371.00	4944696.00				21.4	0.6992	n.a.	0.24	0.16	7.24	0.956
36	44.6544500	-110.4783900	12	541358.00	4944698.00				24.8	0.6982	n.a.	0.13	0.09	3.85	0.851
37	44.6536300	-110.4791100	12	541301.00	4944606.00				27.7	0.6971	n.a.	3.66	2.55	112.00	0.996
38	44.6537400	-110.4791300	12	541299.00	4944619.00				22.7	0.6961	n.a.	7.14	4.97	219.00	0.999
39	44.6539000	-110.4791200	12	541300.00	4944636.00				26.4	0.6950	n.a.	2.34	1.63	71.50	0.998
40	44.6540400	-110.4791300	12	541299.00	4944652.00	29.5	20.2	1.1	23.3	0.6940	n.a.	4.46	3.10	136.00	0.999
41	44.6541800	-110.4791400	12	541298.00	4944667.00				26.4	0.6942	n.a.	0.35	0.24	10.60	0.980
42	44.6543200	-110.4791600	12	541296.00	4944683.00				23.4	0.6944	n.a.	0.32	0.22	9.71	0.965
43	44.6544100	-110.4791500	12	541297.00	4944693.00				22.1	0.6946	n.a.	0.52	0.36	15.90	0.976
44	44.6543300	-110.4793300	12	541283.00	4944684.00				24.8	0.6947	n.a.	0.43	0.30	13.00	0.978
45	44.6542000	-110.4793200	12	541284.00	4944669.00				24.9	0.6949	n.a.	0.65	0.45	19.90	0.979
46	44.6540700	-110.4793200	12	541283.00	4944655.00				23.1	0.6951	n.a.	1.48	1.03	45.20	0.995
47	44.6539200	-110.4793100	12	541285.00	4944638.00				27.0	0.6953	n.a.	0.17	0.12	5.04	0.351
48	44.6537400	-110.4793000	12	541286.00	4944618.00				32.7	0.6955	n.a.	3.71	2.58	114.00	0.999
49	44.6535200	-110.4787700	12	541328.00	4944594.00				30.6	0.6957	n.a.	6.53	4.54	200.00	0.999
50	44.6535100	-110.4789500	12	541313.00	4944593.00	28.7	12.8	3.0	30.5	0.6959	n.a.	3.12	2.17	95.60	0.999
51	44.6535100	-110.4791300	12	541299.00	4944593.00				30.8	0.6959	n.a.	4.69	3.26	144.00	0.999
52	44.6534900	-110.4793100	12	541285.00	4944591.00				27.6	0.6959	n.a.	2.76	1.92	84.50	0.998

53	44.6535000	-110.4794800	12	541271.00	4944592.00				29.5	0.6959	n.a.				5.78	4.02	177.00	0.999
54	44.6535000	-110.4796400	12	541259.00	4944592.00				29.9	0.6959	n.a.				5.88	4.09	180.00	0.998
55	44.6534500	-110.4798400	12	541243.00	4944586.00				25.6	0.6959	n.a.				3.91	2.72	120.00	0.999
56	44.6534700	-110.4800200	12	541229.00	4944588.00				21.2	0.6959	n.a.				0.54	0.38	16.60	0.991

Date: 2014/8/13

Weather: Sunny, rained at 4pm.

Pressure: 1024.38 hPa

Data Collector: Peipei Lin

Notes: the air temperature, air relative humidity and wind speed are measured by Christie at different locations compared to this dataset. Thus the average of Christie's air temperature, humidity and wind speed was used

POINT	**LONGITUDE**	**LATITUDE**	**UTM ZONE**	**UTM LONGITUDE**	**UTM LATITUDE**	**AIR TEMP.**	**AIR RH**	**WIND SPEED**	**SOIL TEMP**	**ACK**	**H_2S**			**H_2S R^2**	**CO_2**		**CO_2 R^2**
						(°C)	(%)	(km/h)	(°C)		(ppm s^{-1})	(mol m^{-2} d^{-1})	(g m^{-2} d^{-1})		(ppm s^{-1})	(mol m^{-2} d^{-1})	(g m^{-2} d^{-1})	
1	44.6537400	-110.4777000	12	541410.00	4944619.00	24.1	47.4	0.6	40.1	0.7055	UD				14.90	10.50	464.00	0.988
2	44.6537500	-110.4779000	12	541396.00	4944620.00				92.3	0.7055	4.55	3.21	141.00	1.000	1900.00	1340.00	58900.00	0.995
3	44.6535700	-110.4777000	12	541414.00	4944600.00				43.2	0.7055	BD				25.00	17.70	777.00	0.976
4	44.6534600	-110.4777000	12	541412.00	4944588.00				48.0	0.7055	UD				30.50	21.50	946.00	0.972
5	44.6535700	-110.4779000	12	541397.00	4944600.00				48.4	0.7055	BD				7.74	5.46	240.00	0.999
6	44.6514400	-110.4797000	12	541255.00	4944362.00				18.6	0.7055	BD				0.31	0.22	9.59	0.963
7	44.6514600	-110.4799000	12	541236.00	4944364.00				23.7	0.7055	BD				0.11	0.08	3.50	0.795
8	44.6514600	-110.4801000	12	541222.00	4944365.00					0.7055	BD				1.48	1.04	45.80	
9	44.6514800	-110.4803000	12	541208.00	4944367.00				24.6	0.7055	BD				0.40	0.28	12.30	0.952
10	44.6516700	-110.4802000	12	541219.00	4944387.00				25.0	0.7055	BD				0.32	0.23	10.00	0.931
11	44.6516100	-110.4800000	12	541236.00	4944381.00				24.0	0.7055	BD				0.12	0.08	3.59	0.571
12	44.6515800	-110.4797000	12	541252.00	4944378.00				21.8	0.7055	BD				0.54	0.38	16.90	0.899

13	44.6515900	-110.4795000	12	541268.00	4944380.00	19.3	0.7055	BD	0.34	0.24	10.60	0.904
14	44.6515800	-110.4794000	12	541282.00	4944378.00	19.0	0.7055	BD	0.31	0.22	9.61	0.976
15	44.6515500	-110.4792000	12	541296.00	4944375.00	17.4	0.7055	BD	0.13	0.09	3.89	0.881
16	44.6517300	-110.4790000	12	541308.00	4944395.00	18.8	0.7055	BD	0.43	0.31	13.40	0.951
17	44.6517100	-110.4793000	12	541291.00	4944393.00	19.7	0.7055	BD	0.09	0.06	2.71	0.596
18	44.6516700	-110.4794000	12	541276.00	4944388.00	21.6	0.7055	BD	0.21	0.15	6.48	0.927
19	44.6517200	-110.4797000	12	541256.00	4944393.00	23.1	0.7055	BD	0.59	0.41	18.20	0.914
20	44.6517500	-110.4800000	12	541236.00	4944397.00	22.6	0.7055	BD	0.13	0.09	3.99	0.785
21	44.6518800	-110.4799000	12	541237.00	4944411.00	24.0	0.7055	BD	0.13	0.09	3.89	0.634
22	44.6518600	-110.4797000	12	541252.00	4944409.00	22.9	0.7055	BD	0.36	0.26	11.20	0.913
23	44.6518800	-110.4796000	12	541267.00	4944411.00	26.1	0.7055	BD	UD			
24	44.6518300	-110.4794000	12	541281.00	4944406.00	19.5	0.7055	BD	0.23	0.16	7.07	0.904
25	44.6519700	-110.4792000	12	541298.00	4944421.00	27.6	0.7055	BD	0.14	0.10	4.23	0.775
26	44.6520000	-110.4794000	12	541281.00	4944425.00	26.5	0.7055	BD	0.12	0.09	3.78	0.764
27	44.6520100	-110.4796000	12	541263.00	4944426.00	28.0	0.7055	BD	UD			
28	44.6520600	-110.4798000	12	541248.00	4944431.00	27.2	0.7055	BD	UD			
29	44.6521400	-110.4796000	12	541267.00	4944440.00		0.7055	BD	UD			
30	44.6521300	-110.4794000	12	541282.00	4944439.00	27.4	0.7055	BD	0.20	0.14	6.08	0.894
31	44.6521200	-110.4792000	12	541296.00	4944438.00	27.1	0.7055	BD	0.19	0.14	6.00	0.881
32	44.6521100	-110.4790000	12	541312.00	4944438.00	23.8	0.7055	BD	0.30	0.21	9.35	0.962
33	44.6520600	-110.4788000	12	541327.00	4944432.00	19.9	0.7055	BD	UD			
34	44.6521200	-110.4786000	12	541342.00	4944439.00	21.4	0.7055	UD	0.24	0.17	7.46	0.965
35	44.6521000	-110.4784000	12	541355.00	4944436.00	21.9	0.7055	BD	0.12	0.08	3.62	0.896
36	44.6520800	-110.4783000	12	541369.00	4944434.00	23.2	0.7055	UD	1.74	1.23	53.90	0.997
37	44.6520700	-110.4781000	12	541384.00	4944433.00	24.2	0.7055	BD	0.77	0.54	23.80	0.990
38	44.6520600	-110.4779000	12	541399.00	4944433.00	22.6	0.7055	UD	0.28	0.20	8.57	0.918

39	44.6519500	-110.4782000	12	541373.00	4944420.00		0.7055	UD				0.46	0.32	14.10	0.983
40	44.6519500	-110.4784000	12	541357.00	4944420.00	24.5	0.7055	UD				0.21	0.15	6.57	0.941
41	44.6519700	-110.4786000	12	541343.00	4944422.00		0.7055	UD				0.35	0.25	10.80	0.114
42	44.6519400	-110.4788000	12	541328.00	4944418.00	23.2	0.7055	UD				0.07	0.05	2.04	0.736
43	44.6519700	-110.4790000	12	541312.00	4944422.00	19.8	0.7055	UD				0.14	0.10	4.34	0.676
44	44.6537700	-110.4794000	12	541274.00	4944621.00	24.7	0.7055	UD				1.43	1.01	44.50	0.995
45	44.6537500	-110.4796000	12	541260.00	4944620.00	32.3	0.7055	UD				9.07	6.40	281.00	0.999
46	44.6537500	-110.4798000	12	541245.00	4944619.00	28.9	0.7055	UD				13.60	9.59	422.00	0.997
47	44.6537500	-110.4800000	12	541232.00	4944619.00	27.8	0.7055	UD				8.46	5.97	263.00	0.998
48	44.6537500	-110.4801000	12	541219.00	4944619.00	44.2	0.7055	UD				25.70	18.10	797.00	0.999
49	44.6537500	-110.4803000	12	541203.00	4944619.00	69.2	0.7055	UD				19.40	13.70	601.00	0.980
50	44.6540000	-110.4804000	12	541200.00	4944646.00	52.2	0.7055	0.08	0.06	2.45	0.935	57.80	40.80	1790.00	0.998
51	44.6540300	-110.4802000	12	541216.00	4944650.00	49.8	0.7055	UD				38.20	26.90	1190.00	0.998
52	44.6540500	-110.4800000	12	541232.00	4944653.00	49.5	0.7055	BD				66.90	47.20	2080.00	0.986
53	44.6540500	-110.4798000	12	541248.00	4944652.00	38.2	0.7055	UD				7.11	5.02	221.00	0.999
54	44.6540400	-110.4796000	12	541263.00	4944652.00	24.0	0.7055	UD				7.85	5.54	244.00	0.999
55	44.6541600	-110.4795000	12	541266.00	4944665.00	26.3	0.7055	UD				5.47	3.86	170.00	0.997
56	44.6541300	-110.4797000	12	541251.00	4944662.00	27.0	0.7055	UD				1.61	1.13	49.90	0.997
57	44.6541300	-110.4799000	12	541235.00	4944662.00	58.0	0.7055	UD				116.00	81.60	3590.00	0.992
58	44.6541100	-110.4802000	12	541216.00	4944659.00	57.3	0.7055	UD				15.50	10.90	482.00	0.997
59	44.6539100	-110.4795000	12	541270.00	4944637.00	25.0	0.7055	UD				2.43	1.71	75.40	0.998
60	44.6538900	-110.4797000	12	541253.00	4944635.00	27.3	0.7055	BD				0.78	0.55	24.20	0.987
61	44.6538900	-110.4799000	12	541237.00	4944635.00	33.5	0.7055	UD				10.30	7.29	321.00	0.999
62	44.6539200	-110.4800000	12	541226.00	4944638.00	40.4	0.7055	UD				39.20	27.70	1220.00	0.976
63	44.6538800	-110.4802000	12	541212.00	4944633.00	42.5	0.7055	UD				27.10	19.10	840.00	0.999
64	44.6538600	-110.4805000	12	541193.00	4944632.00	55.0	0.7055	UD				28.40	20.10	882.00	0.995

65	44.6539000	-110.4806000	12	541182.00	4944635.00	56.9	0.7055	UD				15.60	11.00	484.00	0.997
66	44.6538700	-110.4808000	12	541167.00	4944632.00	54.8	0.7055	UD				47.20	33.30	1470.00	0.999
67	44.6539100	-110.4810000	12	541153.00	4944636.00	53.9	0.7055	0.07	0.05	2.08	0.843	26.80	18.90	833.00	0.995
68	44.6538800	-110.4812000	12	541139.00	4944633.00	37.0	0.7055	UD				14.80	10.40	459.00	0.986
69	44.6538800	-110.4813000	12	541124.00	4944633.00	28.6	0.7055	UD				0.60	0.42	18.50	0.149
70	44.6536400	-110.4814000	12	541117.00	4944606.00	23.8	0.7055	UD				2.18	1.54	67.70	0.997
71	44.6536100	-110.4817000	12	541099.00	4944603.00	20.5	0.7055	UD				1.17	0.83	36.40	0.993
72	44.6536200	-110.4819000	12	541083.00	4944604.00	19.5	0.7055	UD				1.76	1.24	54.70	0.995
73	44.6536200	-110.4823000	12	541051.00	4944603.00	18.9	0.7055	UD				1.01	0.72	31.40	0.995
74	44.6536800	-110.4827000	12	541020.00	4944610.00	16.8	0.7055	UD				0.74	0.52	23.00	0.988
75	44.6536200	-110.4831000	12	540988.00	4944603.00	16.3	0.7055	UD				0.84	0.59	26.00	0.990
76	44.6537100	-110.4833000	12	540966.00	4944613.00	16.6	0.7055	UD				0.79	0.56	24.40	0.992
77	44.6537000	-110.4835000	12	540952.00	4944612.00	17.3	0.7055	UD				0.52	0.36	16.00	0.986
78	44.6536900	-110.4837000	12	540938.00	4944610.00	16.2	0.7055	UD				0.55	0.39	17.00	0.929
79	44.6537400	-110.4839000	12	540922.00	4944616.00	21.8	0.7055	UD				0.17	0.12	5.26	0.931
80	44.6535400	-110.4837000	12	540937.00	4944594.00	18.8	0.7055	UD				0.11	0.08	3.33	0.866
81	44.6535100	-110.4835000	12	540952.00	4944590.00	17.9	0.7055	UD				0.34	0.24	10.60	0.975
82	44.6535500	-110.4833000	12	540969.00	4944595.00	14.9	0.7055	UD				0.59	0.42	18.40	0.986
83	44.6535200	-110.4829000	12	540999.00	4944592.00	16.8	0.7055	UD				0.80	0.56	24.80	0.965
84	44.6535400	-110.4825000	12	541030.00	4944594.00	15.3	0.7055	UD				0.64	0.45	20.00	0.985
85	44.6535100	-110.4822000	12	541053.00	4944591.00	17.9	0.7055	UD				1.41	0.99	43.60	0.973
86	44.6534700	-110.4820000	12	541069.00	4944587.00	18.1	0.7055	UD				0.27	0.19	8.24	0.969
87	44.6534900	-110.4819000	12	541084.00	4944589.00	21.3	0.7055	UD				0.50	0.36	15.60	0.991
88	44.6534700	-110.4817000	12	541099.00	4944588.00	17.0	0.7055	UD				0.39	0.27	12.10	0.959

Date: 2014/8/13

Data Collector: Chirstie E. Torres

POINT	LONGITUDE	LATITUDE	UTM ZONE	UTM LONGITUDE	UTM LATITUDE	AIR TEMP.	AIR RH	WIND SPEED	SOIL TEMP	ACK	H_2S	H_2S R^2	CO_2			CO_2 R^2
						(°C)	(%)	(km/h)	(°C)		(ppm s^{-1})		(ppm s^{-1})	(mol m^{-2} d^{-1})	(g m^{-2} d^{-1})	
1	44.6528100	-110.4788000	12	541330.00	4944516.00	20.2	57.2	1.3	17.3	0.7148	n.a.		0.19	0.14	5.99	0.953
2	44.6528300	-110.4789000	12	541316.00	4944517.00				17.9	0.7139	n.a.		0.27	0.19	8.36	0.971
3	44.6528000	-110.4791000	12	541301.00	4944514.00				19.0	0.7129	n.a.		0.17	0.12	5.23	0.934
4	44.6528000	-110.4793000	12	541286.00	4944514.00				17.5	0.7119	n.a.		0.24	0.17	7.37	0.976
5	44.6528100	-110.4794000	12	541275.00	4944514.00				20.2	0.7110	n.a.		0.23	0.16	7.21	0.951
6	44.6529300	-110.4795000	12	541273.00	4944528.00				20.5	0.7100	n.a.		0.32	0.23	10.00	0.977
7	44.6529400	-110.4793000	12	541288.00	4944530.00				19.3	0.7090	n.a.		0.44	0.31	13.60	0.988
8	44.6529600	-110.4791000	12	541304.00	4944532.00				17.2	0.7081	n.a.		0.13	0.09	4.04	0.801
9	44.6529500	-110.4788000	12	541324.00	4944530.00				18.1	0.7071	n.a.		0.97	0.69	30.30	0.994
10	44.6530800	-110.4788000	12	541328.00	4944545.00	23.8	48.5	0.1	19.9	0.7062	n.a.		0.11	0.08	3.46	0.796
11	44.6530800	-110.4790000	12	541313.00	4944545.00				22.7	0.7058	n.a.		0.50	0.35	15.40	0.071
12	44.6530700	-110.4792000	12	541298.00	4944544.00				19.6	0.7055	n.a.		0.36	0.25	11.10	0.987
13	44.6530600	-110.4793000	12	541284.00	4944543.00				20.8	0.7051	n.a.		0.61	0.43	18.80	0.117
14	44.6530700	-110.4795000	12	541268.00	4944544.00				22.9	0.7047	n.a.		0.59	0.42	18.30	0.978
15	44.6531900	-110.4797000	12	541254.00	4944557.00				22.5	0.7044	n.a.		0.95	0.67	29.30	0.990
16	44.6532000	-110.4795000	12	541268.00	4944559.00				23.6	0.7040	n.a.		0.12	0.09	3.75	0.928
17	44.6532200	-110.4793000	12	541284.00	4944560.00				20.8	0.7037	n.a.		0.56	0.40	17.40	0.985
18	44.6532200	-110.4791000	12	541303.00	4944560.00				19.3	0.7033	n.a.		0.64	0.45	19.90	0.983
19	44.6532400	-110.4789000	12	541318.00	4944563.00				20.9	0.7030	n.a.		2.29	1.61	70.70	0.997
20	44.6532400	-110.4788000	12	541329.00	4944563.00	25.3	44.4	0.1	21.9	0.7026	n.a.		2.54	1.78	78.40	0.998
21	44.6533800	-110.4788000	12	541327.00	4944579.00				25.0	0.7023	n.a.		0.72	0.51	22.30	0.989

22	44.6533900	-110.4790000	12	541312.00	4944579.00				28.5	0.7020	n.a.	4.36	3.06	135.00	0.998
23	44.6533700	-110.4792000	12	541296.00	4944577.00				24.3	0.7016	n.a.	2.78	1.95	85.70	0.999
24	44.6533600	-110.4794000	12	541277.00	4944576.00				24.7	0.7013	n.a.	2.92	2.05	90.00	0.998
25	44.6533500	-110.4796000	12	541261.00	4944574.00				24.0	0.7010	n.a.	1.47	1.03	45.40	0.997
26	44.6533400	-110.4798000	12	541246.00	4944573.00				23.5	0.7006	n.a.	1.86	1.30	57.40	0.997
27	44.6533400	-110.4800000	12	541229.00	4944573.00				17.5	0.7003	n.a.	0.53	0.37	16.40	0.982
28	44.6534200	-110.4806000	12	541183.00	4944583.00				19.5	0.7000	n.a.	3.01	2.11	92.70	0.998
29	44.6534500	-110.4808000	12	541165.00	4944585.00				18.8	0.6997	n.a.	1.04	0.73	32.00	0.995
30	44.6534500	-110.4810000	12	541149.00	4944585.00	26.7	43.8	0.1	17.4	0.6993	n.a.	2.36	1.65	72.70	0.995
31	44.6541200	-110.4828000	12	541006.00	4944659.00				19.0	0.6998	n.a.	1.94	1.36	59.80	0.998
32	44.6541400	-110.4830000	12	540993.00	4944661.00				19.1	0.7003	n.a.	0.41	0.28	12.50	0.983
33	44.6541400	-110.4831000	12	540982.00	4944661.00				18.8	0.7008	n.a.	3.42	2.40	105.00	0.998
34	44.6540300	-110.4832000	12	540980.00	4944649.00				20.9	0.7013	n.a.	1.02	0.72	31.40	0.992
35	44.6540200	-110.4834000	12	540964.00	4944647.00				17.3	0.7018	n.a.	1.17	0.82	36.10	0.992
36	44.6540400	-110.4835000	12	540949.00	4944649.00				18.6	0.7023	n.a.	0.19	0.14	5.95	0.939
37	44.6540600	-110.4837000	12	540937.00	4944652.00				18.9	0.7028	n.a.	UD			
38	44.6540700	-110.4839000	12	540921.00	4944653.00				24.4	0.7033	n.a.	0.39	0.27	11.90	0.977
39	44.6540700	-110.4841000	12	540901.00	4944653.00				28.6	0.7038	n.a.	18.50	13.00	573.00	0.999
40	44.6538700	-110.4841000	12	540902.00	4944630.00	24.6	40.3	1.1	16.9	0.7043	n.a.	0.24	0.17	7.35	0.966
41	44.6538400	-110.4839000	12	540918.00	4944627.00				16.3	0.7044	n.a.	0.19	0.13	5.90	0.943
42	44.6538500	-110.4837000	12	540935.00	4944628.00				16.5	0.7046	n.a.	0.44	0.31	13.80	0.973
43	44.6538200	-110.4835000	12	540954.00	4944625.00				18.9	0.7048	n.a.	0.59	0.41	18.10	0.979
44	44.6538600	-110.4831000	12	540984.00	4944630.00				14.8	0.7049	n.a.	0.72	0.51	22.40	0.992
45	44.6540200	-110.4829000	12	540998.00	4944647.00				20.1	0.7051	n.a.	0.39	0.28	12.10	0.968
46	44.6540000	-110.4828000	12	541011.00	4944645.00				24.3	0.7053	n.a.	1.17	0.83	36.30	0.995
47	44.6539700	-110.4826000	12	541026.00	4944642.00				22.0	0.7054	n.a.	2.44	1.72	75.70	0.999

48	44.6538600	-110.4827000	12	541014.00	4944630.00				17.2	0.7056	n.a.	0.85	0.60	26.30	0.979
49	44.6538100	-110.4823000	12	541044.00	4944625.00				17.4	0.7058	n.a.	1.14	0.80	35.30	0.996
50	44.6538200	-110.4822000	12	541058.00	4944625.00	23.9	50.2	1.0	20.0	0.7059	n.a.	1.15	0.81	35.80	0.995
51	44.6538200	-110.4819000	12	541077.00	4944626.00				27.5	0.7059	n.a.	0.24	0.17	7.33	0.935

Date: 2014/8/15

Weather: Sunny until 11:30, cloudy and rainny later.

Pressure: 1024.72 hPa

Data Collector: Peipei Lin

Notes: the air temperature, air relative humidity and wind speed are measured by Christie at different locations compared to this dataset. Thus the average of Christie's air temperature, humidity and wind speed was used

POINT	**LONGITUDE**	**LATITUDE**	**UTM ZONE**	**UTM LONGITUDE**	**UTM LATITUDE**	**AIR TEMP.**	**AIR RH**	**WIND SPEED**	**SOIL TEMP**	**ACK**	**H_2S**	**H_2S R^2**	**CO_2**		**CO_2 R^2**
						(°C)	(%)	(km/h)	(°C)		($ppm\ s^{-1}$)		($mol\ m^{-2}\ d^{-1}$)	($g\ m^{-2}\ d^{-1}$)	
1	-110.4792800	44.6553000	12	541286.00	4944792.00	23.7	53.6	1.2	17.9	0.7068	BD		0.32	0.23	10.10	0.970
2	-110.4792200	44.6554700	12	541290.00	4944811.00				18.5	0.7068	BD		0.17	0.12	5.37	0.883
3	-110.4791800	44.6556200	12	541294.00	4944827.00				16.4	0.7068	BD		0.24	0.17	7.43	0.979
4	-110.4791700	44.6557600	12	541295.00	4944843.00				18.1	0.7068	BD		1.59	1.13	49.60	0.994
5	-110.4814600	44.6535000	12	541115.00	4944590.00				13.5	0.7068	UD		1.00	0.71	31.20	0.992
6	-110.4812800	44.6534800	12	541129.00	4944588.00				15.2	0.7068	UD		1.37	0.97	42.70	0.990
7	-110.4814200	44.6533600	12	541118.00	4944575.00				12.6	0.7068	UD		0.86	0.61	26.90	0.982
8	-110.4816400	44.6533200	12	541100.00	4944571.00				14.2	0.7068	UD		1.26	0.89	39.30	0.988
9	-110.4818200	44.6533400	12	541086.00	4944573.00				14.3	0.7068	UD		1.41	1.00	43.80	0.987
10	-110.4826800	44.6531800	12	541018.00	4944554.00				15.6	0.7068	UD		0.07	0.05	2.04	0.636
11	-110.4828900	44.6531500	12	541001.00	4944551.00				18.8	0.7068	UD		0.12	0.08	3.67	0.672
12	-110.4830700	44.6531700	12	540987.00	4944553.00				16.5	0.7068	UD		0.35	0.25	10.90	0.968

13	-110.4833000	44.6531900	12	540969.00	4944555.00				15.5	0.7068	UD		0.17	0.12	5.27	0.961
14	-110.4838700	44.6525900	12	540924.00	4944489.00				19.6	0.7068	UD		19.90	14.00	618.00	0.996
15	-110.4839600	44.6525400	12	540917.00	4944483.00				18.9	0.7068	UD		2.54	1.79	78.90	0.987
16	-110.4841200	44.6526600	12	540904.00	4944496.00				17.7	0.7068	UD		0.88	0.62	27.20	0.991
17	-110.4842700	44.6526400	12	540892.00	4944494.00				18.3	0.7068	UD		0.83	0.59	25.80	0.985
18	-110.4843100	44.6527500	12	540889.00	4944506.00				15.6	0.7068	BD		2.47	1.74	76.70	0.988
19	-110.4844700	44.6528400	12	540876.00	4944516.00				15.1	0.7068	UD		2.41	1.71	75.10	
20	-110.4845700	44.6529100	12	540868.00	4944524.00				19.4	0.7068	UD		28.00	19.80	872.00	0.992

Date:2014/8/15

Data Collector: Christie E. Torres

POINT	**LONGITUDE**	**LATITUDE**	**UTM ZONE**	**UTM LONGITUDE**	**UTM LATITUDE**	**AIR TEMP.**	**AIR RH**	**WIND SPEED**	**SOIL TEMP**	**ACK**	**H_2S**	**H_2S R^2**	**CO_2**		**CO_2 R^2**
						(°C)	(%)	(km/h)	(°C)		(ppm s^{-1}) (mol m^{-2} d^{-1}) (g m^{-2} d^{-1})		(ppm s^{-1}) (mol m^{-2} d^{-1}) (g m^{-2} d^{-1})		
1	44.6554800	-110.4793800	12	541278.00	4944812.00	22.2	57.2	2.1	15.4	0.7102	n.a.		0.21	0.15	6.41	0.965
2	44.6556200	-110.4792900	12	541285.00	4944827.00	22.5			13.0	0.7095	n.a.		0.69	0.49	21.40	0.989
3	44.6538200	-110.4816100	12	541102.00	4944626.00	22.8			18.6	0.7087	n.a.		1.07	0.76	33.40	0.996
4	44.6533000	-110.4824800	12	541034.00	4944568.00	23.2			16.0	0.7079	n.a.		1.00	0.71	31.10	0.995
5	44.6533100	-110.4827000	12	541016.00	4944569.00	23.5			13.9	0.7071	n.a.		0.54	0.38	16.90	0.986
6	44.6533100	-110.4828900	12	541001.00	4944569.00	23.8			14.6	0.7064	n.a.		0.57	0.41	17.80	0.990
7	44.6533300	-110.4830500	12	540988.00	4944571.00	24.1			14.0	0.7056	n.a.		0.36	0.26	11.30	0.984
8	44.6533200	-110.4832600	12	540972.00	4944570.00	24.5			13.8	0.7048	n.a.		0.28	0.20	8.66	0.957
9	44.6533500	-110.4834900	12	540953.00	4944573.00	24.8			14.8	0.7041	n.a.		0.10	0.07	3.18	0.875
10	44.6533700	-110.4851900	12	540819.00	4944575.00	25.1	49.9	0.3	19.1	0.7033	n.a.		3.74	2.63	116.00	0.998
11	44.6532700	-110.4850000	12	540834.00	4944563.00	25.1			17.8	0.7033	n.a.		0.25	0.18	7.73	0.870

12	44.6531700	-110.4848500	12	540846.00	4944552.00	25.1	17.9	0.7033	n.a.	0.38	0.27	11.90	0.975
13	44.6530700	-110.4847400	12	540854.00	4944541.00	25.1	16.3	0.7033	n.a.	1.34	0.94	41.50	0.997
14	44.6529800	-110.4846300	12	540863.00	4944531.00	25.1	18.2	0.7033	n.a.	1.02	0.72	31.60	0.994

Appendix II: Detailed data processes of sequential Gaussian simulation

The sequential Gaussian simulation performed was mainly composed of three parts: pre-processing, the simulation itself, and the post-processing. Pre-processing included cell declustering, normal score transformation and variogram modeling. Post-processing included averaging grid values over realizations and adding coordinates.

II.1 Cell Declustering

The ideal dataset is collected from regular sampling with equal spacing, which is difficult to achieve. The resulting clusters in the dataset could cause the uneven weighting of areas, resulting in areas with clusters having a higher weight than those areas void of clusters. Thus, declustering is used to assign new weight values (i.e., clustered data receive less weight and vice versa) so that each datum is more representative of the entire area.

There are two techniques used for declustering: polygonal declustering and cell declustering. Polygonal declustering is applied to determine the polygonal area of influence (Voronoi diagram) and then calculate the weight based on the polygonal area (equation 1).

$$\text{weight(i)}_{poly} = \frac{A_i}{\sum A_i} \tag{1}$$

One disadvantage of the polygonal method is that it is sensitive to the boundary condition. If a boundary is too far from the data, the boundary data would receive a much higher weight than it deserves. However, the cell declustering method is insensitive to the boundary condition. The primary purpose of cell declustering is to separate the area of interest into cells of the same size and to assign weight to the datum based on the number of data in the cell, as illustrated in equation 2,

$$\text{weight(i)}_{cell} = \frac{1}{n_i \cdot L_0} \cdot n \tag{2}$$

where n_i is the number of data in the cell i, L_0 is the number of the cells with data inside, and n is the total number of data.

The weight assigned by cell declustering is sensitive to the cell size. A cell size that is too small would result in a situation where every cell contains only one datum and thus an equal weight of one for each datum. Whereas a cell size that is too large would result in an equal weight for each datum as well as all data locate in that cell. The optimum cell size that identifies the best weight is the coarsest sampling spacing with additional infill sampling. Other than this, a common procedure

is to assign a cell size, which corresponds to the maximum (or minimum) declustered mean. If the sample is clustered at high values, the cell size corresponding to the minimum declustered mean is selected, as the mean is overestimated due to the high-value clusters, and vice versa. The weight by cell declustering is also sensitive to cell origin. In order to remove the influence of a cell's location, the cell declustering procedures are repeated with offsets, and the results are averaged.

Following are parameter descriptions in the cell declustering (declus) program in WinGSLIB.

1) Y, Z cell anisotropy:

   These parameters are used to adjust the Y, Z shape of the cell to conform to major direction of preferential directions. For example, if the measured samples are more closely spaced in the X direction than in the Y direction, the cell size in the X direction should be reduced. The declus program computes cell size for X direction and derives Y, Z direction by multiplying the X cell size by a ratio, which is shown here as Y, Z cell anisotropy. The relations are indicated in the following equations.

$$cell_Y = cell_X \cdot r_Y \tag{3}$$

$$cell_Z = cell_X \cdot r_Z \tag{4}$$

   where $cell_X$, $cell_Y$, $cell_Z$ are the derived cell size in X, Y and Z direction separately; and r_Y and r_Z are the anisotropy ratios of Y, Z direction to cell size in X direction correspondingly.

2) Number of origin offsets:

   Each time the origin is moved at a certain distance in each direction, the number of origin offsets used to remove the sensitivity to the location of origin is defined. The offset distance relates to the number of origin offsets, as shown in the following equation.

$$\mathrm{d} = \mathrm{cell}/\mathrm{n} \tag{5}$$

   where d is the offset distance, cell is the cell size, and n is the number of origin offsets.

3) Declustering: Min or Max

   Here is where the decision is made regarding whether the value corresponding to the minimum or maximum weighted mean will be used.

4) Number of cell sizes, minimum size, maximum size:

   The minimum and maximum size determines the range of the cell size to be located. The number of cell sizes decides the increment of the cell size between min and max, as shown in following equation,

$$\mathrm{increment} = \frac{max_{cell\ size} - min_{cell\ size}}{N_{cell\ number}}, \tag{6}$$

Following are the parameters used in the CO_2 cell declustering program as an example (Figure

33); the setting for the soil temperature is same as the setting of CO_2 except for the variable option. As the spacing in measurements is smaller for a high-value area and is larger for a low-value area, the cell size corresponding to minimum weighted mean becomes the choice. The cell size range of 1 to 50 meters with increment of 1 meter is enough to search for the optimum cell size, as the grid spacing is between 15 and 35 meters.

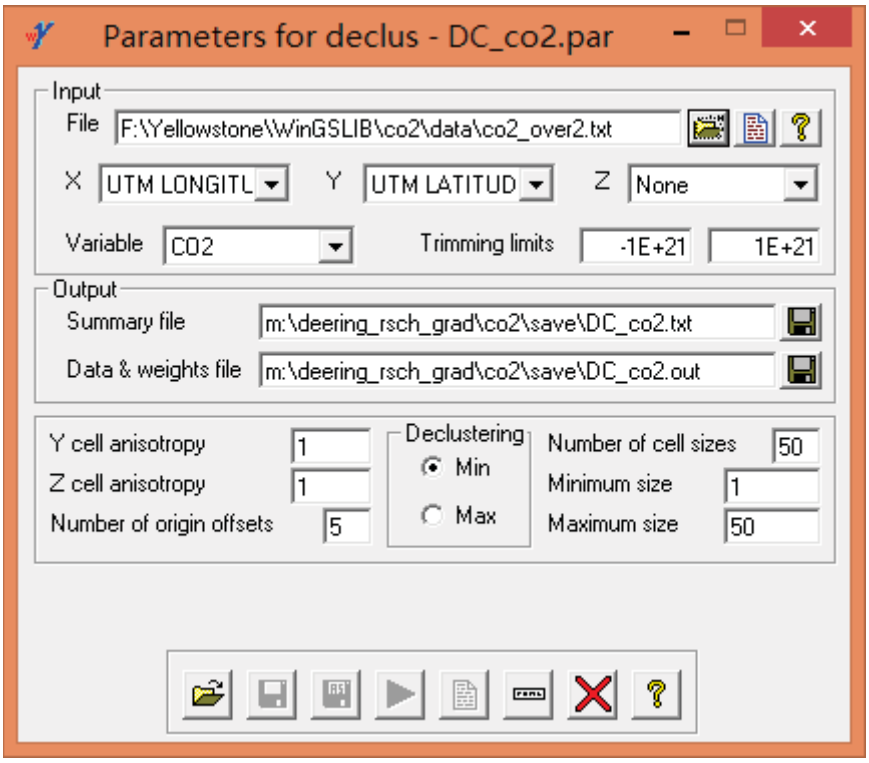

Figure 33. The screenshot for the cell declustering program. The parameters shown here are the values used for the CO_2 flux calculation. Software: WinGSLIB v1.5.8 by Statios

References:

1. Pyrcz, Michael J., and Clayton V. Deutsch. Geostatistical reservoir modeling. Oxford university press, 2014.

2. Pyrcz, M. J., and C. V. Deutsch. "Declustering and debiasing." Newsletter 19 (2003).

3. Deutch, Clyton V., and André G. Journel. "GSLIB: geostatistical software library and user's guide." (1992).

II.2 Normal Score

Generally, the sampled data have an arbitrary distribution that is unable to be described by any predictable equations; however, a normal or Gaussian distribution of the data is required for later

calculation of the variogram. The normal score function in WinGSLIB provide the transformation from an arbitrary distribution to a normal distribution based on the cumulative probability.

II.3 Variogram Modeling

Variogram (Figure 34) plots the variance of the difference between values at two locations, which indicates the spatial dependency of data and is used to assign weights to surrounding sampled data points for interpolation of the unsampled point. Key components in variogram are the sill, nugget, partial sill and range, as shown in Figure 34. Sill is the horizontal part of the graph that levels off, indicating that there is no spatial dependence between the data points at those values of distance. Nugget is the intercept of the line at the y-axis, representing the local error. If the nugget is equal to 0, this means the sampled data at the same location would have the same value every time. If the nugget is not zero, the nugget represents the variance of the measurements at the same location. Partial sill is the distance in variance from the nugget to where the sill begins. Range is the distance from zero to where sill begins, representing the size of neighborhood.

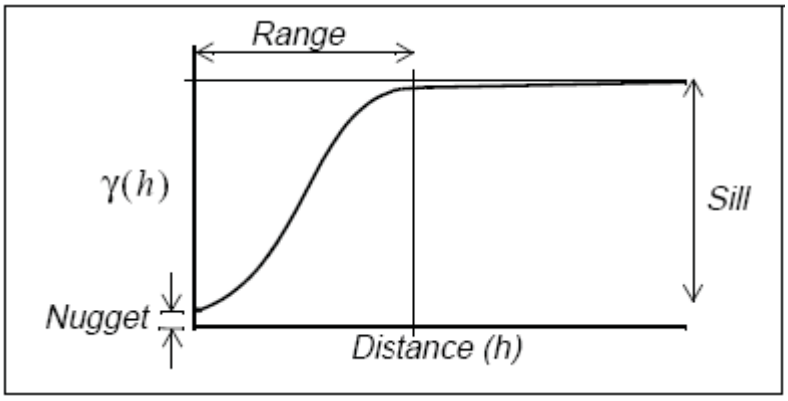

Figure 34. The variogram shows the variance of difference over distance. Its components – nugget, range, sill are also displayed on the graph.

The variogram modeling processes included true variogram calculation, variogram modeling and variogram plotting. These processes could be achieved using *irregularly spaced data variogram computation (gamv)*, *variogram file from model (vmodel)* and *variogram (vargplt)* programs in WinGSLIB separately.

II.3.1 Irregularly spaced data variogram computation (gamv)

This program computed the variance for all pairs of points, and these points were grouped based on the determined lag distance (or bin size). The pairs in the same bin were averaged and plotted as a reprehensive point on the variance-distance plot, the variogram.

The lag distance is one important parameter in this process. If the lag distance is too small, there would not be enough points in a bin to get a representative sample. If the lag distance is too large, the short distance autocorrelation may be masked. The optimum lag distance is the grid spacing in the grid sample, if the spacing varies and then takes an average of the spacing.

The number of lags is another important parameter in the variogram computation. If the number is too small, the variogram would be unable to show the appearance of the spatial independency (the sill). The suggested number of lags for the first attempt is half of the longest distance between a pair of points in the study area divided by the lag distance.

The following screenshots (Figure 35) provide an example of the parameters used in the gamv program for CO_2 flux. All settings for soil temperature were the same, except for the input. Attention should be paid to the input variable, which should be the normal-scored CO_2 flux and soil temperature. Because of the uncertainty regarding parameters for lag distances and lag tolerance, the lag distance from 10m to 35m and lag tolerance from 5m to half lag distance were used for variogram computation to compare the performance of the results.

Figure 36 shows the comparison of the variograms of different lag distance for CO_2 flux. By comparing the lag tolerance in the variograms with lag distance ranging from 15m to 35m (Figure 36), the best-fit were found to always be derived from the lag tolerance of 5m, the smallest tolerance. The rise in lag tolerance normally makes the first few points jump to a comparably high variance and then jump back to a comparably low value. The instability of the first few points would lead to the hardness of defining the nugget.

By plotting the lag distance from 10m to 35m associated with the lag tolerance of 5m in one graph (Figure 37), variograms computed with different lag distances show a similar trend, and the one with the least lag distance of 10m shows the most details. Thus, the lag distance of 10m associated with lag tolerance of 5m (Figure 37) was used as the template for later variogram modeling of CO_2 flux. The comparison result is also the same for soil temperature, thereby requiring no further detailed explanation of soil temperature.

a)

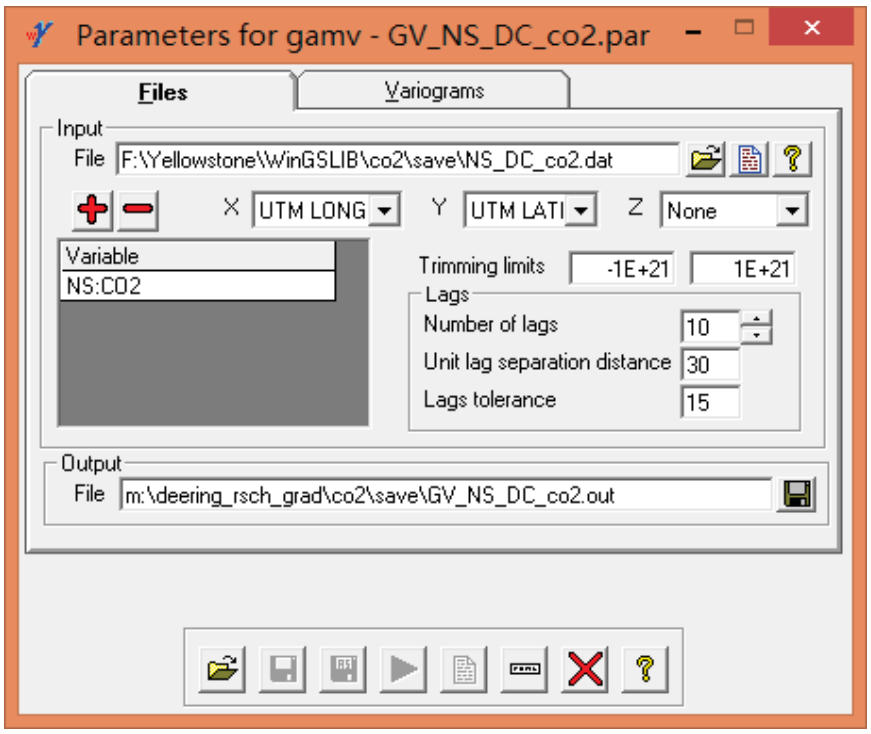

b)

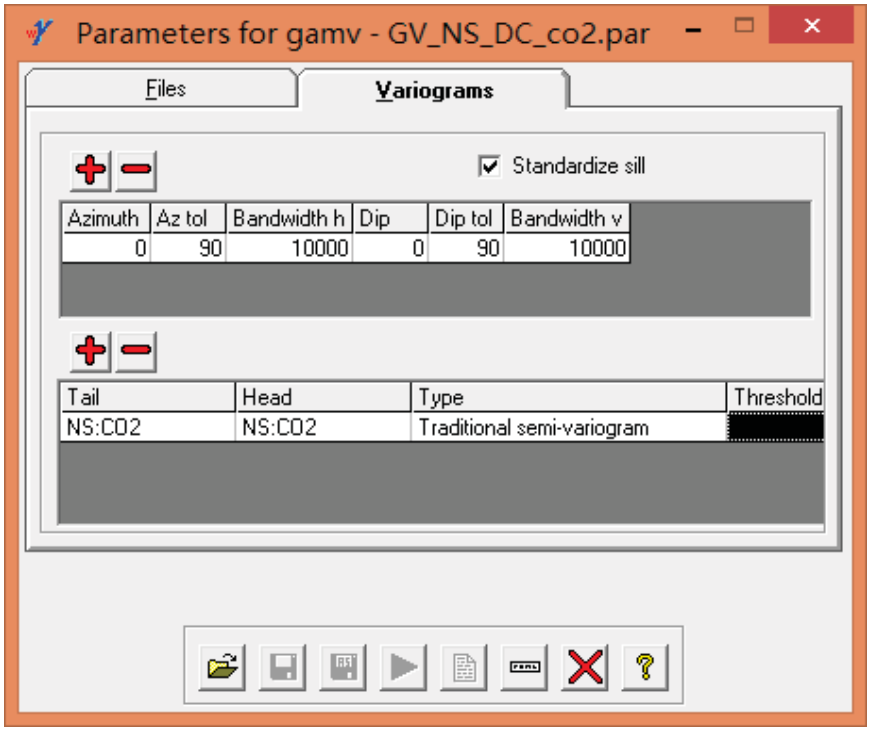

Figure 35. The screenshot for the variogram computation with the parameters for the calculation. Software: WinGSLIB v1.5.8 by Statios

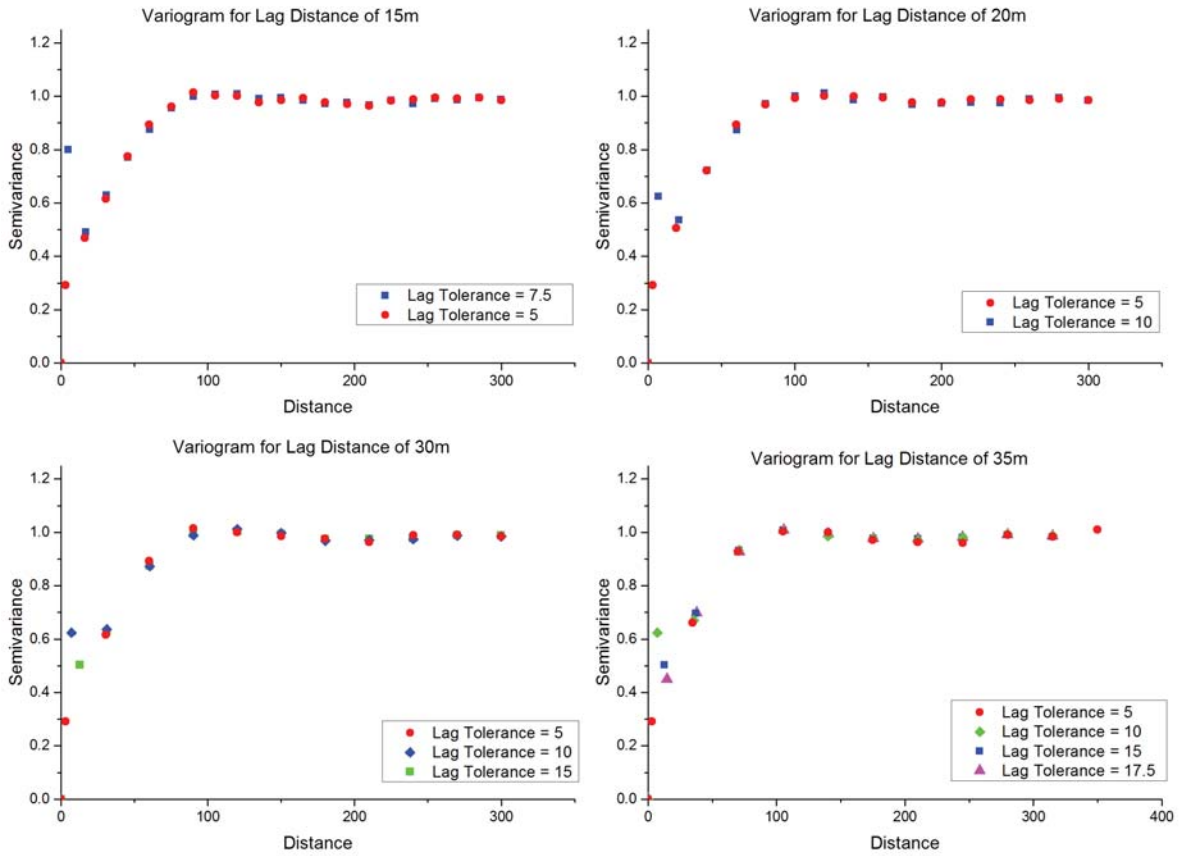

Figure 36. The variogram of various lag distances, ranging from 15m to 35m. In each lag distance, lag tolerances ranging from 5m to half lag distance were plotted.

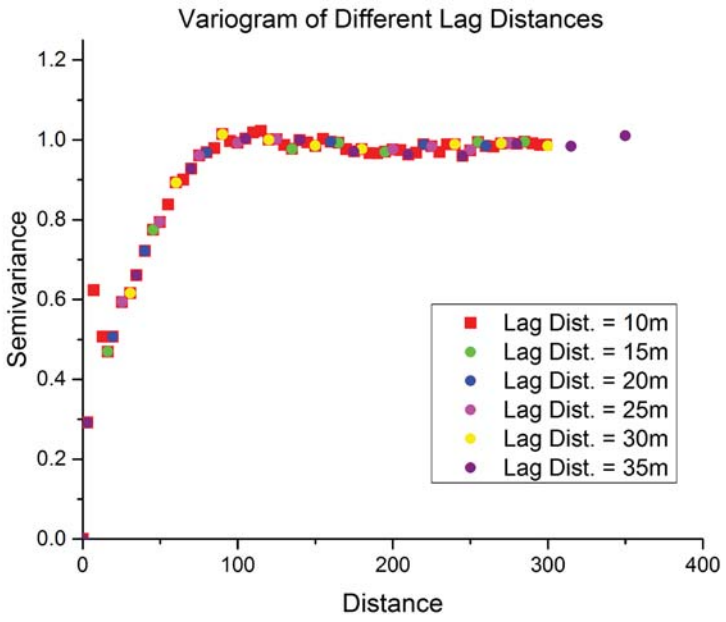

Figure 37 The variogram plotting the lag distance from 10m to 35m together. Most points followed the same trend line. The lag distance of 10m was more detailed with the most points and was then selected as the template for later variogram model fitting.

II.3.2 Variogram Modeling

Variogram models are used to fit a line to the variogram so that the spatial independency can be described mathematically. The frequently used models for variogram fitting are spherical, exponential and Gaussian. Among the three models, spherical and Gaussian models have a more straightforward range and sill than the exponential model. Different variogram model types with different nugget and partial sill values were tried to achieve a best fit variogram model.

The variogram model types of spherical, Gaussian and exponential were used to fit the variogram of CO_2 flux with a lag distance of 10m and lag tolerance of 5m (Figure 38). The best spherical model had the nugget value of 0.28 and the range of 95m. The exponential model utilized the nugget of 0.1 and the range of 110m. The Gaussian model had the nugget of 0.4 and the range of 80m.

From Figure 38, the spherical model is shown to be the best model of these three models, matching the most points and clarifying the trends of CO_2 flux data. The real variogram has a rapid and similar rate of increase from distance of 0 to 80m, and a clear range with a sharp decrease to the variance of 1. The Gaussian model fits well for the part after the distance of 30m, but exhibits

poor performance due to its slow increase at the beginning. Without a clear boundary for the range, the exponential model does not match the variogram well. Thus, the spherical model was finally chosen for the later simulation.

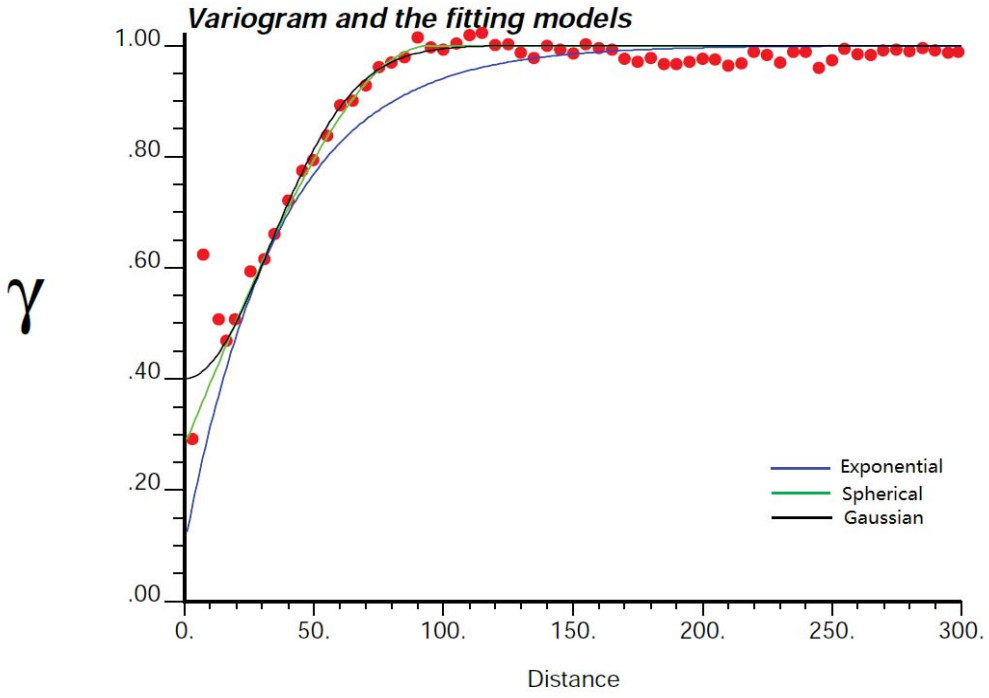

Figure 38 The performance of the spherical, exponential, and Gaussian models. 1) spherical: nugget 0.28, range 95m; 2)exponential: nugget 0.1, range 110m; 3) Gaussian: nugget 0.4, range 80. The red points were the semi-variance values derived from the actual data.

The spherical and exponential models were both tested to utilize for the variogram modeling of soil temperature. The spherical model with a nugget of 0.18 and range of 130m and the exponential model with a nugget of 0.16 and range of 135m worked best in each model; while the spherical model performed better than the exponential one. The Gaussian model was not tested, as the shape of the Gaussian model did not match the shape of the variogram. Figure 39 shows the performance of all three of these models.

II.3.3 Variogram Plotting (vargplt)

This process puts the real variogram and the model in one graph to compare the fitting of the model to the real variogram, where the real variogram is presented in points and the model in a line. The ideal situation is for the line of the model to pass through all the points of the real variogram.

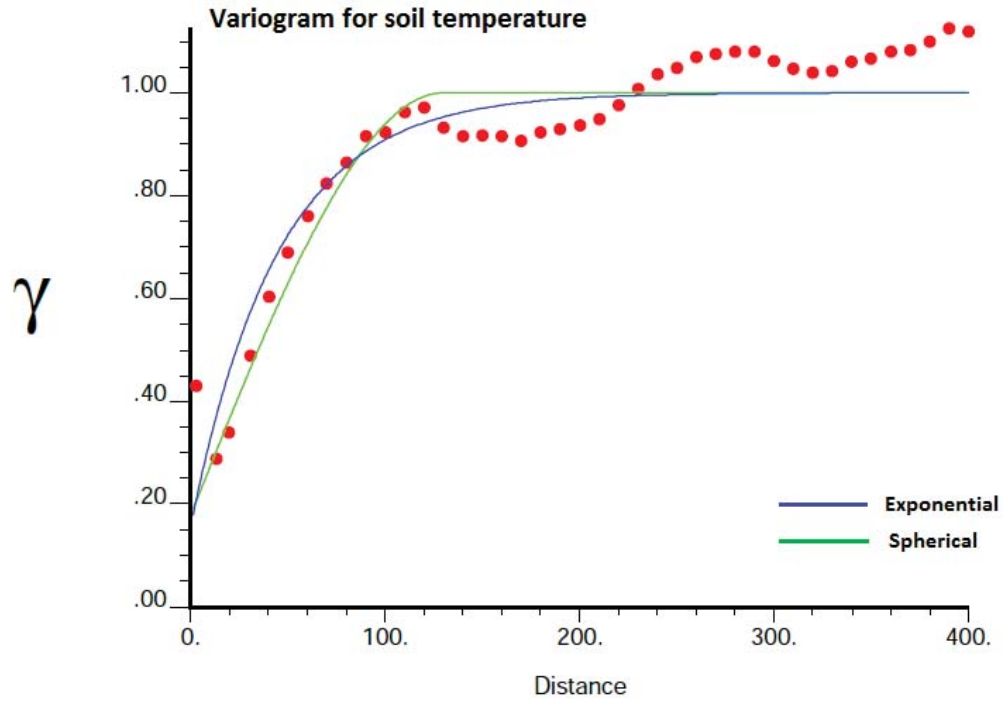

Figure 39. The performance of the spherical and exponential models. 1) Spherical: nugget 0.18, range 130m; 2) exponential: nugget 0.16, range 135m. The red points were the semi-variance values derived from the actual data.

II.3.4 Sequential Gaussian Simulation (sGs)

As mentioned before, the sGs method is used to interpolate values for unsampled points and the sequential Gaussian (sgsim) program in WinGSLIB is used to achieve it. In this program, a random path for the calculation order of the grid was predefined; additionally, the neighboring data and the previously simulated value at the same grid were retained for the simulation. Then a simple kriging –a linear regression technique for estimation of value at unmeasured points, with the variogram model was performed at each grid to determine the mean and variance of the unsampled grid for a probability model. The cumulative distribution function is thus built from the mean and variance to pick a random value as the value of the grid. These steps were performed for all grids to be one realization. In this research, the flux of CO_2 and soil temperature were simulated for 300, 500, 700 and 1000 times separately. Moreover, the performances of different times of simulations were compared to understand whether any large differences in the results associated with the simulation times existed.

In the construction of the probability model of the unsampled value, the simple kriging

technique is employed. Kriging is "a collection of generalized linear regression techniques for minimizing an estimation variance defined from a prior model for a covariance"(Geostatistics, 1991). Simple kriging is the simplest version of kriging, with the calculated mean $Z_{SK}^{*}(u)$ and variance σ_{SK}^{2} shown below (Deutch and Journel, 1992):

$$Z_{SK}^{*}(u) = \sum_{\alpha=1}^{n} \lambda_{\alpha}(u)\mathrm{Z}(u_{\alpha}) - [1 - \sum_{\alpha=1}^{n} \lambda_{\alpha}(u)] \cdot m \quad (7)$$

$$\sigma_{SK}^{2} = C(O) - \sum_{\alpha=1}^{n} \lambda_{\alpha} C(u - u_0) \quad 1) \quad (8)$$

where Z(u) is the random variable model at location u, the u_{α}'s are the n data locations, m is the constant mean of random variable Z(u) at all locations with a prior hypothesis that the random variable Z(u) is stationary, the $\lambda_{\alpha}(u)$ is the weight determined to have minimum estimation variance, $Z_{SK}^{*}(u)$ is the linear regression estimator, and C(h) is the covariance calculated from the variogram model.

For the parameter settings in the sequential Gaussian simulation (sgsim) program in WinGSLIB, several things need to be mentioned here.

1. The input file should be declustered. However, unlike the input in the variogram computation process, no normal score transformation is required. Thus, the input is only declustered.
2. A debugging level is recommended to be set at medium, which could provide all the kriging matrices and data used for the estimation of every point. It is not recommended to set it to high, as the debugging file would be very large with a large grid.
3. For the tail interpolation, the minimum value is the detection limit of 2 g m^{-2} d^{-1}; the maximum value is the measured maximum amount of 58,900 g m^{-2} d^{-1}. The interpolation method set for the lower tail is linear, and the hyperbolic model with the parameter of 1.5 for the upper tail.
4. The variogram used in the program can be directly imported from the previously saved file for the variogram model.
5. The search radii in the search option should be set exactly as the parameters in the variogram. The minimum and maximum data for simulation are 2 and 8 separately in the research. Other search settings are left as the default.

Higher number of simulation times guarantees the higher accuracy for the result, while higher number requires more computation time and larger disk space for output. In addition, how the location of the first simulated grid (seed) and the simulation order for the following grid affect the

final simulation result is unknown. Thus, the three seed value (69069, 4866799, and 6494930) was randomly chosen, and 300, 500, 700 and 1000 realizations were performed for each seed. The following Table 6 shows the minimum, maximum and mean value of the simulated total flux for the whole rectangular area - not the trimmed area for the study area.

The influence of the seed value can be evaluated by comparing each average total flux calculated from 1000 realizations, which is closest to the true data among these numbers of realizations. The differences between the total fluxes derived from these three seed values are quite small, the maximum of which is only 0.008×108 g m-2 d-1 and is about 0.459 percent of the average of these three mean total fluxes. The chosen seed value would make some difference to the simulation result; but the small differences can be ignored.

The simulation results from the different number of realizations were compared for three seed values and indicated the importance of choosing the right number of realizations. The mean total flux of 1000 realizations from three seed values were averaged as a standard for later comparisons which will be called as 1000-average. By comparing the realizations of 300, 500, 700 and 1000 to the 1000-average, the difference showed in the last row under each seed in Table 6 indicated that 300 realizations has a comparably large difference to the 1000-average which is 3 to 4 times larger than the other higher number of realizations, except the seed value of 6494930 showing the same magnitude of difference for all examined number of realizations. This difference was of the same magnitude for the 500, 700 and 1000 realizations for the other two seed values. This comparison result showed that 300 realizations were not enough to obtain a stable result, and at least 500 realizations were required. In addition, the seed value is related to the number of realizations. If a proper seed value is chosen, fewer realizations are needed to approach the true data.

II.4 Post-processing

Post-processing included the processing for multiple simulations and the addition of the coordinates to the simulated data.

The processing of multiple simulations (postim) program in WinGSLIB was able to calculate the average and variance for each grid over all realizations, and to calculate the probability of a grid exceeding a certain value for the generation of the probability map.

The Add Coordinate (addcoord) program in WinGSLIB was easy to use by just adding the grid information previously defined.

II.5 Data trimming

The sequential Gaussian simulated result was in a rectangular area rather than the desired study

area. Thus, data trimming is required to extract the study area out. Two software programs are involved in this process: Google Earth to draw a polygon for the study area, and surfer for data trimming and total flux calculation. The drawing of the polygon for the study area was based on the satellite image where there was a barren ground surface and the sampled points. The trimming process is accomplished by setting the study area as a boundary file, and using the Blank program under Grid toolbar for trimming. The output trimmed grid file was used for total flux calculation using the Volume program under the Grid toolbar.

Table 6 *The mean of CO2 emission (t/day) derived from different times of simulation and different seed values.*

Seed	69069			
realizations	300	500	700	1000
min	89	89	89	85
max	205	205	205	205
mean	125	124	124	124
standard deviation	17	16	16	16
difference between mean and average(1000)	2.2	1.4	0.8	0.5

Seed	4866799			
realizations	300	500	700	1000
min	89	89	89	89
max	192	206	206	206
mean	123	124	124	124
standard deviation	17	18	17	17
difference between mean and average(1000)	1.0	0.2	0.2	0.3

Seed	6494930			
realizations	300	500	700	1000
min	92	92	84	82
max	223	223	223	223
mean	123	124	124	124
standard deviation	17	17	17	17
difference between mean and average(1000)	0.3	0.7	0.8	0.8

Average(1000): average value of the means of 1000 simulations for each seed value

Appendix III: CO_2 and H_2S correlation analysis

The linear regression was performed for CO_2 and H_2S where H_2S was a dependent variable and CO2 as an independent variable. The least square method was utilized to obtain the best linear model which have the least square of difference between predicted and observed value. Several statistical diagnostics were utilized to evaluate the performance of the linear regression.

1) The performance of the model is assessed by the adjusted R-squared, which is 0.72 in this case. This indicates that the model explains approximately 72% of the variation in the H_2S flux.
2) A T-test is used to speak for the significance of the independent variable CO_2 flux in the linear model. The null hypothesis for the T-test is that the coefficient for the independent variable is zero; in other words, the variable do no help for the model. The t-test for CO_2 indicate CO_2 plays an important role for the model, revealed by the p-value of 0.000005, which is statistically significant to reject the null hypothesis.
3) The Koenker (BP) Statistic is a test to determine whether the independent variable CO_2 flux is consistent to the dependent variable H_2S both in geographic space (similar behavior across the study area) and in data space (similar change for independent and dependent variables in magnitude). The statistical insignificant of BP test, revealed by the p-value of 0.96, shows the CO_2 flux and H_2S flux are consistent both in data space and geographic space.
4) Although previous test indicated a good performed model and consistent between CO_2 flux and H_2S flux, the non-normal distribution of residuals indicated that the linear model was biased. The Jarque-Bera statistic is used to assess whether the residuals are normally distributed. Its null hypothesis is that the residuals are normally distributed. While the p-value of this test for the H_2S-CO_2 model is 0, which is statistically significant, indicating a not normal distribution and a biased model. The biased prediction could also be seen from the residual vs. predicted plot (Figure 40). For a proper model, the scatter plot would have little structure and look random; while for this scatter plot, the residuals are concentrated at low values. This phenomena is due to the influence of a significantly high value and insufficient data points in between. This problem currently cannot be fixed and the standard deviation shown in Figure 40 is also acceptable except the two points with significant deviation. In summary, the linear regression is proper to predict H_2S flux based on CO_2

flux.

The best-performed linear regression is:

$$H_2S = 0.00238 \times CO_2 + 3.707167 \quad (1)$$

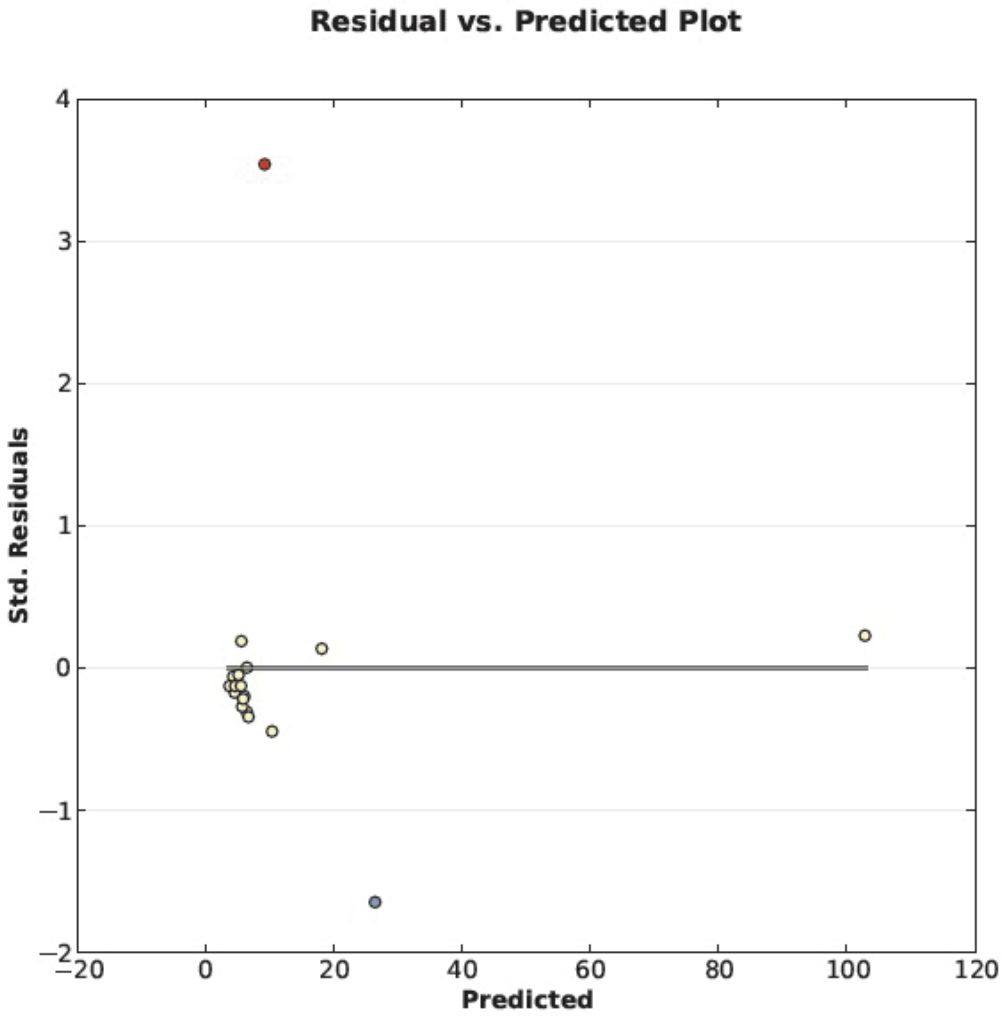

Figure 40 residual vs. predicted plot, indicating a non-random distribution of the residuals.

Appendix IV: Documentation for copyright materials

IV.1 Satellite image from Google Earth

This document is for Figure 5, Firuge6, Figure 8, Figure 9, Figure 14, and Figure28.

Fair Use Analysis Summary from https://www.lib.umn.edu/copyright/fairthoughtssummary

Work considered: Satellite image from Google Earth

Date: 07-31-2015

Here's your "Thinking Through Fair Use" results! As a reminder, these results have not been analyzed or processed in any way, except to format the input you provided into one document. These results don't claim to tell you whether a proposed use is fair or not, and do not constitute legal advice. For formal legal advice, please contact an attorney.

You thought that **purpose** was *strongly favorable* towards fair use.

You highlighted these elements as relevant to your proposed use:

Favors Fair Use	Weighs Against Fair Use
• Educational, scholarly, and research uses, and/or news reporting	

You thought that **nature** was *strongly favorable* towards fair use.

You highlighted these elements as relevant to your proposed use:

Favors Fair Use	Weighs Against Fair Use
• Published source	

You thought that **amount** was *somewhat favorable* towards fair use.

You highlighted these elements as relevant to your proposed use:

Favors Fair Use	Weighs Against Fair Use
• Portion used is peripheral or not significant to the entire work	

You thought that **market** was *strongly favorable* towards fair use.

You highlighted these elements as relevant to your proposed use:

Favors Fair Use	Weighs Against Fair Use
• One or few copies made • No impact on market for original work	

IV.2 Image of Isotech® gas bag

This document is for Figure 12.

Permission given through email contact

Peipei Lin <peipeil@mtu.edu>

Copyright of the picture on your website

Ohlsson, Julia M <Ohlsson@isotechlabs.com> Thu, Jul 30, 2015 at 4:31 PM
To: Peipei Lin <peipeil@mtu.edu>

Yes – please use the photo from our website.

Thank you,

Julie Ohlsson

Purchasing

Isotech Laboratories, Inc. (A Weatherford Company) | 1308 Parkland Court | Champaign | IL | 61821

Main: +1.217.398.3490 | Fax: +1.217.398.3493 | Toll Free: +1.877.362.4190

ohlsson@isotechlabs.com | www.isotechlabs.com

From: Peipei Lin [mailto:peipeil@mtu.edu]
Sent: Thursday, July 30, 2015 2:13 PM
To: Ohlsson, Julia M
Subject: Copyright of the picture on your website

Hi Ms. Ohlsson,

Our research team utilized your gas bags for carbon isotope analysis last year. I am going to show your gas bags in my thesis; however unluckily, I seems to lose the photo of the gas bags taken by myself and would like to know if your company could give me the permission to use the photo of gas bag shown in your website (shown below)?

Thanks. I am looking forward to hear from you.

Regards,

Peipei

IV.3 Image of Statios® WinGSLIB

This document is for Figure 33 and Figure 35.

Permission given through email contact

Michigan Tech

Peipei Lin <peipeil@mtu.edu>

Permission for screenshot of WinGSLIB

Emmanuel Schnetzler <manu@statios.com> Fri, Jul 31, 2015 at 12:02 PM
Reply-To: Emmanuel Schnetzler <manu@statios.com>
To: Peipei Lin <peipeil@mtu.edu>

Dear Peipei,

Feel free to use any snapshot from WinGslib. Please do credit Statios.

Best regards,

Manu

Manu Schnetzler
Statios LLC
www.statios.com

From: Peipei Lin <peipeil@mtu.edu>
To: wingslib@statios.com
Sent: Friday, July 31, 2015 7:05 AM
Subject: Permission for screenshot of WinGSLIB

Dear WinGSLIB team,

I am going to illustrate the software and the settings for parameters of some programs in WinGSLIB using its screenshot in my thesis. I would like to know if I am able to use the screenshot of WinGSLIB.

Thanks.

Regards,
Peipei Lin